การสังเคราะห์นาโนคอมพอสิตของพอลิไอโซพรีน/มอนต์มอริลโลไนต์ โดยใช้ดิฟเฟอเรนเชียลไมโครอิมัลชันพอลิเมอไรเซชัน

นางสาวปารัช บุญชู

วิทยานิพนธ์นี้เป็นส่วนหนึ่งของการศึกษาตามหลักสูตรปริญญาวิทยาศาสตรมหาบัณฑิต
สาขาวิชาปิโตรเคมีและวิทยาศาสตร์พอลิเมอร์
คณะวิทยาศาสตร์ จุฬาลงกรณ์มหาวิทยาลัย
ปีการศึกษา 2555

SYNTHESIS OF POLYISOPRENE/MONTMORILLONITE NANOCOMPOSITES VIA DIFFERENTIAL MICROEMULSION POLYMERIZATION

Miss Parat Boonchoo

A Thesis Submitted in Partial Fulfillment of the Requirements
for the Degree of Master of Science Program in Petrochemistry and Polymer Science
Faculty of Science
Chulalongkorn University
Academic Year 2012

Thesis Title	SYNTHESIS OF POLYISOPRENE/MONTMORILLONITE NANOCOMPOSITES VIA DIFFERENTIAL MICROEMULSION POLYMERIZATION
By	Miss Parat Boonchoo
Field of Study	Petrochemistry and Polymer Science
Thesis Advisor	Professor Pattarapan Prasassarakich, Ph.D.

Accepted by the Faculty of Science, Chulalongkorn University in Partial Fulfillment of the Requirements for the Master's Degree

..…….. Dean of the Faculty of Science
(Professor Supot Hannongbua, Dr.rer.nat.)

THESIS COMMITTEE

…….. Chairman
(Associate Professor Supawan Tantayanon, Ph.D.)

…….…… Thesis Advisor
(Professor Pattarapan Prasassarakich, Ph.D.)

…….. Examiner
(Assistant Professor Varawut Tangpasuthadol, Ph.D.)

…….. External Examiner
(Associate Professor Ittipol Jangchud, Ph.D.)

ปารัช บุญชู: การสังเคราะห์นาโนคอมพอสิตของพอลิไอโซพรีน/มอนต์มอริลโลไนต์โดยใช้ดิฟเฟอเรนเชียลไมโครอิมัลชันพอลิเมอไรเซชัน. (SYNTHESIS OF POLYISOPRENE/MONTMORILLONITE NANOCOMPOSITES VIA DIFFERENTIAL MICROEMULSION POLYMERIZATION) อ.ที่ปรึกษาวิทยานิพนธ์หลัก: ศ.ดร.ภัทรพรรณ ประศาสน์สารกิจ, 97 หน้า.

งานวิจัยนี้เป็นการศึกษาการสังเคราะห์นาโนคอมพอสิตของพอลิไอโซพรีนและมอนต์-มอริลโลไนต์ด้วยวิธีดิฟเฟอเรนเชียลไมโครอิมัลชันพอลิเมอไรเซชัน ซึ่งใช้ 2,2-เอโซบิวทิโรไน-ไทรล์เป็นตัวริเริ่ม PIP-CS15A นาโนคอมพอสิตมีขนาดอนุภาคเฉลี่ย 30 นาโนเมตรและมีการกระจายขนาดอนุภาคแคบ PIP กระจายตัวแบบแทรกสอดระหว่างชั้นของ CS15A พิสูจน์โดยเอ็กซเรย์ดิฟแฟรคโตมิเตอร์พบว่า ช่องว่างระหว่างชั้นของ CS15A ขยายเพิ่มขึ้นจาก 3.11 นาโนเมตรเป็น 3.82 นาโนเมตร ศึกษาสัณฐานวิทยาของ PIP-CS15A นาโนคอมพอสิตโดยใช้ทรานสมิสชันอิเล็กตรอนไมโครสโคป ตัวแปรที่มีผลต่อการเปลี่ยนแปลงมอนอเมอร์ ปริมาณของแข็งและขนาดอนุภาคของ PIP-CS15A นาโนคอมพอสิต ได้แก่ ความเข้มข้นของสารลดแรงตึงผิว อัตราส่วนของมอนอเมอร์ต่อน้ำและปริมาณของ CS15A พบว่า ค่าการเปลี่ยนแปลงมอนอเมอร์ร้อยละ 81 เมื่อเติม CS15A ร้อยละ 10 โดยน้ำหนักลงในระบบ ที่อัตราส่วนของมอนอเมอร์ต่อน้ำเท่ากับ 0.24:1 ร้อยละความเข้มข้นของตัวริเริ่มเท่ากับ 0.25 โดยน้ำหนัก และร้อยละความเข้มข้นของสารลดแรงตึงผิวเท่ากับ 12 โดยน้ำหนัก

PIP-MMT นาโนคอมพอสิต สามารถใช้เป็นสารตัวเติมนาโนในน้ำยางธรรมชาติสำหรับการเตรียม NR/PIP-MMT คอมพอสิตโดยกระบวนการพรีวัลคาไนเซชัน สำหรับสมบัติเชิงกลของ NR/PIP-CS15A คอมพอสิต ค่าความต้านทานแรงดึง มอดูลัสของความยืดหยุ่นและความแข็งมีค่าสูงขึ้นเมื่อเทียบกับยางธรรมชาติ ค่าความต้านทานแรงดึงของ NR/PIP-CS15A มีค่าเท่ากับ 17.7 เมกะปาสคาล ที่ร้อยละการเติม CS15A เท่ากับ 2 เสถียรภาพของ NR/PIP-CS15A คอมพอสิตหลังการทดสอบการบ่มความร้อนเพิ่มขึ้นเมื่อเทียบกับยางธรรมชาติ โดยยังคงรักษาค่ารีเทนชันของความต้านทานแรงดึงเท่ากับร้อยละ 87.6 และรีเทนชันของมอดูลัสของความยืดหยุ่นเท่ากับร้อยละ 84 ที่ร้อยละการเติม CS15A เท่ากับ 2.

สาขาวิชา ปิโตรเคมีและวิทยาศาสตร์พอลิเมอร์ ลายมือชื่อนิสิต……..…..….

ปีการศึกษา 2555 ลายมือชื่อ อ.ที่ปรึกษาวิทยานิพนธ์หลัก…..……....

5272707523: MAJOR PETROCHEMISTRY AND POLYMER SCIENCE
KEYWORDS: NANOCOMPOSITES/ MONTMORILLONITE/ DIFERENTIAL MICROEMULSION POLYMERIZATION

PARAT BOONCHOO: SYNTHESIS OF POLYISOPRENE/ MONTMORILLONITE NANOCOMPOSITES VIA DIFFERENTIAL MICROEMULSION POLYMERIZATION. ADVISOR: PROF. PATTARAPAN PRASASSARAKICH, Ph.D., 97 pp.

Polyisoprene-montmorillonite nanocomposites were successfully synthesized via differential microemulsion polymerization by using 2,2-azoisobutylronitile. PIP-CS15A nanocomposites with particle size of 30 nm and narrow size distribution were obtained. PIP was intercalated in the layer of CS15A, as confirmed by X-ray diffractometer that d-spacing of CS15A layer was expanded from 3.11 nm to 3.82 nm. Morphology of PIP-CS15A nanocomposites was determined by transmission electron microscope (TEM). Surfactant concentration, monomer to water ratio and CS15A loading were found to affect monomer conversion, solid content and particle size of PIP-CS15A nanocomposites. The monomer conversion of 81% was achieved at 10 %wt CS15A loading, monomer to water ratio of 0.24:1, initiator concentration of 0.25 %wt and surfactant concentration of 12 %wt based on isoprene monomer.

PIP-MMT nanocomposites could be used as an effective nano-filler in natural rubber (NR) latex for the preparation of NR/PIP-MMT composites by pre-vulcanization. For NR/PIP-MMT composites, the mechanical properties in tensile strength and modulus of elasticity were dramatically improved as compared to unfilled NR. The tensile strength of NR/PIP-CS15A composites of 17.7 MPa was obtained at 2 %wt of CS15A content. The stability of NR/PIP-CS15A composites after thermal ageing increased as compared to unfilled NR by maintaining 87.6% of its tensile strength and 84% of its modulus of elasticity at 2 %wt of CS15A content.

Field of Study:Petrochemistry and Polymer Science Student's Signature……

Academic Year: 2012 Advisor's Signature……...

ACKNOWLEDGEMENTS

The author would like to express her gratitude to her supervisors, Prof. Pattarapan Prasassarakich, for her encouraging guidance, supervision and helpful suggestion throughout this research. The author also would like to acknowledge Associate Professor Supawan Tantayanon, Assistant Professor Varawut Tangpasuthadol, and Associate Professor Ittipol Jangchud for their participation on the dissertation chairman and members of thesis committee, respectively.

The gratefully acknowledged to Southern Clay Product Co., Ltd. that supported the montmorillonite clay for this research, Program of Petrochemistry and Polymer Science and Department of Chemical Technology, Faculty of Science, Chulalongkorn University.

A warm thank is expressed to all of her friends in the laboratory for their friendships and help during the course of her graduate research.

Finally, and most of all, the author would like to express her deep appreciate to her family for their love, inspiration and endless encouragement throughout her entire study.

CONTENTS

Page

Page

Page

LIST OF TABLES

LIST OF FIGURES

Figure **Page**

Figure **Page**

Figure **Page**

LIST OF ABBREVIATIONS

AIBN	:	2,2-Azoisobutyronitrile
CS15A	:	Cloisite15A
CS30B	:	Cloisite30B
DSC	:	Differential Scaning Calorimetry
D_n	:	Mean Number Diameter (average particle size)
FTIR	:	Fourier Transform Infrared spectroscopy
GE	:	Grafting efficiency
MMT	:	Montmorillonite clay
NF15	:	Nanofil15
NF116	:	Nanofil116
NR	:	Natural rubber
NRL	:	Natural rubber latex
PIP	:	Polyisoprene
phr	:	Parts per hundred of rubber by weight
PSD	:	Particle Size Distribution
SC	:	Solid content
TEM	:	Transmission Electron Microscope
TGA	:	Thermogravimatric Analysis
VTS	:	Vinyl trimethoxysilane
XRD	:	X-Ray Diffraction

CHAPTER I

INTRODUCTION

1.1 The Purpose of the Investigation

Recently, polymer-clay nanocomposites (PCN) and rubber-clay nanocomposites (RCN) have good potential for industrial applications. Synthetic polyisoprene (PIP) has a green strength lower than that natural rubber (NR), however, PIP has the narrow molecular weight distribution and regular structure [1]. Therefore, the addition of montmorillonite clay into PIP matrix could improve the mechanical properties, thermal stability, flame retardant and gas barrier properties [2-3]. Modification of montmorillonite clay layer with organic compounds is necessary in order to render the clay layers more compatible with polymer chain. The PCN can be classified into three patterns by their structure, i.e. nanocomposites with intercalated, exfoliated or both intercalated and exfoliated. The greatest reinforcement of nanocomposites was completely exfoliated structure [4].

PCN can be prepared by many methods, such as in situ intercalative polymerization, solution or melts or emulsion intercalation. Emulsion intercalation is a suitable method for industries due to simple method, low cost and superior performance of PCN [5]. For the synthesis of polymer nanoparticles, nanosized polymer can be prepared by miniemulsion polymerization and microemulsion polymerization. However, both techniques require high amount of surfactant. Therefore, the differential microemulsion polymerization was proposed [6]. Poly(methyl methacrylate) nanoparticles were synthesized by differential microemulsion polymerization at low surfactant concentration. The system consists of non-aggregated surfactant, water-insoluble monomer and water or oil soluble initiator. The monomer was continuously and slowly added as small droplet to the polymerization system under mild agitation [7]. In the present work, the synthesis of polyisoprene-montmorillonite (PIP-MMT) nanocomposites via differential microemulsion polymerization was firstly reported, nanosized PIP particles are well

dispersed and intercalated in MMT layer resulting composites with good mechanical properties from polymer latex.

1.2 The Objective

The objectives of thesis can be summarized as follows:

1. To prepare the PIP-MMT nanocomposites via differential microemulsion polymerization.
2. To investigate the effects of MMT loading and monomer to water ratio on the monomer conversion, particle size and solid content.
3. To characterize the structural of PIP-MMT nanocomposites and study the mechanical properties, thermal properties and morphology of PIP-MMT nanocomposites filled natural rubber.

1.3 Scope of the Investigation

The experimental procedure for this research was presented as follows:

1. Literature survey and in-depth study research work.
2. Prepare the PIP-MMT latex via differential microemulsion polymerization and study the effects of variables:
   - Surfactant concentration: 6-14 %wt based on monomer
   - Monomer to water ratio: 0.24:1, 0.27:1, 0.30:1 and 0.40:1
   - Montmorillonite loading: 0-20 %wt based on monomer
3. Investigate of the monomer conversion, particle size and solid content of PIP-MMT nanocomposites.
4. Characterize the PIP-MMT latex by X-ray diffractometer and transmission electron microscope.
5. Prepare NR/PIP-MMT vulcanizates at various blend ratio of NR/PIP-MMT: 100/0, 70/30 and 60/40
6. Investigate the mechanical properties, thermal properties and thermal ageing properties (ASTM D573) of NR/PIP-MMT composites.

7. Characterize the NR/PIP-MMT composites morphology by scanning electron microscope.
8. Analyze data and summarize the results.

CHAPTER II

THEORY AND LITERATURE REVIEW

2.1 Synthesis of Polymer Nanoparticles [8-10]

Polymer nanomaterials have obtained much attention because of the improved properties of nanosized polymers and many attractive applications such as in textiles, coatings, paints, packaging and pharmaceuticals. Miniemulsion and microemulsion polymerization are the common methods used to synthesize polymer nanoparticles [11].

2.1.1 Miniemulsion Polymerization [12, 13]

Miniemulsion is an emulsion polymerization which has some similar to conventional emulsion polymerization containing two immiscible liquid phases. The reaction approximates an emulsion and miniemulsion polymerization depending on the monomer droplet size [12]. Miniemulsion polymerization has droplet sizes of less than 500 nm, large surface area and most of the surfactant is adsorbed at the droplet surface. Miniemulsion polymerization is a technique that uses highly water-insoluble monomers to provide very small particles. This method is useful for producing high solid content latexes and both of water-soluble and oil-soluble initiators have been used in miniemulsion polymerization. Miniemulsion polymerization uses an equal or even a lower amount of surfactant than that employed in conventional emulsion polymerization. The particle sizes from miniemulsion are smaller than those obtained by emulsion polymerization but larger than those obtained by microemulsion polymerization.

The miniemulsion polymerization is introduced for nanoparticle synthesis [13]. The particle sizes of miniemulsion are usually within a range of 50-500 nm related to the monomer droplet size. Then, the monomer droplet can be prepared by shearing a system containing oil, water, a surfactant, and an osmotic pressure agent. The process

of miniemulsion polymerization is illustrated in Figure 2.1. In the first stage, the stirrer employed in conventional emulsion polymerization is used to make the monomer emulsion with larger droplets. After that, high shear equipment is used to make the smaller droplets. Subsequently, initiator is added and polymerization starts to produce fine polymer particles.

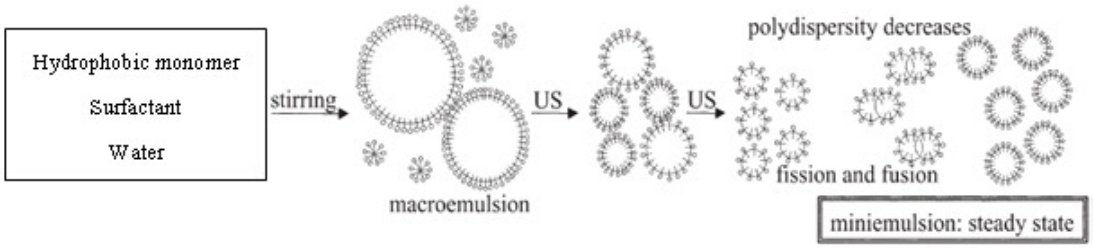

Figure 2.1 Illustration for the formation of a miniemulsion polymerization induced by ultrasound [13].

2.1.2 Microemulsion Polymerization [13]

The microemulsion polymerization method is different from the conventional emulsion polymerization method. The microemulsion polymerization is thermodynamically stable and small particle size in the range of 10 to 100 nm can be achieved. Microemulsion polymerization, which first came into being in the early 1980s, can produce transparent or translucent polymer microlatexes [14, 15]. The particle size from microemulsion polymerization is considerably smaller (10-50 nm) while the particle size that obtained by conventional emulsion polymerization is in the range of 100 to 1000 nm. It was due to the initial surface area of micelles is larger by several orders of magnitude than the total surface area of the final polymer particle. The small fraction of micelles is nucleated to stabilize the polymer particles. A comparison of micelle size in heterophase polymerization processes is presented in Figure 2.2.

The locus of initiation in the microemulsion polymerization of hydrophobic monomer (styrene, butyl acrylate, etc.) initiated by a water or oil soluble initiator is the microemulsion droplet. The initiation is a two-step process. In the first step, the initiating radicals are formed by the decomposition of initiator in the aqueous phase.

In the second step, the formed oligomers radicals enter the micelles and start the growth events (the nucleation of monomer-swollen micelles, re-initiation, etc.) or terminate the particle growth [16].

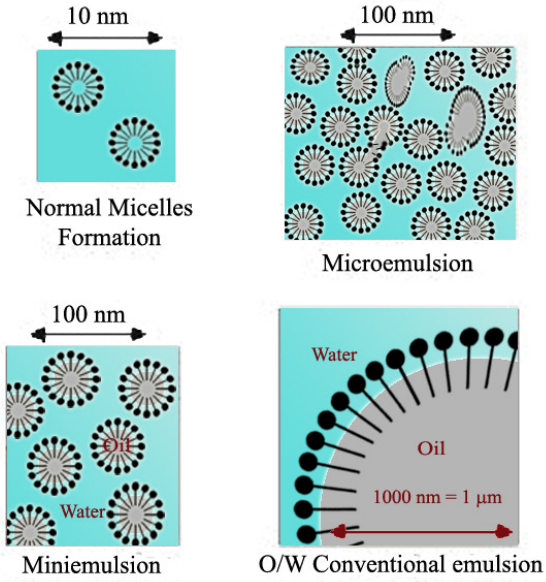

Figure 2.2 Schematic representation of micelles size in heterophase polymerization processes. [11]

In the oil-soluble case, two main approaches are suggested for the production of radicals: (1) in the monomer swollen polymer particles, formed radicals desorbed to the aqueous phase; and (2) in the aqueous phase, formed radicals are generated from the fraction of the oil-soluble initiator dissolved in water and initiate the growth of the polymer chains in both the aqueous phase (the formation of oligomers radicals) and the monomer-swollen micelles or polymer particles (by radical entry) [16]. The principle behind the formation of microemulsion (with a droplet diameter 10–50 nm) is penetration of co-emulsifier into the water/oil interface, thereby decreasing surface tension and increasing interface area. Coemulsifier also decreases the rigidity of interface film due to increasing the molecular disorder. Coemulsifier promotes the formation of a more curved interfacial area and this is reflected in smaller size of oil droplets [17].

2.1.3 Differential Microemulsion Polymerization [18]

In the previous section, a few microemulsion polymerization methods have been described for the preparation of nanosized polymers. Conventional or the modified microemulsion polymerization has many advantages such as small particle size and no need for solvent in the system, however, the major disadvantage of these polymerization methods is the requirement of a high amount of surfactant. Surfactants are not only expensive but they also have a significantly negative impact on the properties of the synthesized polymer. Thus, the differential microemulsion polymerization method has been developed. This method is expected to be a practical route that the amount of surfactant required can be decreased while still providing the nanoparticle size. Differential microemulsion polymerization, similar to emulsion polymerization, is performed with water, surfactant, water-insoluble monomer and water or oil soluble initiator. In addition, it still requires a certain temperature to initiate polymerization and agitation to form an emulsion. For the differential method, the monomer is continuously and slowly added to the polymerization system with mild agitation [18]. Smaller monomer-swollen micelles were formed by this monomer addition method. In addition, the continuous feeding of monomer will cause the monomer amount in the reaction system to be much lower and hence there are no monomer droplets during polymerization. In this case, there usually exist monomer droplets which act as a monomer reservoir. The free radical in the micelles can propagate with enough monomer transferred quickly from the monomer reservoir. The process of differential microemulsion polymerization is shown in Figure 2.3

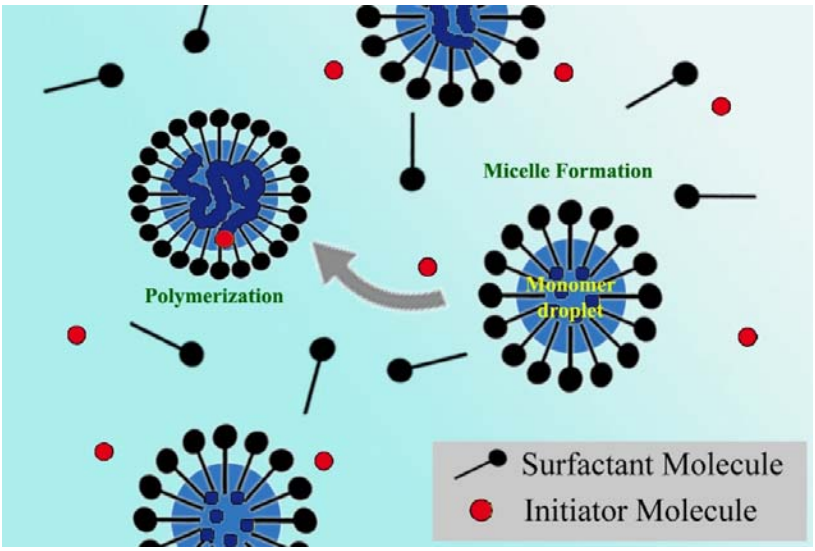

Figure 2.3 Schematic of differential microemulsion polymerization of hydrophobic monomer. [19]

2.2 Polymer-Clay Nanocomposites [20, 21]

Polymer-clay nanocomposites (PCN) materials are a class of organic-inorganic hybrids consisting of organic polymers as the matrix and inorganic clay as the reinforcing filler. The unique characteristics of PCN materials had the nanometer-scale mixing of the two components and the molecular-level interactions between them. It has a wide variety improved mechanical, thermal and barrier properties as compared to pure polymers.

2.2.1 Types of Polymer-Clay Nanocomposites [20]

Polymer-clay nanocomposites or rubber-clay nanocomposites (RCN) have potential for many industries and academic researchers. PCN exhibit the remarkable properties at low filler loading compared with unfilled rubber compounds or conventional filled composites. The rubber-clay nanocomposites have been studied mainly on four well-known rubbery materials, natural rubber (NR), ethylene propylene diene rubber (EPDM), styrene-butadiene rubber (SBR), and nitrile rubber

(NBR). However, some other types of elastomers such as silicon rubber, polybudiene rubber, and ethylene propylene rubber also exist.

2.2.2 Polymer-Clay Nanocomposites Preparation Methods [20]

In general, the method for the preparation of PCN and RCN can be divided into four major groups according to the processing techniques:

- in-*situ* polymerization
- intercalation of rubber via solution blending
- direct melt intercalation method
- intercalation of rubber via latex compounding

In-situ polymerization

In this method, layered silicate is swollen within the monomer solution (or liquid monomer), thus the formation of rubber can be occurred between and around the intercalated layers. The polymerization can be initiated either by heat or radiation, by the diffusion of suitable initiator or by an organic initiator, by the incorporating of curing or initiator and by the increasing temperature.

Intercalation via solution

This method uses a solvent system in which the rubber is soluble and the layered silicate is swellable. The organo modified layered silicate is first swollen and comes apart in the solvent. The rubber is dissolved in solvent and added to the solution. Upon solvent removal, the clay layers reassemble around the polymer, resulting in polymer-clay nanocomposites.

Direct melt intercalation method

This is the simple method that has many advantages for the industrial process and mild environmental effect, due to the absence of solvents. In this method, rubber and modified layered silicate mixture are blended in the molten state under high shear. The rubber chains was melt into the silicate galleries to form intercalated or delaminated nanocomposites

Intercalation of rubber via latex compounding

Latex compounding is also a promising method for preparing polymer-clay nanocomposites. The latex compounding technique starts with dispersing layered silicates in water that acts as a swelling agent owing to hydration of the intergallery cations. Then, the rubber latex is added and mixed for a period of time, with the dispersion of layered silicate in water followed by coagulation.

2.2.3 Types of Polymer-Clay Nanocomposites Structure [20]

The incorporation of a few weight percent of modified layered silicates which are properly dispersed in the polymer matrix results in very high surface areas for polymer-clay interactions, as compared to the conventional polymer-filler composites. According to the strength of the interfacial interactions between polymer matrix and layered silicate three types of polymer-clay composites can be produced (Figure 2.4):

- Phase separated microcomposites or conventional composites: the polymer is unable to intercalate between the silicate sheets and the clay agglomerate is formed.

- Intercalated nanocomposites: intercalated nanocomposites are formed by the insertion of a rubber chains between the unaltered silicate layers, maintaining their regular alternation of galleries and laminas.

- Exfoliated nanocomposites: the individual layers of the nanoclay are totally delaminated and dispersed in the rubber matrix. The ordered structure of layered silicate is lost and the average distances between the exfoliated layers depend on clay loading.

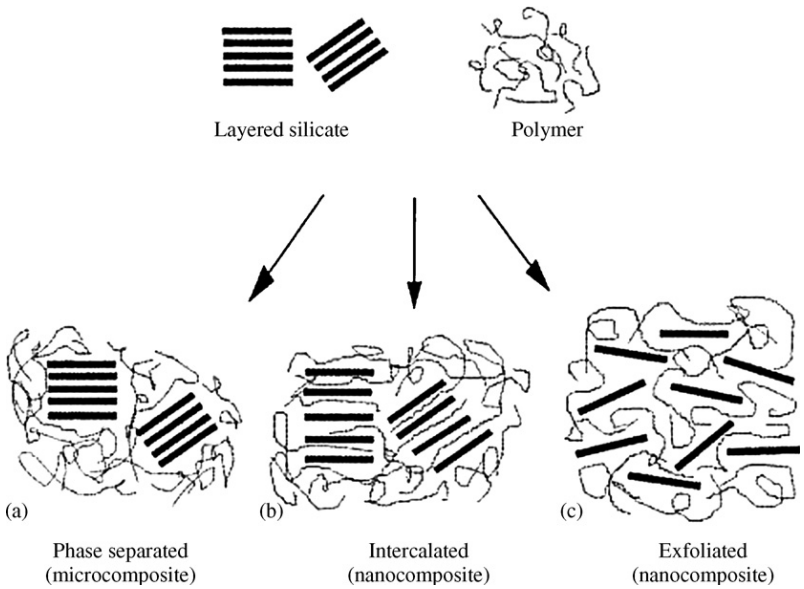

Figure 2.4 Probable polymer/layered silicate structure. [22]

2.2.4 Characterization of Polymer-Clay Nanocomposites [20]

There are mainly two methods to characterize the structure of PCN. The most is X-ray diffraction (XRD) to determine the spacing between the clay layers. The sample preparation is relatively easy and the X-ray analysis can be performed within a few hours. However, one needs to be very careful with the interpretation of the results. Lack of sensitivity of the analysis and limits of the equipment can lead to wrong conclusions about the nanocomposites structure. Therefore, transmission electron microscopy (TEM) is a necessary complement to XRD. TEM gives a direct measurement of the special distribution of the layers but requires significant skills in specimen preparation and analysis.

X-Ray Diffraction

XRD is used to identify intercalated structures. In such nanocomposites, the repetitive multilayer structure is well preserved, allowing the interlayer spacing to be determined. The intercalation of the polymer chains usually increased the interlayer spacing, as compared with the spacing of the organoclay used, leading to a shift of the

diffraction peak towards lower angle values. Angle and layer spacing values are being related to the Bragg's relation:

$$\lambda = 2d \sin\theta \qquad (2.1)$$

where λ corresponds to the wave length of the X-ray radiation used in the diffraction experiment, d is the spacing between diffraction lattice planes and θ is the measured diffraction angle or glancing angle.

When exfoliated structure is concerned, no more diffraction peaks are visible in the XRD diffractograms due to large spacing between the layers (i.e. exceeding 8 nm in the case of ordered exfoliated structure) and loss of structure.

Transmission Electron Spectroscopy

Transmission Electron Spectroscopy (TEM) is used to characterize the nanocomposites morphology. Besides these two well-defined structures, other intermediate organizations can exist presenting both intercalation and exfoliation was observed by TEM.

2.2.5 Properties of Polymer-Clay Nanocomposites [20]

Layered silicate nanofillers can improve the polymers properties such as modulus (tensile or Young's modulus and flexural modulus) of nanocomposites at a low loading of filler. Additionally, thermal stability and fire retardancy were obtained by nanocomposites. Those new materials have also been studied and applied for their superior barrier properties of gas and vapor transmission.

i) Mechanical Properties

-Tensile Properties

The dramatic improvements of the tensile strength and tensile modulus given by the delaminated nanocomposites structure on polyamide 6-clay hybrids were first reported by the Toyota researchers [23]. The tensile strength of polyamide 6-clay was increased of 55% and the modulus of 90% from pure polyamide 6 with the addition of

only 4 %wt of delaminated clay. Later, Lan et al. [24] reported that tensile strength and modulus in rubbery epoxy matrix increased more than a ten-fold with only 15 %wt of delaminated organoclay. Furthermore, the modulus of intercalated PMMA-clay nanocomposites with 20 %wt of clay was reported to be greater by 60% to the pristine polymer [25]. The improvement of tensile properties of polymer-clay nanocomposites is related to the degree of delamination of the clay in the polymer matrix that increases the interaction between the clay layers and the polymer.

-Impact Properties

Impact properties have been measured for nylon-6 nanocomposites prepared either by in *situ* intercalative polymerization of ε-caprolactam using protonated aminododecanoic acid-exchanged montmorillonite [26]. Both methods lead to exfoliated nanocomposites especially at the filler content less than 10 %wt. At higher filler loading, melt-intercalation provides partially-exfoliated-partially-intercalated materials. Although using the exfoliation process, impact properties of nylon-6-based nanocomposites does not decrease too much. In the case of in *situ* intercalative polymerization, the Izod impact strength is decreased from 20.6 to 18.1 J/m^2 when 4.7 %wt of nanoclay is incorporated. Charpy impact testing shows similar reduction in the impact strength with a drop from 6.21 kJ/m^2 of unfilled rubber matrix to 6.06 kJ/m^2 of the 4.7 %wt nanocomposites.

ii) Barrier Properties

-Permeability

The substantial decrease of permeability brought is also a major advantage of polymer-clay nanocomposites. It was first reported by the Toyota researchers [23] that their polyamide 6-clay hybrid had a rate of water absorption reduced by 40% as compared with the pristine polymer. Later, Messersmith et al. [27] observed a dramatically decreasing of water permeability with their poly(ε-caprolactone) layered silicate nanocomposites, up to 80% with 4.8 %vol clay loading. The gas permeability in rubber-clay hybrid was reduced by 30% with 4 %vol of delaminated clay loading [28].

-Solvent Resistance

The better barrier properties of polymer-clay nanocomposites also increased the solvent resistance. A recently study reported that epoxy-clay nanocomposites showed a high resistance to organic solvents such as alcohol, toluene and chloroform.

iii) Thermal Properties

-Thermal Stability

The thermal stability of a material is usually determined by thermogravimetric analysis (TGA). When the heating is operated under an inert gas flow (nitrogen, helium, etc.), a non-oxidative degradation occurs while the use of air or oxygen allows following the oxidative degradation of the sample. The improvement of thermal stability in nanocomposites appears in the work by Blumstein et al. [29] who studied the thermal stability of PMMA intercalated within montmorillonite. It found that the thermal stability of the PMMA extracted from the montmorillonite was higher than that of PMMA conventionally produced in solution. The higher stability of PMMA synthesized by in situ intercalative polymerization is more likely due to a decrease in the relative amount of PMMA encapped by carbon-carbon double bond, as a result of reduced propensity to disproportionate reactions.

-Flame Ratardancy

The flame retardant properties of nanocomposites have been recently reviewed in detail by Gilman et al. [30] The main bench-scale method used to measure important parameters in the flame retardant behavior of a material (heat release rate, peak of heat release rate, heat of combustion, etc.) is Cone calorimetry. In a typical experiment, the sample is exposed to a given heat flux (often taken as 35 kW/m^2) and the heat release rate (HRR) as well as the mass loss rate are recorded as a function of time. It is worth noting that the reduction of the peak HRR is the most clear-cut evidence for the efficiency of a flame retardant. Moreover, gas and smoke production are also measured. Cone calorimetry experiments have been carried out on other nanocomposites such as exfoliated nylon-12, exfoliated poly(methylmethacrylate-co-dodecylmethacrylate), [31] intercalated PS (3 %wt) or intercalated PP (2 %wt). HRR

is decreased while the heat of combustion as smoke and the carbon monoxide are usually not increased.

iv) Optical Properties

Traditional composites tend to be largely opaque due to light scattering by the particles or fibres embedded within the continuous phase. In nanocomposites, the domain sizes are reduced to a level such that true “molecular composites” are formed. Wang et al. [32] demonstrated that magadiite-nanocomposites filled in an epoxy matrix were much more transparent than smectite-nanocomposites at the same loading. It is indicated that the refractive index of magadiite is more nearly that of the organic matrix or the magadiite was more fully delaminated than smectite. Moreover, it has been reported the high transparency of smectite-nanocomposites based on a polyurethane matrix [33].

2.3 Clay and Clay Mineral [34-35]

Natural clay contains pure clay, clay mineral and non-clay minerals. Impurities such as calcite, quartz, feldspars, iron oxides and humic acids are the most common components in addition to the pure clay mineral. Calcite, iron oxides and humic acids can be removed by chemical treatments. Quartz and feldspars can be removed by sedimentation. However, traces of quartz are often found in the purified samples [34].

Type of clay can be identified by mainly chemical composition of clay mineral. Clay minerals are hydrous silicates which contain tetrahedral silicate sheet and octahedral alumina or magnesium sheet. There are four important clay mineral groups, including kaolinites, illites, smectites and vermiculites which have different structure and composition.

The clay mineral usually classifies by layer type and position of cations which replace in octahedral sheet [35] as shown in Table 2.1.

Table 2.1 Type of clay minerals [35].

Characters	Kaolinites	Illites	Smectites	Vermiculites
Structure Type	1:1	2:1	2:1	2:1
Octahedral component	di-octahedral	Mostly di-octahedral	di- or tri-octahedral	Mostly tri-octahedral
Principal interlayer cations	Nil	K	Ca, Na	Mg
Interlayer water	Only in halloysite (one layer)	Some in hydromuscovite	Ca two layers; Na one layer	Two layer
Basal Spacing	7.1Å (10Å in halloysite)	10Å	Variable, moat ~15Å(for Ca)	Variable, 14.4Å when fully hydrated
Glycol	Taken up by halloysite only	No effect	Takes two layers glycol, 17Å	Takes one layers glycol, 14Å
Chemical formula	$Al_4Si_4O_{10}(OH)_8$	$K_{1.0\text{-}1.5}Al_4(Si,Al)_8O_{20}(OH)_4$	$M^+_{0.7}(Y^{3+},Y^{2+})_{4\text{-}6}(Si,Al)_8O_{20}(OH)_4 nH_2O$	$M^{2+}_{0.66}(Y^{2+},Y^{3+})_6(Si,Al)_8O_{20}(OH)_4 8H_2O$
Paragenesis	Alterlation of acid rocks, feldspars, etc. Acidic condition	Alterlation of micas, feldspars, etc. Akaline condition	Alterlation of basic rocks, or volcanic material. Akaline condition	Alterlation of biotite flakes or volcanic material, chlorites, hornblende, etc.

- Kaolinites group is 1:1 type of layer silicate and clay minerals in this group are kaolinite, dickite, nacrite and halloysite
- Illites group is 2:1 type of layer silicate which has potassium ion compensate charge in interlayer, including illite, hydrous mica, phengite, brammalite, glauconite and celadonite
- Smectites group is 2:1 type of layer silicate, including montmorillonite, beidellite, nontronite, hectrorite, saponite and sauconite

- Vermiculites group is 2:1 type of layer silicate which has magnesium ion compensate charge in interlayer

Smectite Clay [35]

Smectite clay is the group of clay mineral that can be expanded and attracted crystal structure when immerse in water or some organic solvent. The clay minerals in this group are montmorillonite, beidellite, nontronite, hectrorite, saponite and sauconite with different in chemical composition.

The clay mineral type 2:1 structural units include one octahedral sheet of aluminium oxide, called alumina sheet, sandwiched between two tetrahedral sheets of silicon oxide, called silica sheet, one unit layer is close to another tetrahedral sheet of another layer as shown in Figure 2.5. The unit layers are stacked together face-to-face to form the crystal lattice. The distance between the plane in one layer and the corresponding plane in the next layer is called the *basal spacing* or *d*-spacing. The sheets in the unit layer are tied together by covalent bonds; therefore, the unit layer is stable.

The layers in the lattice layer are held together by Van der Waals forces and secondary valences between adjacent atoms. Therefore, the lattice splits along the basal surfaces. The repulsive potential on the surface of the layers depends on an isomorphous substitution and these two factors contribute to the increase of the *d*-spacing between the layers due to the penetration of water.

The smectites have an expanding lattice that the layer surfaces are available for hydration and cation exchange. Interlayer surface and cation hydration between smectite structure units is a unique property of smectite clays. The crystal structure of smectite clay can be detected by X-ray diffraction. The layer thickness is approximately 1 nm and the lateral dimensions may vary from 300Å to several microns, giving an aspect ratio (length/thickness) greater than 1000 [36-39].

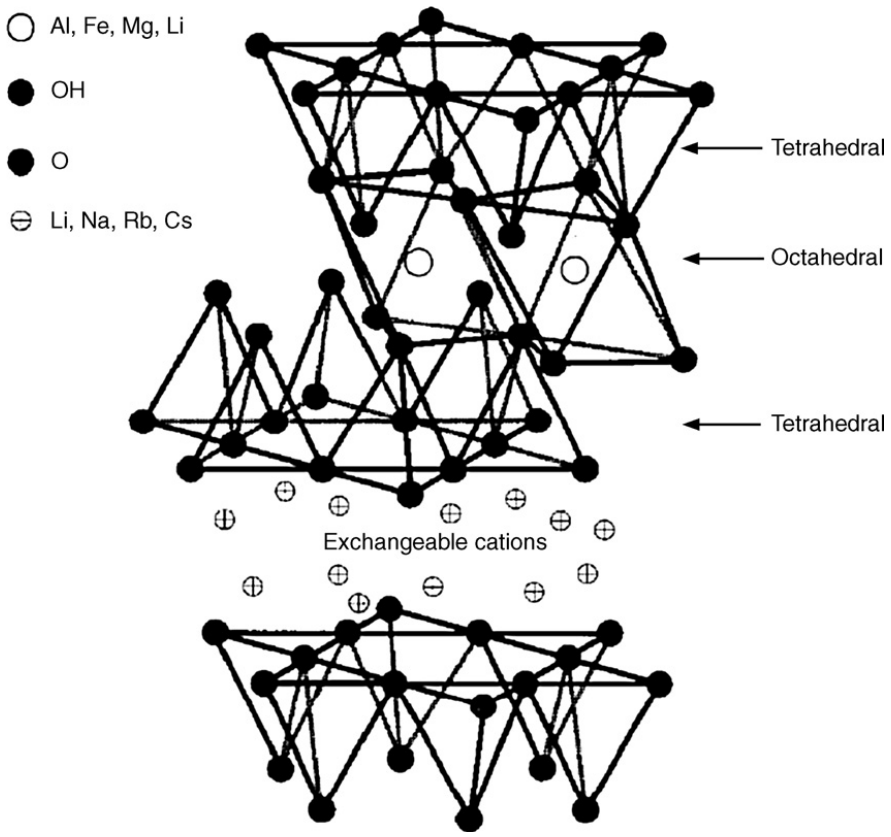

Figure 2.5 Illustration of T:O:T structure of montmorillonite clay. [40]

Montmorillonite (MMT)

Montmorillonite (MMT) is normally applied for polymer nanocomposites because it has a potentially high-aspect ratio and high surface area. MMT has a low thermal expansion coefficient and high gas barrier property. Stacking of this structure leads to a regular weak dipolar or Van der Waals interaction between the layers. Isomorphic substitution in each layer generates negative charges that are counterbalanced by hydrated sodium or potassium ions residing in the interlayer spacing [41]. In aqueous suspension, cations in interlayer may exchange with ions in the bulk solution. They are known as exchangeable cations. The total amount of cations adsorbed in the clay interlayer, expressed in miliequivalents per hundred grams of dry clay, is called the cation exchange capacity (CEC). It is an important characteristic of clay mineral. The high cation exchange capacity was obtained by using sodium montmorillonite, as compared to the other clay minerals.

There are many methods to investigate the CEC values. The principle method suggested by Rhoades et al. in 1982 is displacement of saturating index cation and displacement of saturating index cation after washing free from saturating salt. The last step, the detection of the saturating index cation by many techniques such as titration, atomic emission spectroscopy depends on the type of index. Methylene blue index is the simple method to detect the CEC values according to the ASTM C 337-99 for the characterization of clays [42].

Organoclay

The use of clays greatly limits the class of miscible polymers only to hydrophilic ones, mainly poly(ethylene oxide) and poly(vinyl alcohol). There are many methods using to modification natural clay to be organoclay such as by (a) an adsorption of the organic molecule into an interlayer, (b) a covalently bonding of the surfactant to a free hydroxyl group on the clay surface and (c) an exchanging of an interlayer cation with a cation surfactant. Sodium cations on montmorillonite can ion exchange with alkyl ammonium, phosphonium, imidazolium, or any other +1 cation to yield an organoclay as shown in Figure 2.6. It should be noted that ion exchange with sodium montmorillonite is facile with many different cations. Clay was exchanged the inorganic cations in the interlayer with organic cations to convert the clay into organophillic compound as shown in Figure 2.7 which suitable for use in organic system [35].

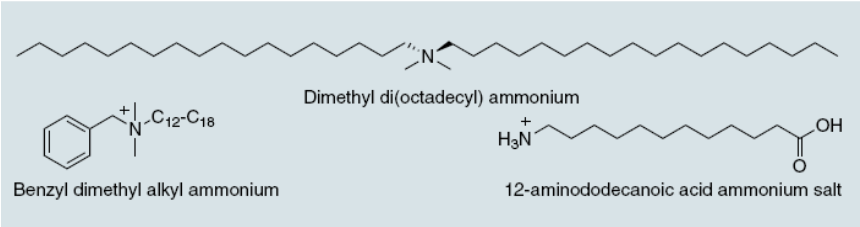

Figure 2.6 Typical alkylammonium organic treatments [43]

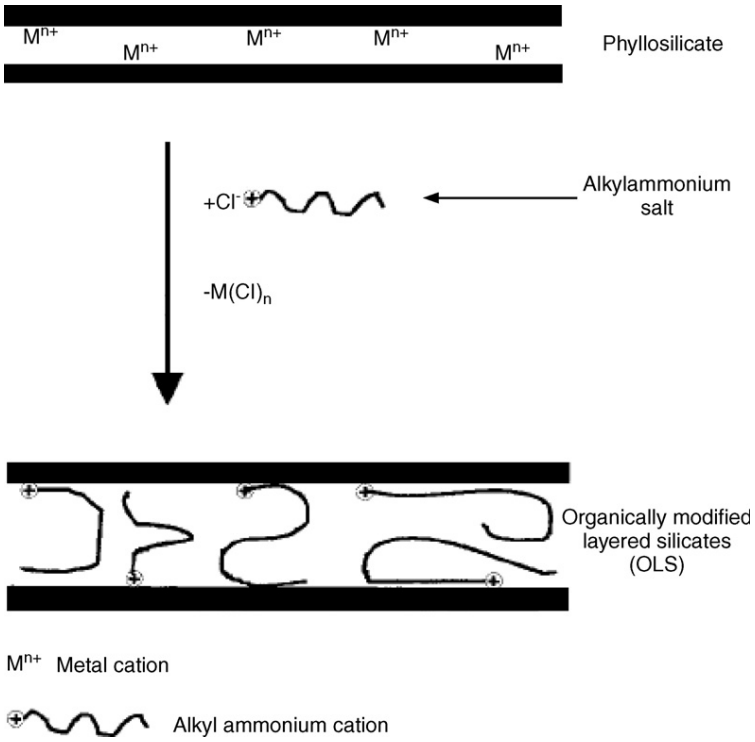

Figure 2.7 Schematic demonstration of clay organic modification. [38]

The replacement of inorganic exchange cations by surfactant on the clay surface was neutralized the clay surface and expanded the interlayer spacing. Three types of surfactant arrangement in interlayer; a monolayer, a lateral bilayer and a pseudo-trimolecular layer, or an inclined paraffin structure as illustrated in Figure 2.8. At very high charge densities, large surfactant can adopt lipid bilayer orientations in the clay interlayer. The orientations of surfactant chains in organoclay were deduced based on infrared and XRD measurements [44]. More recent molecular dynamics (MD) simulations were used to study molecular properties such as density profiles, normal forces, chain configurations and trans-gauche conformer ratios. For mono-, bi- and pseudo-trilayers with respective *d*-spacings of 13.2, 18.0 and 22.7 Å, a disordered liquid-like arrangement of chains do not remain flat, but instead, overlap and co-single with onium ions in opposing layers within the galleries. However, for the trilayer arrangement, the methylene groups are primarily found within a span of two layers and only occasionally they continue into the layer opposite to the positive head group. The onium head group is also noted to reside near the silicate surface relative

to the aliphatic portion of the surfactant. The highest preference conformation is trans over gauche for the maximum surfactant chain length just before the system progresses to the next highest layering pattern. This is expected since the alkyl chains must be optimally packed under such dense surfactant concentrations. The MD simulation experiments have agreed well with experimental XRD data and FTIR spectroscopy for the stacked interlayer alkyl chains. However, the inclined paraffin association is not addressed for < C15 surfactants with clays of CEC less than 1.2 meq/g.

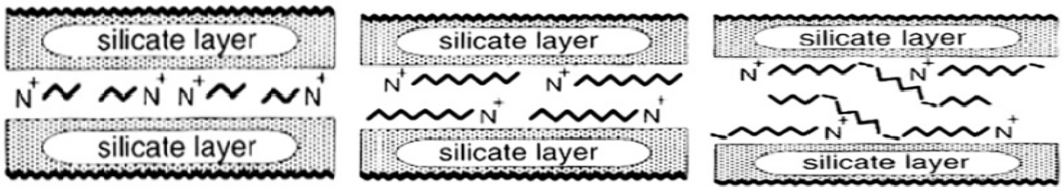

Figure 2.8 Orientation of alkylammonium ions in the interlayer silicate with different layer charge densities. [45]

2.4 Literature Review

Microemulsion and differential microemulsion polymerization

Zhang et al. [46] studied the preparation of nanosized polystyrene by ultrasonic technique induced microemulsion polymerization, processing many merits such as high polymerization rate, the formation of small latex particles with a narrow size distribution, the absence of the initiator and relatively low surfactant concentration. The monomer conversion reached 70% in 1h, and the average diameter of polystyrene (PS) latex was about 30 nm which could be prepared with 3% SDS concentration. The molecular weight of PS was around 10^6 g/mol and the poly-distribution index was 1.06, indicating a very narrow distribution.

Xu et al. [47] studied the synthesis of nanosized poly(methyl methacrylate)(PMMA) initiated with benzoyl peroxide (BPO) in oil/water microemulsion system using sodium 12-butinoyloxy-9-octadecenoic acid as

stabilized. The growth of monomer-swollen PMMA particles was investigated by photon correlation spectroscopy. It found that nucleation process continues to very high conversion and the polymerization in large polymer particles formed at the early state could not be ignored. Hydrodynamic diameter of polymer latex was about 50 nm at high conversion and high rate of polymerization.

He et al. [6] studied the synthesis of PMMA nanoparticles via differential microemulsion polymerization. Sodium dodecyl sulfate (SDS) and ammonium persulfate (APS) were used as a surfactant and initiator, respectively. A particle size of less than 20 nm in diameter was achieved at surfactant/monomer and surfactant/water weight ratios of 1:18 and 1:120, respectively. These result showed that the amount of the surfactant required was certainly lower when compared with other methods. This technique is a novel method for preparing nanosized polymer particle.

He et al. [18] studied the preparation of acrylonitrile-butadiene copolymer latex (NBR) and styrene-butadiene copolymer latex (SBR) nanoparticle via differential microemulsion polymerization initiated by APS. For NBR latex, the particle size could be reduced to less than 20 nm at surfactant/monomer and surfactant/water weight ratios of 1:9 and 1:80, respectively. The nanoparticle size of SBR (30 nm) was larger than that of NBR. However, the nanoparticle size of PMMA/SBR with core-shell morphology was decreased as compared to PMMA-NBR core-shell particle.

Norakankorn et al. [48, 49] investigated the synthesis of PMMA nanoparticles initiated by 2,2'-Azoisobutyronitrile (AIBN) via differential microemulsion polymerization. Nanosized poly(methyl methacrylate)(PMMA) particles was about 20 nm with a high molecular weight of 106 g/mol and a polydispersity index of about 1–2 were synthesized was obtained. The kinetics of the polymerization, the glass transition temperature, tacticity, the particle size distribution, and the morphology of the nanosized PMMA synthesized were investigated. The dependence of the number of the polymer particles (Np) and the number of the micelles (Nm) on the concentration of the surfactant was discussed. The molecular weight distribution was found to be nearly constant over the polymerization time, which was attributed to the significance of micellar polymerization. The resultant nanosized PMMA has a rich syndiotactic configuration (53–57% rr triads) with a glass transition temperature of

about 125°C. A beneficial operation condition was discovered where the conversion reached a maximum at a high monomer-to-water ratio.

Suppaibulsuk et al. [7, 50] studied the synthesis of nanosized polyisoprene via differential mocroemulsion polymerization using 2,2' -azoisobutyronitrile (AIBN) as initiator. The optimum conditions gave highest monomer conversion of 90% and average particle of PIP of 27 nm. Moreover, the graft copolymerization of styrene (ST) onto nanosized polyisoprene (PIP) was synthesized by using cumene hydroperoxide (CHPO) and tetraethylene pentamine (TEPA) as redox initiators. The high conversion and high degree of grafting could be achieved when a small particle was used as the core polymer. The grafting efficiency and monomer conversion increased with increasing reaction temperature and monomer concentration. Transmission electron microscopy indicated that the small PIP nanoparticles were completely coated with polystyrene (PS) by grafting resulting in a core shell morphology of nanosized graft PIP. The particle size of graft copolymers was larger than PIP. Moreover, nanosized PIP and ST-g-PIP could be used as colloid stabilizer for pre-vulcanized natural rubber latex (NRL). Mechanical properties of rubber blends were reduced by addition of nanosized PIP and ST-g-PIP. For thermal ageing properties, the retention of tensile strength and elongation at break of compounds was higher than that of unfilled NR.

Polymer-montmorillonite nanocomposites

Jankovic et al. [51] studied the characterization of systematically selected organo-montmorillonites for polymer nanocomposites. Eight carefully selected organoclays from monoalkyl- to tetraalkylammonium type were prepared from Na+-MMT. Four samples contained 1–4 octylammonium chains, from mono-octylammonium (1C8) to tetraoctylammonium (4C8). Two cations had chains with 16 carbons each, hexadecylammonium(1C16) and dihexadecyldimethylammonium (2C16). Two cations contained a benzene ring, either without reactive bonds benzyltrimethylammonium, C10) or with a double bond in 4-vinylbenzyl-trimethylammonium (C12). The d_{001} values depended on the size and structure of the organocation. The most interlayer expanded of 3.16 nm when using dihexadecyldimethylammonium as a modifier. The suitability of the prepared

materials to be used as fillers for polymer nanocomposites was estimated according to rheological measurements of dispersions in solvents taking solubility parameters as primary factors for comparison of particular solvent and polymer.

Valadares et al. [52] studied the preparation of NRL/MMT nanocomposites by using dispersion shear blending method. Nanocomposites of natural rubber latex and layered silicates were prepared by a mild dispersion shear blending process. The results of X-ray diffraction (XRD) and transmission electron microscopy (TEM) show that clay particles were well dispersed in the dry latex and the platelets have a preferential orientation, forming translucent nanocomposites. These showed tensile mechanical properties analogous to those obtained with vulcanized rubber as well as an increased solvent resistance, which was expected considering that there was significant adhesion between clay lamellae and rubber. Nanocomposite swelling was strongly anisotropic. Natural rubber properties may thus be strongly modified by nanocomposite formation producing unprecedented combinations of properties.

Gu et al. [53] studied the preparation of SBR/NR/organo-bentonite nanocomposites from latex dispersion. SBR/NR/organo-bentonite nanocomposites were prepared from emulsions. The structure of the nanocomposites was characterized by TEM and XRD. The effect of organobentonite on the mechanical properties, thermal stability and swelling behavior was investigated. TEM and XRD confirmed that rubber chains were intercalated into the organo-montmorillonite particles. When the organo-bentonite content was lower than 12 %wt, the nanocomposites showed excellent mechanical properties. The addition of a small amount of OMMT greatly improved thermal stability and swelling behavior, which was attributed to the good barrier properties of the dispersed and partially exfoliated organo-montmorillonite particles. Organo-bentonite addition had little effect on the score and cure times of the nanocomposites, while increased the maximum and minimum torque.

Pojanavaraphan et al. [54] studied the preparation of sodium-montmorillonite (Na^+MMT) areogels/pre-vulcanized natural rubber latex by using freeze-drying technique. The composites exhibited densities in the range of 0.36–0.51 g/cm^3, which was in good agreement with the content of polymer in the aqueous solutions. The dispersion of the Na+-MMT particles and the microstructure of the composites were investigated by X-ray diffraction and scanning electron microcopy. The influence of

the Na+-MMT particles on the mechanical, rheological and swelling properties of the composites was investigated. A composite made from 7 phr of Na+-MMT showed the greatest improvement in material properties. Such Na+-MMT aerogel/polymer composites would be candidate for structural and insulation applications.

CHAPTER III

EXPERIMENTAL

3.1 Chemicals

1. Isoprene monomer (IP, 99%) : Sigma-Aldrich
2. Montmorillonite clay (Cloisite15A, Cloisite30A, Nanofil15 and Nanofil116), Appendix A : Southern Clay Products
3. Vinyl trimethoxysilane (VTS) : Sigma
4. High ammonium natural rubber latex (60 %wt dry rubber content) : Rubber Research Institute of Thailand
5. 2,2'-Azoisobutyronitrile, AR grade : Polyscience
6. Sodium dodecyl sulphate, 99% : Aldrich
7. Sodium bicarbonate, 99.7% : Sigma-Aldrich
8. Normal-dodecyl mercaptan, 97% : Sigma-Aldrich
9. Sulfur (50 %wt) : Rubber Research Institute of Thailand
10. Zinc oxide (ZnO, 50 %wt) : Rubber Research Institute of Thailand
11. Zinc diethyl dithiocarbamate (ZDEC, 50 %wt) : Rubber Research Institute of Thailand
12. Methyl ethyl ketone, AR grade : Fisher Scientific
13. Toluene, AR grade : Fisher Scientific
14. Petroleum Ether, AR grade : Fisher Scientific
15. Acetone, AR grade : Fisher Scientific
16. Chloroform D : Sigma-Aldrich
17. Nitrogen gas, 99.9% : Prax Air
18. De-ionized water

3.2 Glasswares

1. 500 mL four-necked round bottom reactor
2. Soxhlet extractor apparatus
3. Glass mold
4. Other general laboratory glassware

3.3 Equipments

1. Parr Reactor	: Parr 4843
2. Dynamic Light Scattering Analyzer	: Nanotrac NPA252
3. Fourier Transform Infrared Spectrophotometer	: Thermo 470 FT-IR Spectroscope
4. ^{1}H Nuclear Magnetic Resonance Spectrometer	: Bruker 300 MHz
5. X-ray Diffractometer	: Bruker AXS Model D8
6. Thermal Gravimetric Analyzer	: Perkin-Elmer Pyris Diamond
7. Differential Scanning Calorimeter	: METTLER DSC822e
8. Transmission Electron Microscope	: JEOL JEM-2100
9. Scanning Electron Microscope	: JEOL JSM-6400
10. Universal tensile machine	: LLOYD Instrument LR 5K Plus
11. Hardness testing machine	: Durometer Hardness Tester REX2000

3.4 Synthesis of Nanosized Polyisoprene-Montmorillonite via Differential Microemulsion Polymerization

PIP-MMT nanocomposites was prepared via differential microemulsion polymerization in a 300 mL Parr reactor. AIBN, SDS, SHC, MMT and n-DM were dissolved in de-ionized water and charged into the reactor. However, SDS was used to disperse MMT into water before the initiation of polymerization. Then the mixture was heated to the reaction temperature of 70°C, isoprene monomer was continuously and slowly added to the reactor using a peristaltic pump at flow rate of 0.6 mL/min for designated time. After the addition of monomer was completed, the reaction system was kept at the reaction temperature with constant agitation for 20 h. Afterwards, PIP-MMT nanocomposites latex was precipitated using an excess of methyl ethyl ketone and then dried in a vacuum oven. The effects of process variable were studied.

- Organoclay loading: 0, 5, 10, 15 and 20 %wt based on monomer
- Monomer to water ratio: 0.24:1, 0.27:1, 0.30:1 and 0.40:1

A schematic diagram for the synthesis of polyisoprene-clay nanocomposites is showed in Figure 3.1.

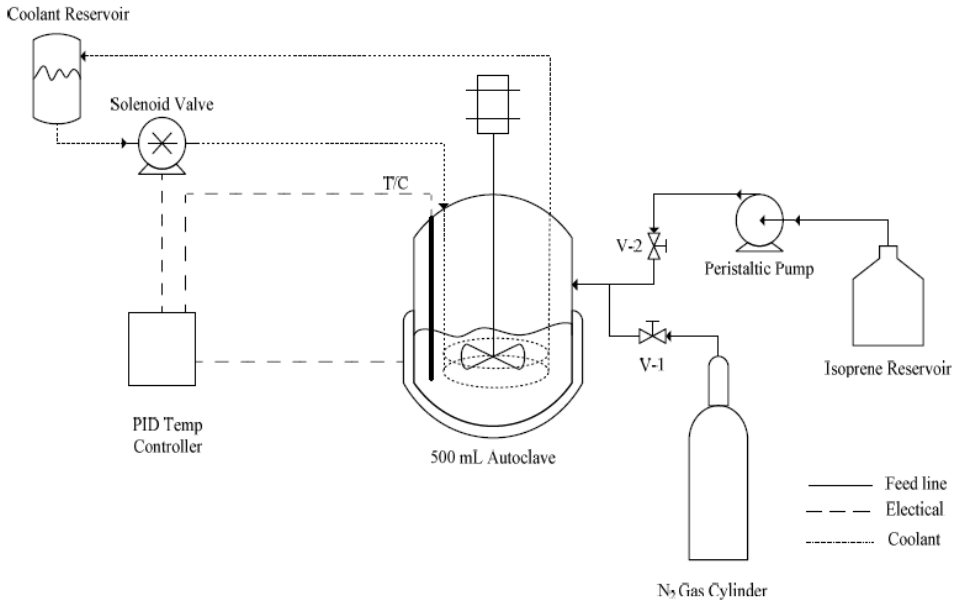

Figure 3.1 The schematic diagram for synthesis of nanocomposites. [51]

The monomer conversion and solid content were determined by gravimetric method and calculated using following equations:

$$\text{Monomer conversion (\%)} = (M_0\text{-}M_1 / M_2) \times 100 \quad (3.1)$$

$$\text{Solid content (\%)} = (M_3 / M_4) \times 100 \quad (3.2)$$

where; M_0 = Mass of the resulting composite particles
M_1 = Mass of the charged MMT particles
M_2 = Mass of the charged isoprene monomer
M_3 = Mass of dried PIP-MMT
M_4 = Mass of PIP-MMT latex

The experimental procedure for nanosized PIP-MMT synthesis was summarized and shown in Figure 3.2.

3.5 Blending and Vulcanization

3.5.1 Latex Compound Preparation

Natural rubber latex (NRL) was filled with nanosized PIP-MMT latex at various blend ratios (100:0, 90:10, 80:20, 70:30 and 60:40 by weight ratio). The latex was mixed with the compounding ingredients according to the formulation given in Table 3.1. The latex compounds were pre-vulcanized in a water bath at 40^{o}C and stirred well for 1 h providing a homogeneous mixture. After that the compound latex was cooled to room temperature and then casted on raised glass plates with a dimension of 13 cm x 13 cm x 2 mm. The cast film was then allowed to dry in an air until transparent and then vulcanized at 70^{o}C for 4 h in the air circulated oven [7]. The vulcanized samples obtained were kept in the desiccators prior mechanical testing.

Table 3.1 Formulation of the NR latex compound.

Ingredients	Dry (parts by weight, phr)
60% DRC Natural Rubber Latex	Variable 100, 90,80, 70, 60
20% Solid content of PIP-MMT nanocomposites latex	Variable 0, 10, 20, 30, 40
50 %wt Sulfur dispersion	1.5
50 %wt ZDEC dispersion	1.0
50 %wt ZnO dispersion	2.0

*phr = part per hundred

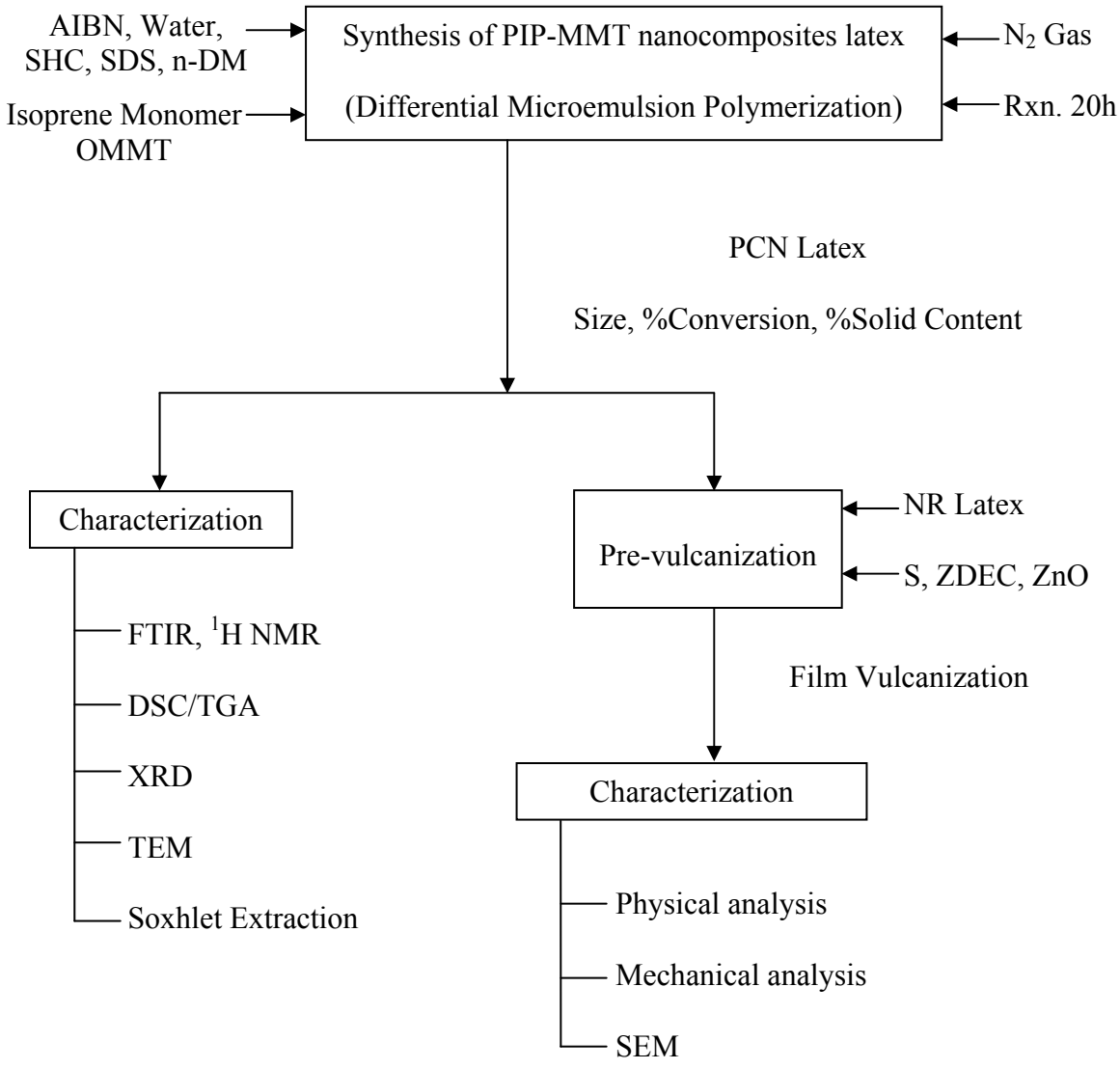

Figure 3.2 The experimental procedure for PIP-MMT nanocomposites synthesis and vulcanization.

3.5.2 Accelerated Thermal Ageing of Vulcanized Products

Vulcanized rubber-clay nanocomposites sheets were aged at 100°C for 24 h in the air-circulating ageing oven. The tensile properties of the aged samples were determined according to ASTM D 573 (1994). Tensile test (ASTM D 412-99) was carried out on a dumbbell test specimen before and after ageing to estimate ageing resistance.

3.6 Characterization Methods

3.6.1 Fourier Transform Infrared Spectroscopy

The structure of PIP-MMT nanocomposites was characterized using Fourier Transform Infrared Spectroscopy. The samples were prepared by dissolving the composites in toluene (2 %w/v) and then cast as a film on a sodium chloride (NaCl) disk. The solvent was evaporated at ambient temperature before recording the infrared spectra.

3.6.2 Number-average Diameter Measurement

The number-average particle diameter (D_n) and particle size distribution (PSD) of polyisoprene (PIP) and nanocomposites latex were examined using Dynamic light scattering (DLS, the Nanotrac NPA252) in latex form of nanocomposites.

3.6.3 Thermogavimatric Analysis (TGA)

Thermogravimetric analysis (TGA) of the sample was performed using a Perkin-Elmer Pyris Diamond TG/DTA under nitrogen atmosphere with heating rate of 10^oC/min. The initial decomposition temperature (T_{id}) and the temperature at the maximum mass loss rate (T_{max}) were recorded.

3.6.4 Differential Scaning Calorimetry (DSC)

Differential scanning calorimeter (DSC) was carried out on DSC Mettler DSC822e. The instrument signal was derived from the temparature difference between the sample and reference. The sample was cooled to -100°C with liquid nitrogen and then heated at a constant rate of 10^{o}C/min under a nitrogen atmosphere to 30^{o}C. The glass transition temperature (T_g) was calculated from the midpoint of the baseline shift of the DSC thermogram.

3.6.5 X-ray Diffraction (XRD)

X-ray diffraction (XRD) measurements were performed in Bruker AXS Model D8 Discover at a scan rate of 0.5°/min, 2θ =1.5-35° with CuKα X-ray radiation (1.5406 Å). The measurements were operated by EVA program.

3.6.6 Morphological Study

The morphology of PIP-MMT nanocomposites was stained by OsO_4 and investigated by transmission electron microscope (TEM, a JEOL JEM-2100) at acceleration voltage of 80 kV. Scanning electron microscope (SEM) was used to observe the morphology of the vulcanized film. The fracture surfaces after tensile testing were cut and stitched on a SEM stub using double-sided tape. Then, the sample was sputter-coated with gold and examined using SEM, JEOL model JSM-6480LV operated at 15 kV.

3.7 Measurement of Mechanical Properties

3.7.1 Tensile Properties

The pre-vulcanized samples were cut into tensile specimens using a die C. The cutting die punched the specimen into dumbbell test piece as shown in Figure 3.3. The dumbbell samples used were 25 mm in gauge length, 25 mm in width and 2.0 mm in thickness. Testing was carried out on LLOYD Universal Testing Machine model

LR5K according to ASTM D412. The crosshead speed of 500 mm/min was used with a full scale force at 5 kN. Five specimens were used for each tensile measurement. The elongations at break were also measured.

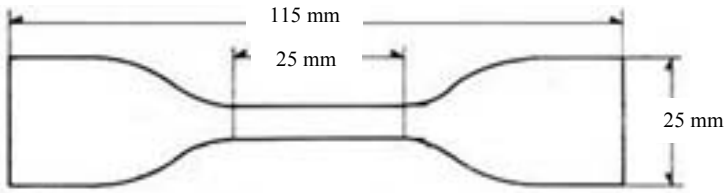

Figure 3.3 Tensile test specimens.

3.7.2 Hardness

The hardness testing was measured using Durometer Hardness Tester REX2000 (Shore A) according to ASTM D2240 at room temperature. The measurements taken from five different points distributed over the sample and the reported values were averaged of five measurements.

CHAPTER V

RESULTS AND DISCUSSION

Polyisoprene-montmorillonite (PIP-MMT) nanocomposites were successfully synthesized by differential microemulsion polymerization using AIBN as an initiator at reaction temperature of 70°C for 20 h. The particle size of PIP-MMT nanocomposites latex was investigated by dynamic light scattering method. The monomer conversion and solid content of PIP-MMT nanocomposites latex were determined. The PIP-MMT nanocomposites were also characterized by FTIR and XRD.

4.1 Synthesis of Polyisoprene-Montmorillonite Nanocomposites via Differential Microemulsion Polymerization

4.1.1 Effect of Surfactant Concentration

In this work, SDS was used as an anionic surfactant for preparation of PIP-CS15A nanocomposites. The effects of surfactant concentration (6 to 14 %wt) on monomer conversion, particle size and solid content of PIP-CS15A nanocomposites latex are shown in Table 4.1 and Figure 4.1. The particle size of PIP-CS15A nanocomposites decreased with increasing surfactant concentration. The number of monomer-swollen micelles was increased and size of monomer-swollen micelles was decreased with increasing the surfactant concentration. Therefore, the particles size was decreased implying that the particle size could be controlled by surfactant concentration. The similar results were earlier reported for preparation of poly(methyl methacrylate)(PMMT) [6] and styrene-g-polyisoprene nanoparticles initiated by using AIBN via differential microemulsion polymerization [7, 50].

The monomer conversion and solid content increased with increasing surfactant concentration. An increase in the SDS concentration increased the number of monomer-swollen micelles and therefore the number of particles led to an increase in the polymerization rate and the final conversion. This phenomenon suggests that the conversion and solid content in the differential microemulsion polymerization were determined by micelle numbers. For the synthesis of PIP-CS15A nanocomposites

initiated by oil-soluble initiator, the polymerization is believed to occur in micelles. Micelle numbers increased with increasing SDS concentration, resulting in the high polymerization rate. Hence, a higher SDS concentration resulted in higher monomer conversion and solid content. The similar results were observed for the synthesis of PMMA [6]. For the synthesis of PIP-CS15A nanocomposites, high monomer conversion of 81.4%, high solid content of 21.5%, and small PIP-CS15A nanocomposites size of around 26.3 nm with narrow particle size distribution (PSD) were obtained at SDS concentration of 12 %wt based on monomer weight. The particle size distribution of PIP/MMT nanocomposites are shown in Figure 4.2.

Table 4.1 Effect of SDS concentration on monomer conversion, average particle size and solid content of PIP-CS15A nanocomposites

Sample	% Surfactant	%Solid Content	%Monomer Conversion	D_n (nm)	PSD (nm)
PIP-CS15A_5-S6	6	14.7 (0.65)	56.0 (0.99)	45.8	15.5
PIP-CS15A_5-S8	8	16.7 (0.38)	62.6 (0.81)	38.2	13.5
PIP-CS15A_5-S10	10	20.3 (0.35)	80.4 (1.21)	31.7	10.7
PIP-CS15A_5-S12	12	21.5 (0.17)	81.4 (0.62)	26.3	10.8
PIP-CS15A_5-S14	14	22.6 (0.83)	80.5 (1.15)	25.5	11.6

Condition: [CS15A] = 5 %wt; [AIBN] = 0.25 %wt; IP:H_2O= 0.27:1; [SHC] = 0.60 %wt; [n-DM] = 0.20 %wt; temperature = 70°C; stirring speed = 300 rpm; reaction time = 20 h.
D_n = Mean Number Diameter (average particle size); PSD = Particle Size Distribution

%Monomer conversion: calculated from nano-latex (was not included PIP and MMT agglomeration)
(-): Standard diviation, SD

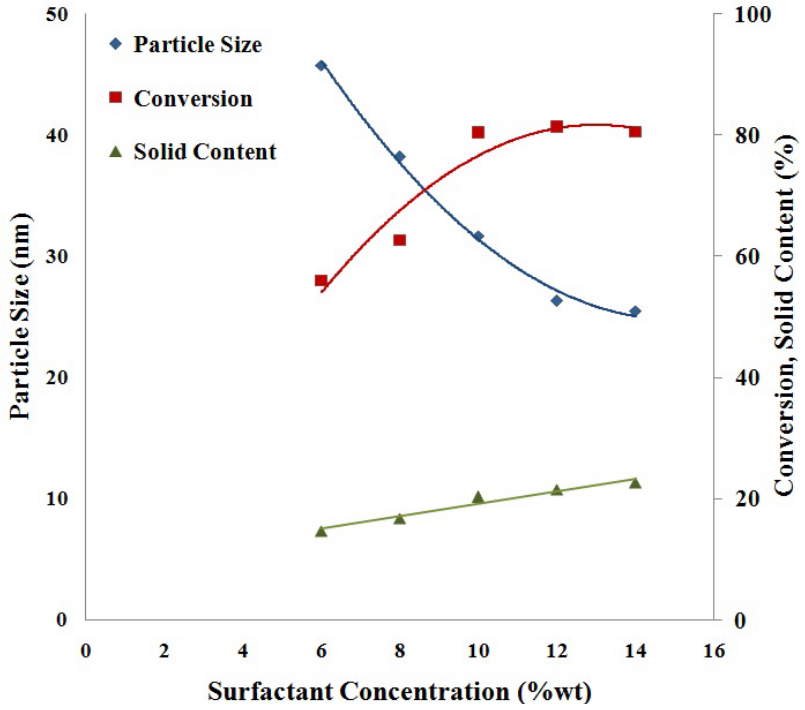

Figure 4.1 Effect of SDS content on monomer conversion, particle size and solid content of PIP-CS15A nanocomposites.

Condition: [CS15A] = 5 %wt; [AIBN] = 0.25 %wt; IP:H_2O= 0.27:1; [SHC] = 0.60 %wt; [n-DM] = 0.20 %wt; temperature = 70°C; stirring speed = 300 rpm; reaction time = 20 h.

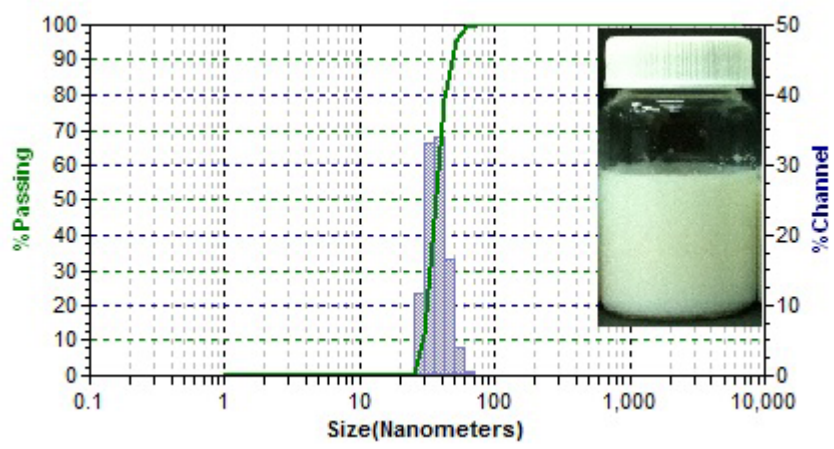

a)

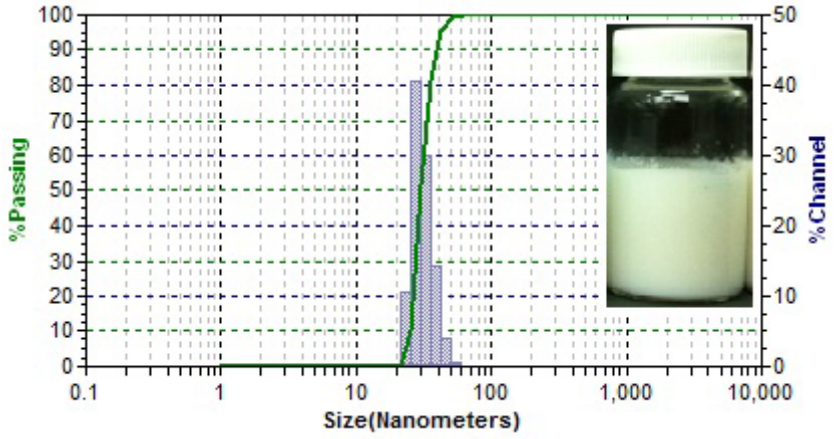

b)

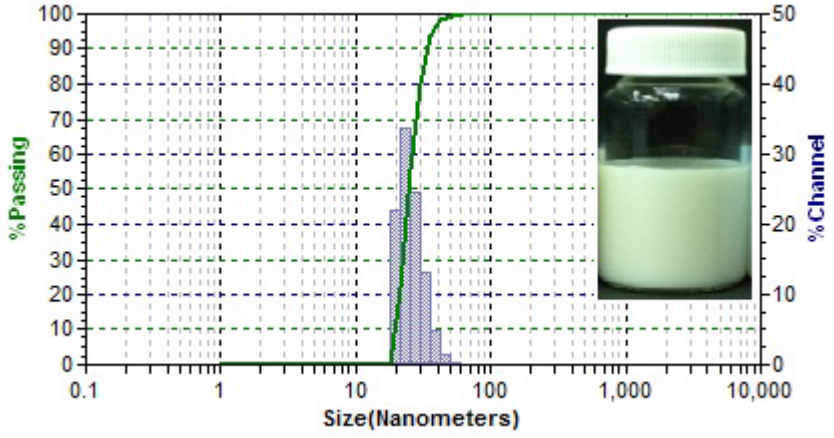

c)

Figure 4.2 Histograms of particle size distribution of PIP-CS15A nanocomposites: a) 8 %wt of SDS, b) 10 %wt of SDS and c) 12 %wt of SDS.

Condition: [CS15A] = 5 %wt; [AIBN] = 0.25 %wt; IP:H_2O= 0.27:1; [SHC] = 0.60 %wt; [n-DM] = 0.20 %wt; temperature = 70°C; stirring speed = 300 rpm; reaction time = 20 h.

4.1.2 Effect of Montmorillonite Loading

The concentration of CS15A loading had a significant effect on monomer conversion, particle size and solid content as shown in Table 4.2 and Figure 4.3. The effect of CS15A loading was studied over the range of 5-20 %wt based on monomer weight. The average particle size increased from 26.3 nm to 44.5 nm and monomer conversion and solid content linearly decreased with increasing clay loading (5-20 %wt). This indicates that at high CS15A loading, more aggregation of CS15A particles was observed and large particle size of PIP-CS15A nanocomposites was produced. It is also probable that, the aggregation of CS15A particles tended to decrease the number of monomer-swollen micelles and particle stability, and therefore the final conversion was decreased. The similar results were earlier reported for synthesis of monodispersed PIP-silica nanoparticles via differential microemulsion polymerization [55]. The particle size distribution of PIP-CS15A nanocomposites at various CS15A loading are shown in Figure 4.4.

Thus, the PIP-CS15A nanocomposites with high monomer conversion of 81.4% and 67.8%, small particle size of around 26.3 and 29.8 nm and high solid content of 23.3% and 21.5% were obtained at an appropriate CS15A loading of 5 and 10 %wt, respectively.

Table 4.2 Effect of CS15A loading on monomer conversion, average particle size and solid content of PIP-CS15A nanocomposites

Sample	CS15A (%wt)	%Solid Content	%Monomer Conversion	Dn (nm)	PSD (nm)
PIP-CS15A_5	5	21.5 (0.17)	81.4 (0.62)	26.3	10.8
PIP-CS15A_10	10	21.9 (0.61)	67.8 (1.22)	29.8	11.9
PIP-CS15A_15	15	16.9 (0.56)	53.5 (0.65)	30.1	12.5
PIP-CS15A_20	20	12.6 (0.45)	30.8 (0.33)	44.5	15.0

Condition: [AIBN] = 0.25 %wt; IP:H_2O= 0.27:1; [SHC] = 0.60 %wt; [n-DM] = 0.20 %wt; temperature = 70°C; stirring speed = 300 rpm; reaction time = 20 h.
D_n = Mean Number Diameter (average particle size); PSD = Particle Size Distribution
(-): Standard diviation, SD

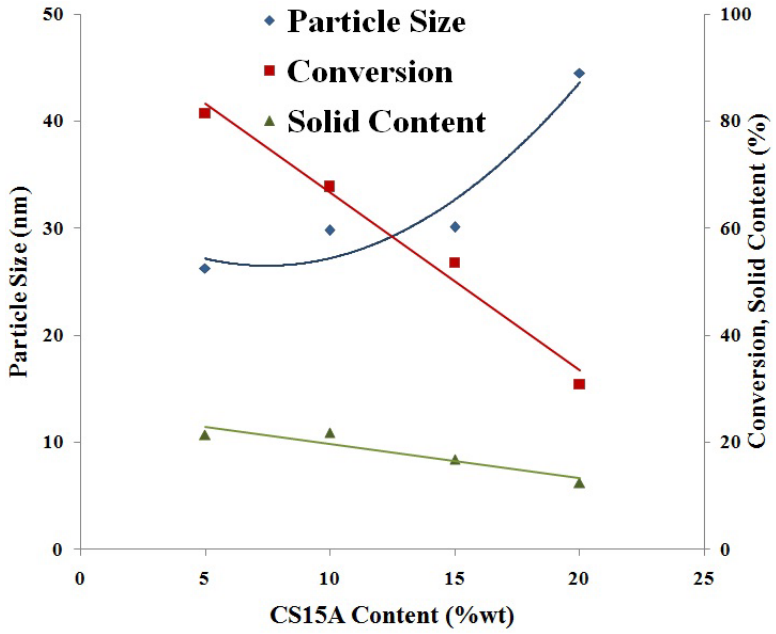

Figure 4.3 Effect of CS15A content on monomer conversion, particle size and solid content of PIP-CS15A nanocomposites.

Condition: [AIBN] = 0.25 %wt; IP:H_2O= 0.27:1; [SHC] = 0.60 %wt; [n-DM] = 0.20 %wt; temperature = 70°C; stirring speed = 300 rpm; reaction time = 20 h.

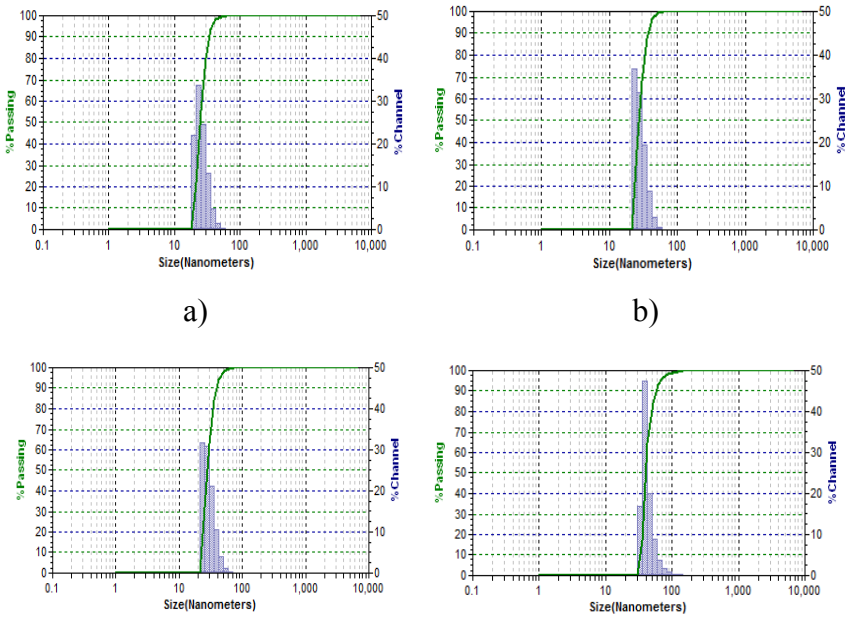

Figure 4.4 Histograms of particle size distribution of PIP-CS15A nanocomposites: a) PIP-CS15A_5, b) PIP-CS15A_10, c) PIP-CS15A_15 and d) PIP-CS15A_20

Condition: [AIBN] = 0.25 %wt; IP:H_2O= 0.27:1; [SHC] = 0.60 %wt; [n-DM] = 0.20 %wt; temperature = 70°C; stirring speed = 300 rpm; reaction time = 20 h.

For appearance of PIP-CS15A latex, the agglomeration of PIP-CS15A latex were observed at 15 and 20 %wt CS15A loading (Figure 4.5). The low volume of PIP-CS15A latex with high viscosity and more bubbles was obtained (Figure 4.6). This is due to the fact that, the active sites of isoprene monomer were hindered by CS15A particles resulting the decrease in monomer conversion and solid content. Furthermore, the white flake of CS15A was observed in PIP-CS15A latex at 20 %wt CS15A loading due to the over loading of CS15A (Figure 4.6d).

Figure 4.5 The agglomeration of PIP24-CS15A latex in the Parr reactor at high CS15A loading

a) b) c) d)

Figure 4.6 PIP24-CS15A latex at a) 5, b) 10, c) 15 and d) 20 %wt CS15A loading.

Figures 4.7a and 4.7b show the decomposition of CS15A, PIP, PIP with 5, 10, 15 and 20 %wt of CS15A loading. The thermogram of CS15A shows three-step decomposition. The first and second steps correspond to decomposition of the organic matters present in the organo-modifier (desurfactant), the onset occurs near 200°C with two maxima at 247°C and 310°C, respectively. The last-step is dehydroxylation of the CS15A layer at 387°C. The similar results were earlier reported for characterization of systematically selected organo-montmorillonites [51].

The thermograms of PIP and PIP-CS15A nanocomposites of 5, 10 and 15 %wt CS15A show one-step polymer degradation and provide smooth weight loss curves. PIP-CS15A nanocomposite of 20 %wt CS15A shows two steps decomposition. The first step corresponds to the decomposition of the organic matter of long chain carbon with amine group (desurfactant), the onset occurs near 200°C with maxima at 234°C and the second step is dehydroxylation of the CS15A layer at 384°C.

Furthermore, the CS15A loading affected the decomposition temperature of PIP-CS15A nanocomposites as presented in Table 4.3. In comparison of TGA and DTG of all samples, the decomposition temperatures (T_{id}) of PIP-CS15A nanocomposites (325°C) was slightly decreased with increasing CS15A loading and was lower than that of PIP (358°C). This implies that organic compound in the layer of CS15A did not affect the thermal properties of PIP-CS15A nanocomposites. However, maximum temperatures (T_{max}) of PIP-CS15A nanocomposites were the same as that of PIP. The residue of PIP-CS15A nanocomposites increased with increasing CS15A loading and PIP-CS15A nanocomposites at high CS15A loading had the highest residue. The similar results were earlier reported for characterization of natural rubber nanocomposites filled with organoclay [59].

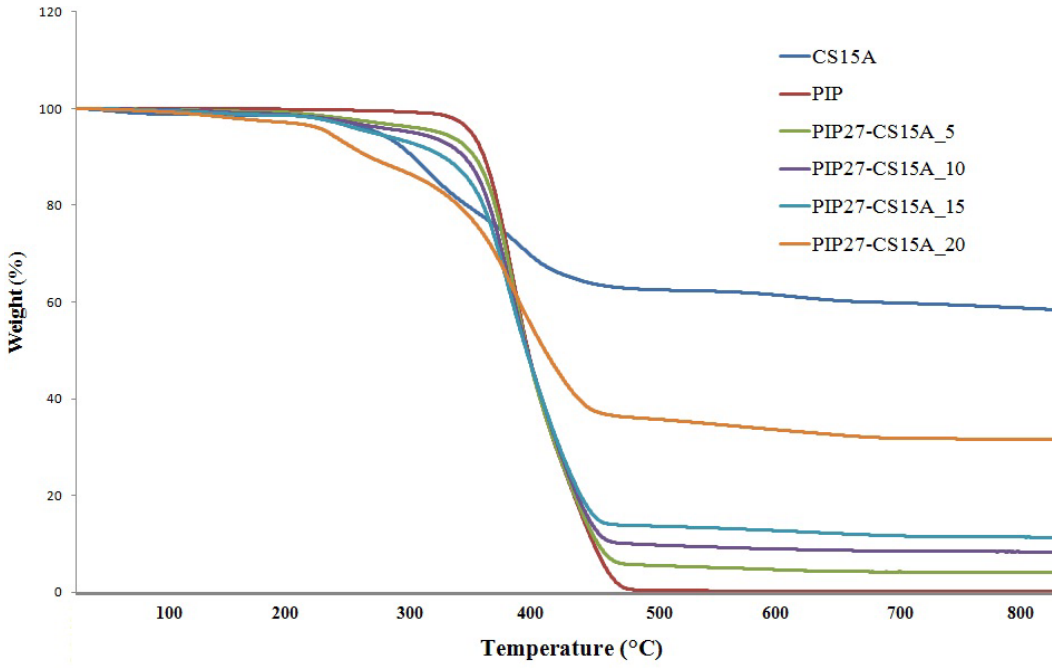

a)

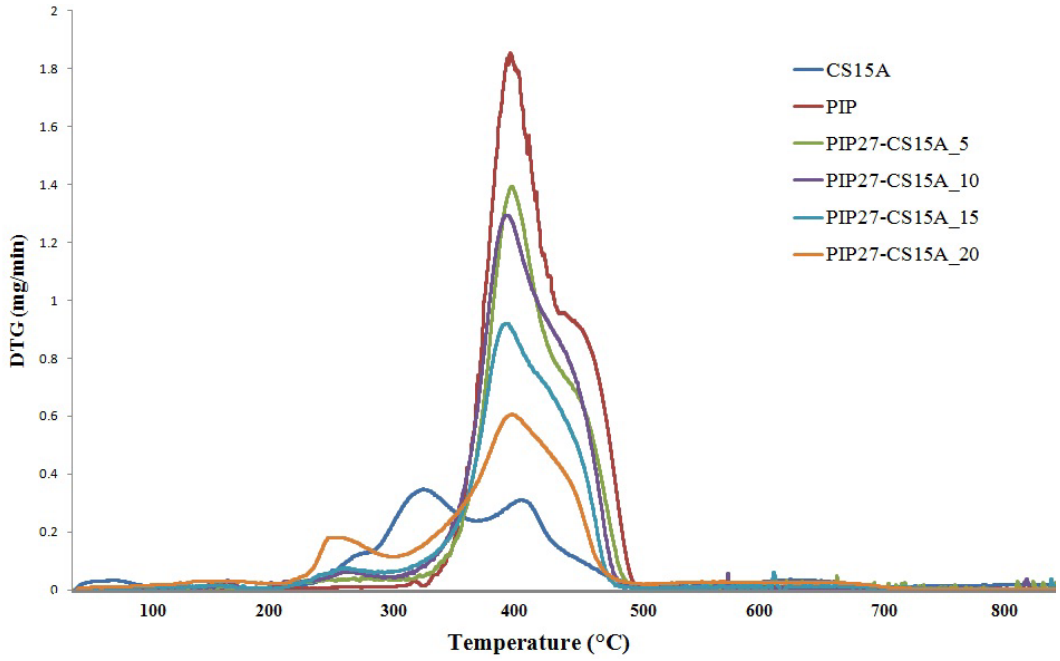

b)

Figure 4.7 a) TGA and b) DTG curves of the PIP-CS15A nanocomposites with various CS15A loading

Condition: [AIBN] = 0.25 %wt; IP:H_2O= 0.27:1; [SHC] = 0.60 %wt; [n-DM] = 0.20 %wt; temperature = 70°C; stirring speed = 300 rpm; reaction time = 20 h.

Table 4.3 Decomposition temperature of PIP-CS15A nanocomposites with various CS15A loading

Sample	%wt Loss	T_{id} (°C)	T_{max} (°C)
CS15A	35	268	408
PIP	99	358	429
PIP-CS15A_5	92	358	426
PIP-CS15A_10	87	354	429
PIP-CS15A_15	81	351	428
PIP-CS15A_20	62	325	433

Condition: [AIBN] = 0.25 %wt; IP:H_2O= 0.27:1; [SHC] = 0.60 %wt; [n-DM] = 0.20 %wt; temperature = 70°C; stirring speed = 300 rpm; reaction time = 20 h.

4.1.3 Effect of Monomer to Water Ratio

The effect of monomer to water ratio (0.24-0.40) on monomer to water ratio on monomer conversion, particle size and solid content of PIP-CS15A nanocomposites are shown in Table 4.4 and Figure 4.8. The average particle size and solid content of PIP-CS15A nanocomposites (5 and 10 %wt of CS15A loading) were decreased with decreasing monomer to water ratio. At monomer to water ratio of 0.24:1, the maximum conversion of 85% and 81% were obtained for adding 5 %wt and 10 %wt of CS15A, respectively. This indicated that the particle size was increased proportional to the increasing monomer to water ratio. The monomer to water ratio above 0.3 caused the decreasing monomer conversion that was obviously observed at 10 %wt of CS15A loading. The particle size distribution of PIP-CS15A nanocomposites at various monomer to water ratios is shown in Figure 4.9. In this work, a hydrophobic initiator was an oil-soluble type for isoprene monomer. Therefore, the nucleations were most likely occurred within the micelles, the size of the micelle increased with increasing isoprene monomer concentration. Thus, the ratio of monomer to water significantly affected the particle size. The similar results were earlier reported for styrene-g-polyisoprene nanoparticles initiated by using AIBN via differential microemulsion polymerization [7] and synthesis of monodispersed PIP-silica nanoparticles via differential microemulsion polymerization [55].

However, the appropriate monomer to water ratio for synthesis of PIP-CS15A nanocomposites was 0.24:1. A small particle size around 24.5 nm and 29.1 nm, monomer conversion of 85% and 81.3% and solid content of 24.2% and 19.9% were obtained at optimum condition for 5 %wt and 10 %wt of CS15A loading, respectively. Furthermore, increasing the monomer to water ratio above 0.24 caused an increase in the micelles size and diffusion resistance resulting in a slow polymerization rate and a decrease in the stabilization of nanoemulsion.

Table 4.4 Effect of monomer to water ratio on monomer conversion, average particle size and solid content of PIP-CS15A nanocomposites

Sample	IP/water ratio	%Solid Content	%Monomer Conversion	Dn (nm)	PSD (nm)
5 %wt of CS15A loading					
PIP24-CS15A_5	0.24:1	24.2 (0.23)	85.0 (0.05)	24.5	10.8
PIP27-CS15A_5	0.27:1	21.5 (0.17)	81.4 (0.62)	26.3	10.8
PIP30-CS15A_5	0.30:1	21.6 (0.51)	76.6 (1.28)	24.2	10.2
PIP40-CS15A_5	0.40:1	28.0 (0.43)	72.8 (1.41)	37.0	14.0
10 %wt of MMT loading					
PIP24-CS15A_10	0.24:1	19.9 (0.87)	81.3 (0.91)	29.1	11.2
PIP27-CS15A_10	0.27:1	21.9 (0.61)	80.2 (0.53)	29.8	11.9
PIP30-CS15A_10	0.30:1	21.4 (0.62)	43.8 (0.76)	29.8	11.5
PIP40-CS15A_10	0.40:1	23.7 (0.58)	31.5 (0.13)	32.6	12.8

Condition: [AIBN] = 0.25 %wt; [SHC] = 0.60 %wt; [n-DM] = 0.20 %wt;
Temperature = 70°C; stirring speed = 300 rpm; reaction time = 20 h.
D_n = Mean Number Diameter (average particle size); PSD = Particle Size Distribution
(-): Standard diviation, SD

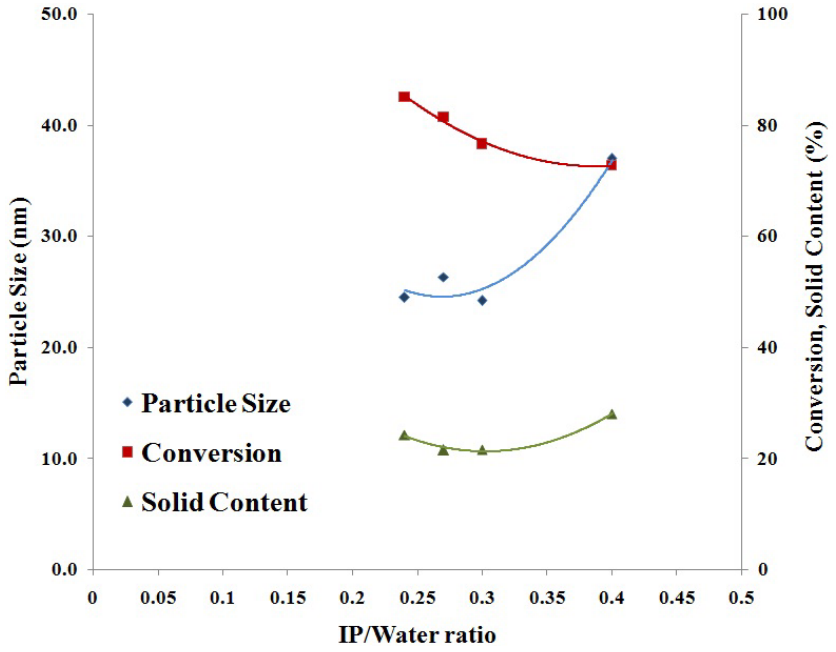

a)

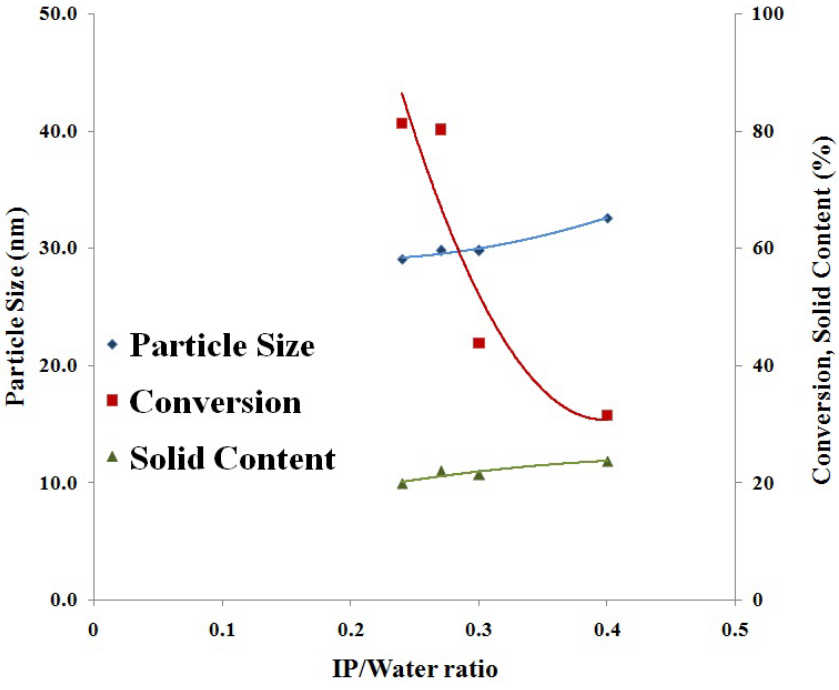

b)

Figure 4.8 Effect of monomer to water ratio on monomer conversion, particle size and solid content of PIP-CS15A nanocomposites:
a) 5 %wt of CS15A loading and b) 10 %wt of CS15A loading

Condition: [AIBN] = 0.25 %wt; [SHC] = 0.60 %wt; [n-DM] = 0.20 %wt;
Temperature = 70°C; stirring speed = 300 rpm; reaction time = 20 h.

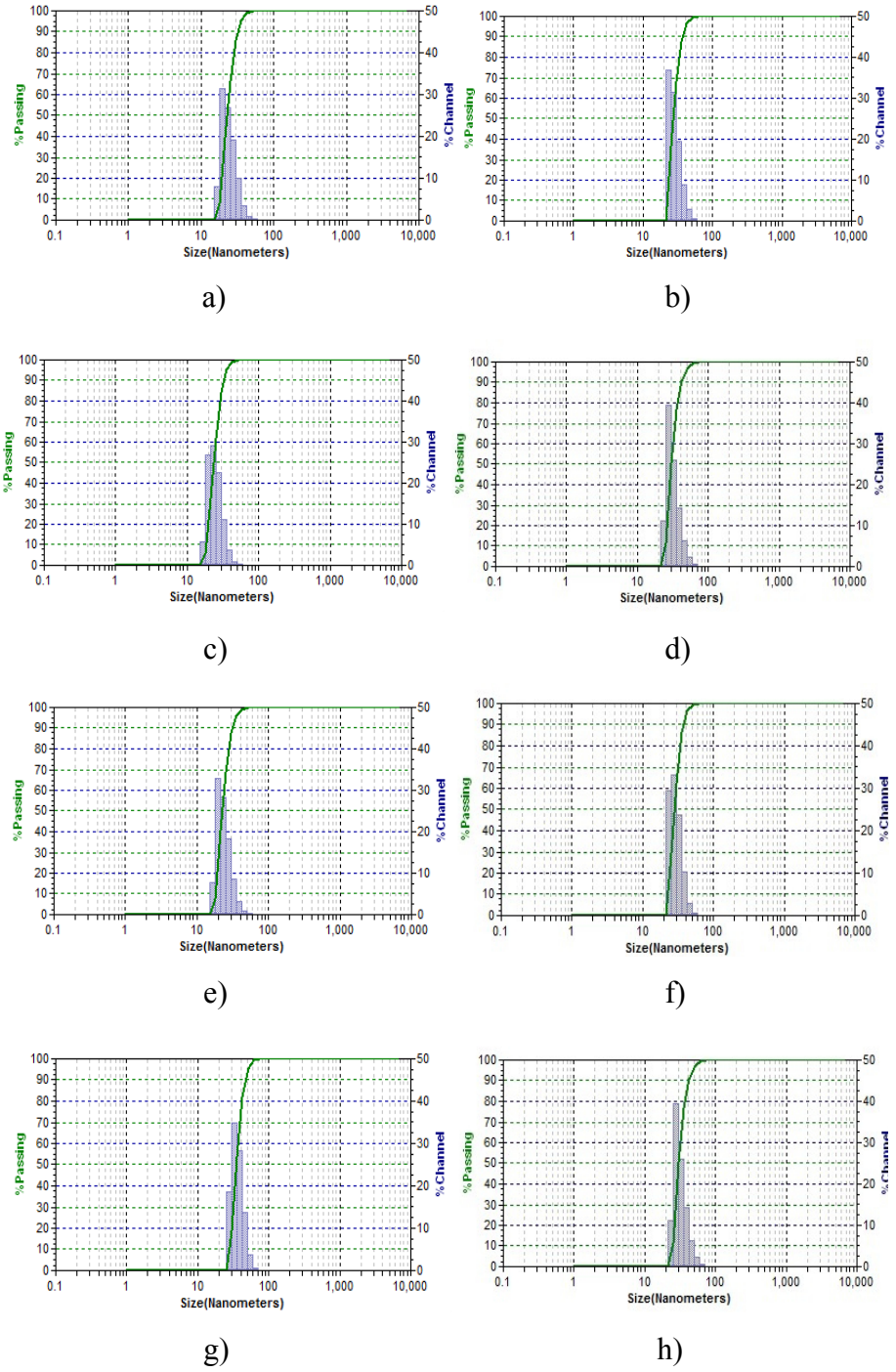

Figure 4.9 Histograms of particle size distribution of PIP-CS15A nanocomposites with various monomer to water ratios: a) PIP24-CS15A_5, b) PIP24-CS15A_10, c) PIP27-CS15A_5, d) PIP27-CS15A_10, e) PIP30-CS15A_5, f) PIP30-CS15A_10, g) PIP40-CS15A_5 and h) PIP40-CS15A_10

Condition: [CS15A] = 5, 10 %wt [AIBN] = 0.25 %wt; [SHC] = 0.60 %wt; [n-DM] = 0.20 %wt; Temperature = 70°C; stirring speed = 300 rpm; reaction time = 20 h.

For direct mixing of CS15A and PIP latex, the phase separation and CS15A agglomeration were observed due to the precipitation of CS15A particles at the bottom phase with top phase of PIP latex (Figure 4.10a). Moreover, PIP-CS15A at 10 %wt of CS15A loading was kept for period of 1-4 months to investigate the colloidal stability. The homogeneous and stable colloidal latex were observed (Figure 4.10b). This can be explained that the synthesis of PIP-CS15A nanoparticles via differential microemulsion polymerization had a high colloidal stability and reduction of CS15A aggregation.

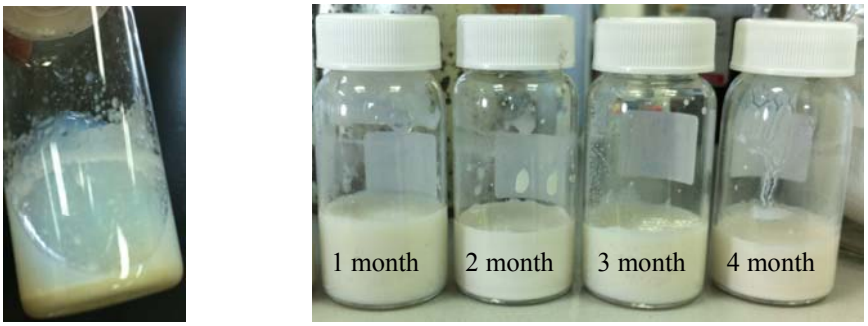

a) b)

Figure 4.10 Appearance of a) PIP-CS15A directed load and b) PIP-CS15A nanocomposites

In addition, the thermograms of PIP and PIP-CS15A nanocomposites (Figure 4.11a and 4.11b) are shown one step polymer degradation and provided smooth weight loss curves. The decomposition temperatures of PIP-CS15A nanocomposites of 10 %wt CS15A loading (354°C) was slightly lower than that of PIP (358°C). However, T_{max} of PIP-CS15A nanocomposites was the same that of PIP.

Furthermore, the thermal properties of PIP-CS15A nanocomposites (T_{id} = 354-358°C and T_{max} = 428-432°C) were the same which was not affected by monomer to water ratio. The similar results were earlier reported for synthesis of monodispersed PIP-silica nanoparticles via differential microemulsion polymerization [55] and characterization of natural rubber nanocomposites filled with organoclay [59].

Table 4.5 Decomposition temperature of PIP-CS15A nanocomposites with virous monomer to water ratios

Sample	%wt Loss	T_{id} (°C)	T_{max} (°C)
CS15A	35	268	408
PIP	99	358	429
10 %wt of CS15A loading			
PIP24-CS15A_10	83	358	432
PIP27-CS15A_10	87	354	429
PIP30-CS15A_10	82	356	430
PIP40-CS15A_10	84	356	428

Condition: [CS15A] = 10 %wt [AIBN] = 0.25 %wt; [SHC] = 0.60 %wt; [n-DM] = 0.20 %wt; Temperature = 70°C; stirring speed = 300 rpm; reaction time = 20 h.

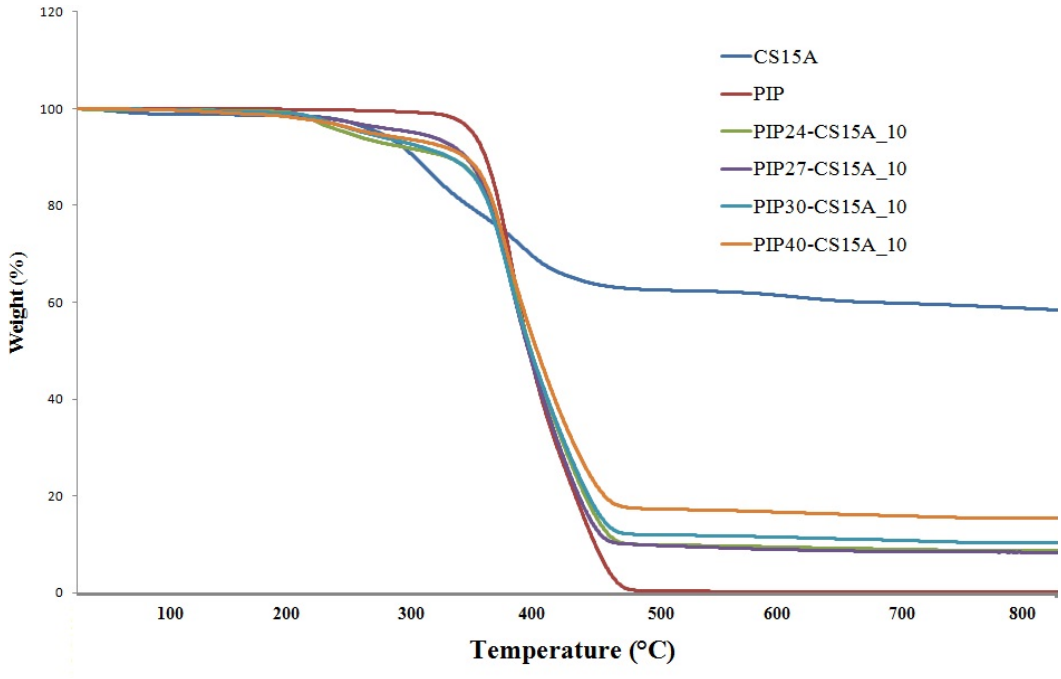

a)

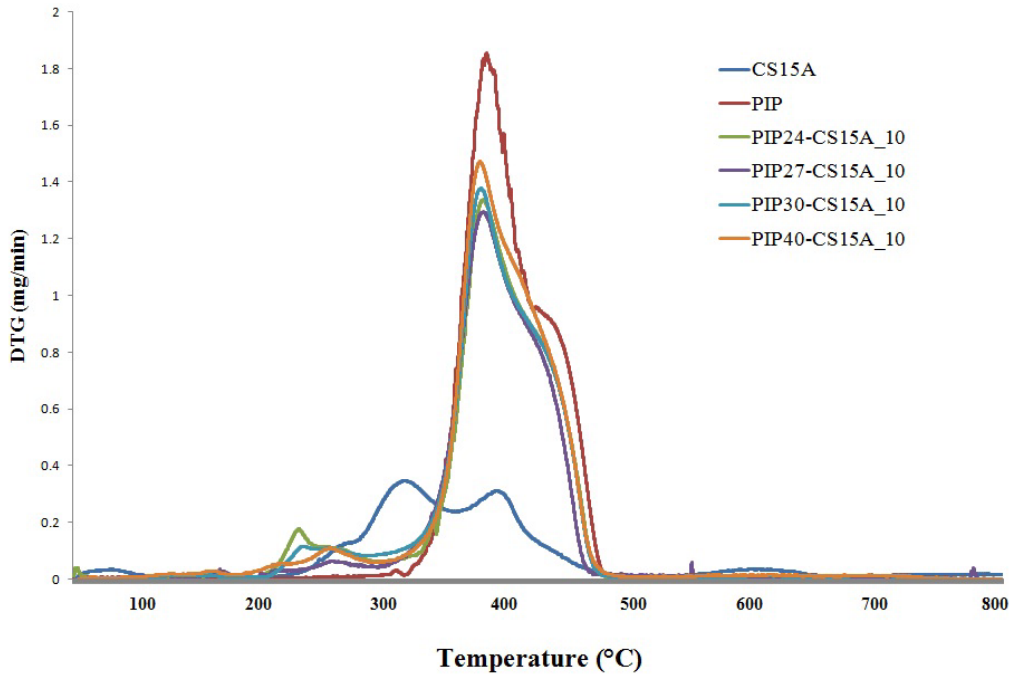

b)

Figure 4.11 a) TGA and b) DTG curves of the PIP-CS15A nanocomposites with various monomer to water ratios

Condition: [CS15A] = 10 %wt [AIBN] = 0.25 %wt; [SHC] = 0.60 %wt; [n-DM] = 0.20 %wt; Temperature = 70°C; stirring speed = 300 rpm; reaction time = 20 h.

4.1.4 Effect of Clay Types

Four types of montmorillonite clay, CS15A, CS30B, NF15 and NF116-VTS were used in this work. The composition and properties of all MMT types are shown in Table A-2 (Appendix A). CS15A and NF15 were modified by the same quaternary ammonium salt (hydrophobic modifier), resulting well dispersion of PIP in CS15A and NF. CS30B was modified by quaternary ammonium salt with –OH group. It was found that CS30B was well dispersed in water phase than other MMT (CS15A and NF15). Therefore, CS30B could be loaded up to 20 %wt for preparation PIP-CS30B nanocomposites. The MMT, NF116-VTS and NF116 were modified with vinyl trimethoxysilane (VTS) in similar method to modified silica nanoparticles [55].

At the same MMT loading and condition, the maximum monomer conversion of 80.2% and 20.9% solid content with small particle size of 26.3 nm of PIP-CS15A nanocomposites was obtained (Table 4.6). This indicates that organo-modifier affected the polymerization of PIP-MMT nanocomposites. However, the condition at SDS concentration of 12 %wt, monomer to water ratio of 0.24 and MMT loading of 10 %wt was studied for PIP-CS15A nanocomposites. Therefore, this appropriate condition for preparation of PIP-NF15, PIP-CS30B and PIP-NF116-VTS was not studied in this work. In addition, for low monomer conversion of PIP-NF15 (67.8%), PIP-CS30B (67.4%) and PIP-NF116-VTS (30%) was obtained due to the agglomeration of PIP-MMT in the reactor).

Furthermore, for PIP-CS30B nanocomposites of 10-20 %wt loading (Table 4.7), monomer conversion was decreased with increasing CS30B loading. This indicated that CS30B was not well-dispersed into monomer droplet resulting low polymerization rate due to the agglomeration of PIP-CS30B in the reactor at high loading of CS30B.

Table 4.6 Effect of clay types on monomer conversion, average particle size

and solid content of PIP-MMT nanocomposites

Sample	MMT (%wt)	%Solid Content	%Monomer Conversion	Dn (nm)	PSD (nm)
PIP-CS15A	10	19.9 (0.87)	81.3 (0.91)	29.1	11.2
PIP-NF15	10	20.3 (0.28)	67.8 (0.52)	26.1	12.8
PIP-NF116-VTS	10	21.4 (0.38)	30.0 (0.09)	30.1	12.5
PIP-CS30B	10	22.5 (0.53)	67.4 (0.52)	25.6	12.8

Condition: [MMT] = 10 %wt; [AIBN] = 0.25 %wt; IP/H_2O = 0.24; [SHC] = 0.60 %wt; [n-DM] = 0.20 %wt; temperature = 70°C; stirring speed = 300 rpm; reaction time = 20 h.
D_n = Mean Number Diameter (average particle size); PSD = Particle Size Distribution

%Monomer conversion: calculated from nano-latex (was not included PIP and MMT agglomeration)
(-): Standard diviation, SD

Table 4.7 Effect of CS30B loading on monomer conversion, average particle size and solid content of PIP-CS30B nanocomposites

Sample	CS30B (%wt)	%Solid Content	%Monomer Conversion	Dn (nm)	PSD (nm)
PIP-CS30B_10	10	22.5 (0.53)	67.4 (0.52)	25.6	12.8
PIP-CS30B_15	15	21.9 (0.74)	63.0 (1.03)	30.8	13.3
PIP-CS30B_20	20	21.7 (0.81)	59.4 (0.19)	30.7	12.7

Condition: [AIBN] = 0.25 %wt; IP/H_2O = 0.24; [SHC] = 0.60 %wt; [n-DM] = 0.20 %wt; Temperature = 70°C; stirring speed = 300 rpm; reaction time = 20 h.
D_n = Mean Number Diameter (average particle size); PSD = Particle Size Distribution
(-): Standard diviation, SD

4.2 Characterization of PIP-CS15A Nanocomposites Latex

4.2.1 FTIR Analysis Results

FTIR spectra of CS15A, PIP and PIP-CS15A nanocomposites are shown in Figure 4.12. For the FTIR spectrum of nanosized polyisoprene (Figure 4.12a) the methylene stretching at 2,925 and 2,854 cm^{-1}, the methyl stretching at 2,962 cm^{-1}, the methyl deformations at 1,450 and 1,377 cm^{-1} and the prominent =C-H out-of-plane wag at 837 cm^{-1} were observed. The distinctive peaks at 3,035 cm^{-1} corresponded to

the =C-H stretching, 2,727 cm^{-1} related to the overtone of the methyl deformation and 1,664 cm^{-1} for C=C stretching. The similar results were earlier reported for preparation nanosized polyisoprene via differential microemulsion polymerization [7].

For FTIR spectra of CS15A (Figure 4.12b), the peaks at 3632, 3442, 2929, 2854, 1640, 1479, 1041 and 523 cm^{-1} can be assigned as the O-H stretching, O-OH stretching, C-H stretching of methyl and methylene group, RCONHR of ammonium salts, CH_3 deformation, Si-O stretching and Al-O stretching, respectively. These results indicate that the sample have organo-modifier in the layer of CS15A [57]. FTIR spectras were confirmed that PIP-CS15A nanocomposites consisted of PIP and MMT as shown in Figure 4.12c.

4.2.2 XRD Analysis Results

The d_{001} values were obtained from XRD patterns as shown in Figure 4.14. The CS15A shows a diffraction peak at 2θ of 2.83° corresponding to the d_{001} of 3.11 nm. The similar result was reported in production bulletin of CS15A from Southern Clay Products that shows d_{001} of 3.15 nm [58]. The d_{001} diffraction shifted to 2θ of 2.30° to 2.34°, which is assigned to d_{001} of 3.76 to 3.82 nm for PIP-CS15A nanocomposites (Table 4.8) and diffraction peak intensity of 10 %wt CS15A loading was higher than that of 5 %wt CS15A loading due to high loading of CS15A. These result indicated that clay layer was intercalated by polyisoprene due to the expanding basal space of clay. The similar results were earlier reported for characterization of natural rubber nanocomposites filled with organoclay [59].

Moreover, XRD patterns of all clay types and PIP-MMT nanocomposites are shown in Figure 4.15. From Table 4.9, the d_{001} of PIP-MMT nanocomposites are expanded from the original MMT. This indicated that PIP dispersed into the interlayer of all clays (NF15, CS30B and NF116-VTS). The similar results were earlier reported for SBR/NR/organo-bentonite nanocomposites prepared from latex dispersion [53, 59].

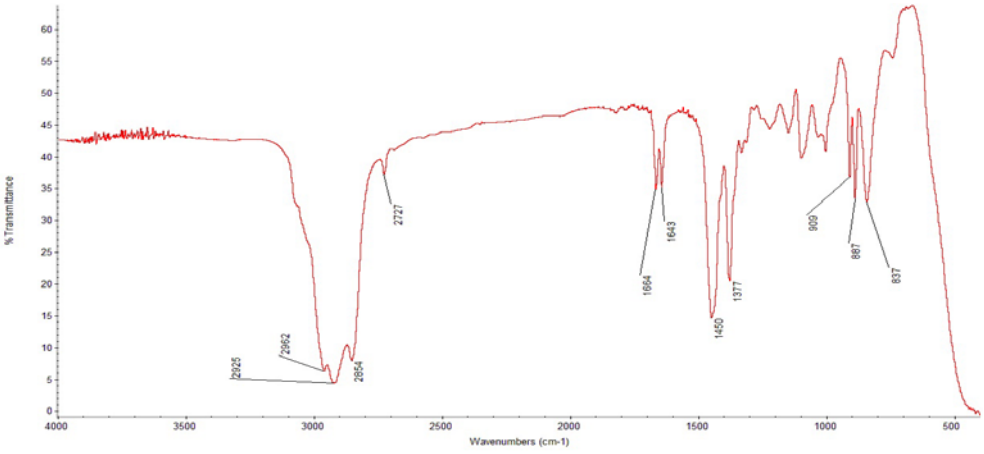

a)

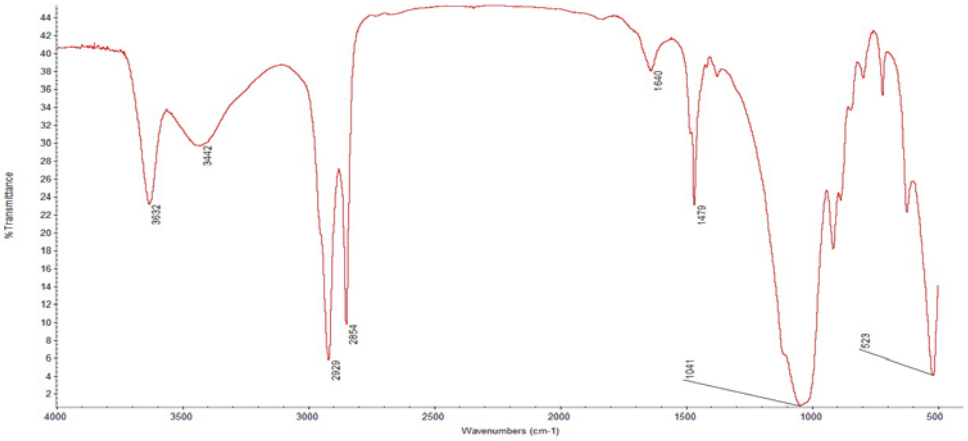

b)

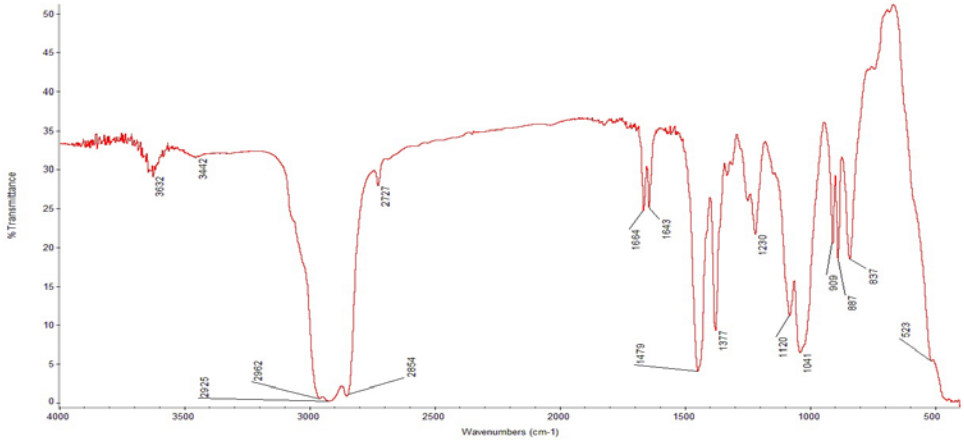

c)

Figure 4.12 FT-IR spectras of the PIP-CS15A nanocomposites:
a) PIP, b) CS15A and c) PIP-CS15A nanocomposites

Table 4.8 2θ and d-spacing of XRD spectra of CS15A and PIP-CS15A nanocomposites

Sample	%CS15A	2θ (Degree)	d_{001} (nm)
CS15A		2.84	3.11
PIP24-CS15A_5	5	2.30	3.82
PIP24-CS15A_10	10	2.31	3.81
PIP27-CS15A_5	5	2.32	3.80
PIP27-CS15A_10	10	2.34	3.76

Condition: [CS15A] = 5, 10 %wt; [AIBN] = 0.25 %wt; IP/H_2O = 0.24, 0.27; [SHC] = 0.60 %wt; [n-DM] = 0.20 %wt; Temperature = 70°C; stirring speed = 300 rpm; reaction time = 20 h.

Table 4.9 2θ and d-spacing of XRD spectra of clay type effect

Sample	2θ (Degree)	d_{001} (nm)
CS15A	2.84	3.11
NF15	2.73	3.23
NF116	6.92	1.27
NF116-VTS	6.92	1.27
CS30B	4.77	1.85
PIP-CS15A_10	2.31	3.81
PIP-NF15_10	2.21	3.99
PIP-NF116-VTS_10	4.57	1.93
PIP-CS30B_10	2.25	3.91

Condition: [AIBN] = 0.25 %wt; IP/H_2O = 0.27; [SHC] = 0.60 %wt; [n-DM] = 0.20 %wt; temperature = 70°C; stirring speed = 300 rpm; reaction time = 20 h.

In addition, d-spacing of NF116 and NF116-VTS was not expanded (d_{001}= 1.27 nm) due to modifying the –OH group by silane group of VTS occurring only at the edge of NF116 (Figure 4.12).

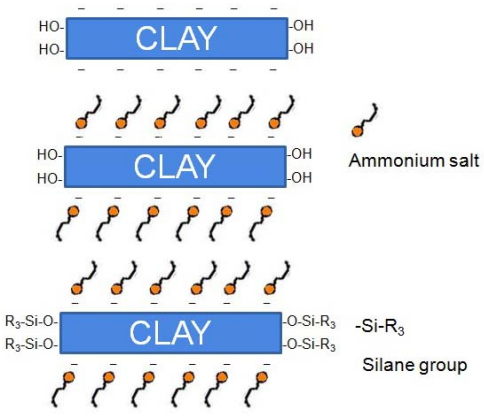

Figure 4.13 Model of clay modification with ammonium salt and silane group

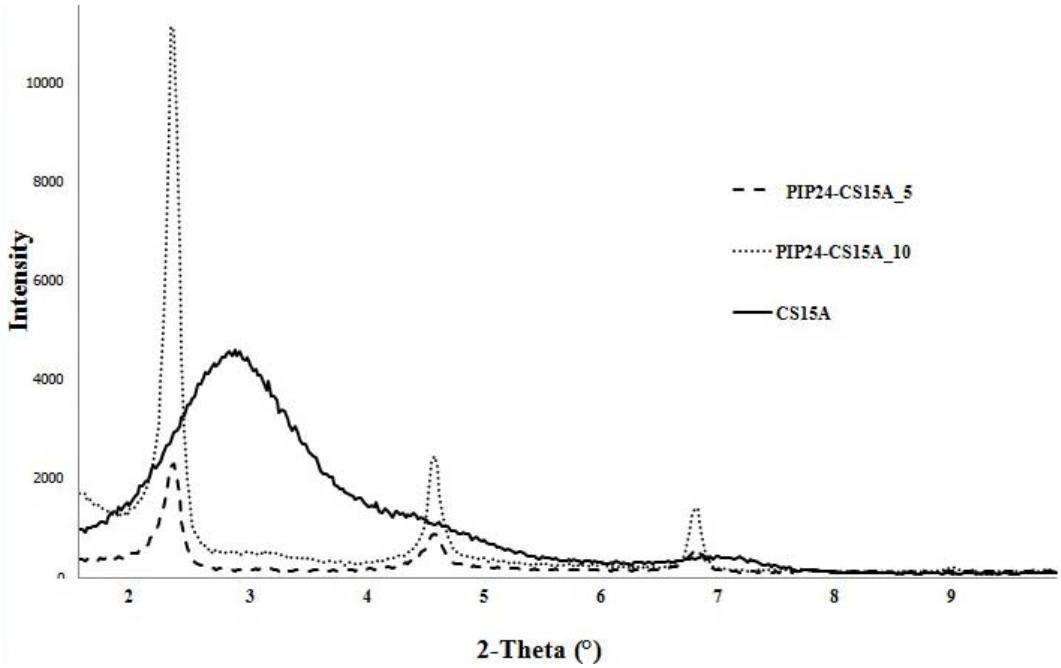

a)

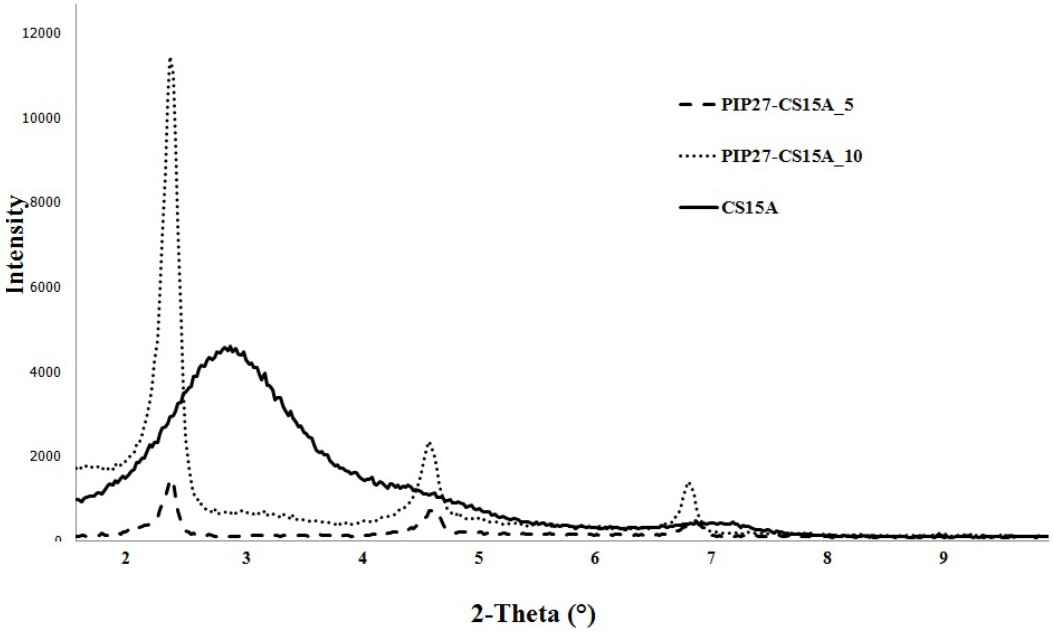

b)

Figure 4.14 XRD patterns of the PIP-CS15A nanocomposites:

a) CS15A, PIP24-CS15A_5 and PIP24-CS15A_10

b) CS15A, PIP27-CS15A_5 and PIP27-CS15A_10

Condition: [AIBN] = 0.25 %wt; IP/H_2O= 0.27; [SHC] = 0.60 %wt; [n-DM]=0.20 %wt; temperature=70°C; stirring speed=300 rpm; reaction time = 20 h.

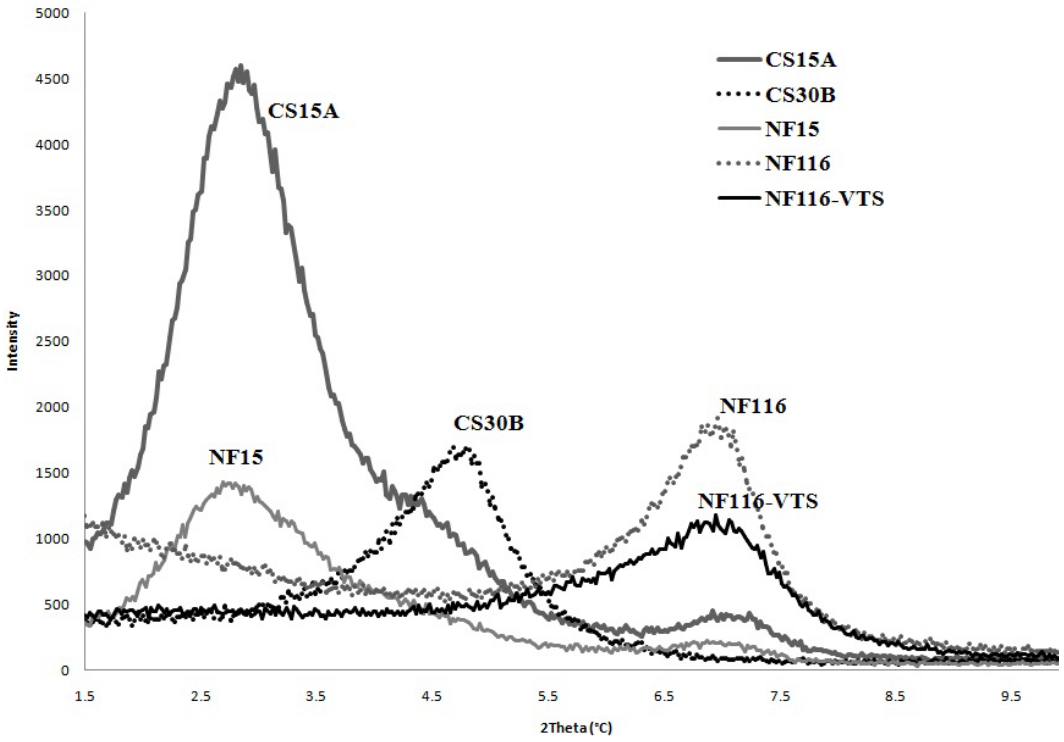

a)

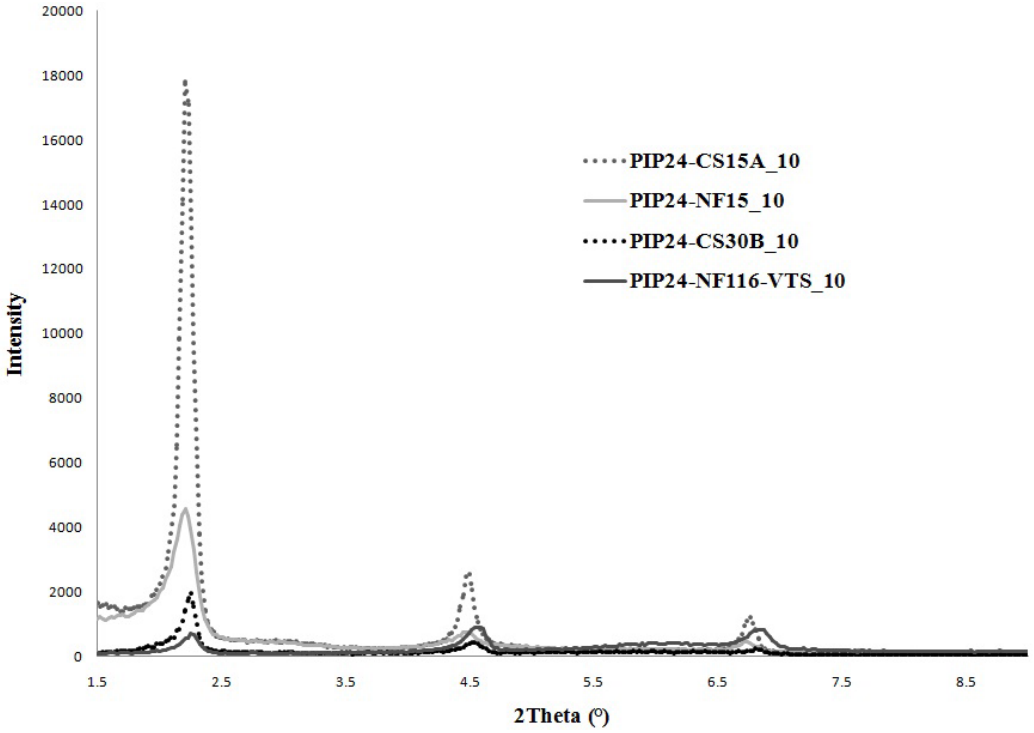

b)

Figure 4.15 XRD patterns of a) clay types and b) PIP-MMT nanocomposites at various clay types

4.2.3 Morphology of PIP-MMT Nanocomposites

The morphologies of nanosized PIP and PIP-MMT nanocomposites examined by TEM micrographs are shown in Figure 4.16. OsO_4 can stain only the carbon-carbon double bonds of PIP. This result was similar to nanosized PIP in the earlier reported for preparation nanosized polyisoprene via differential microemulsion polymerization [7].

From Figure 4.16a, the nanosized PIP had spherical shape around 30 nm. For the PIP filled with 5 %wt of CS15A (Figure 4.16b) and 4.16c) and 10 %wt of CS15A (Figure 4.16d) and 4.16e), it can be seen that the spherical PIP and dark flake shape of CS15A are well-dispersed due to some dark line of CS15A (thickness of CS15A at 20-30nm) was observed and some of PIP intercalated in the layer of CS15A that confirmed the expanding of basal space in XRD result. However, PIP with 10 %wt of CS15A was darker than that of 5 %wt of CS15A due to the stack of CS15A. The thickness of CS15A was 20-30 nm and the length was about 100-200 nm. Furthermore, CS15A morphology had been observed similar to morphology NR-MMT nanocomposites prepared in aqueous medium [52] and SBR/NR/OMMT nanocomposites [53].

Moreover, the morphology of PIP nanocomposites with other clay types is shown in Figure 4.17. Morphology of PIP-NF15 and PIP-CS30B nanocomposites (Figure 4.17a and c) had darker flake of NF15A and CS30B than that of PIP-CS15A according to more PIP-NF15A and PIP-CS30B agglomeration in the reactor and low monomer conversion (67.8% and 67.4%, respectively) was observed. Furthermore, for low monomer conversion (30%) due to the agglomeration of NF116-VTS, this can be explained by PIP-NF116-VTS morphology as shown in Figure 4.17b that the stack of NF116-VTS with the thickness larger than 100 nm was observed.

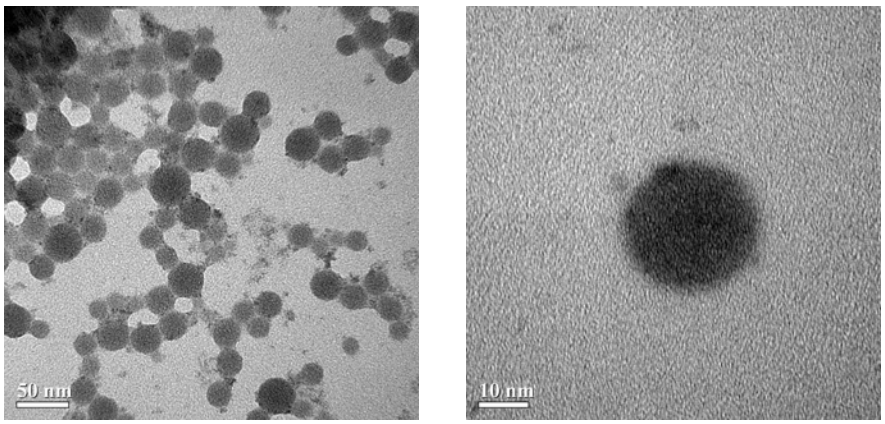

a) PIP

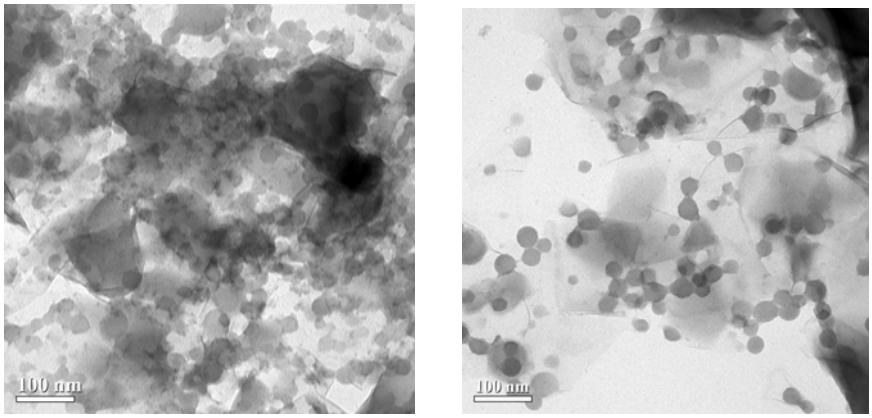

b) PIP24-CS15A_5 c) PIP27-CS15A_5

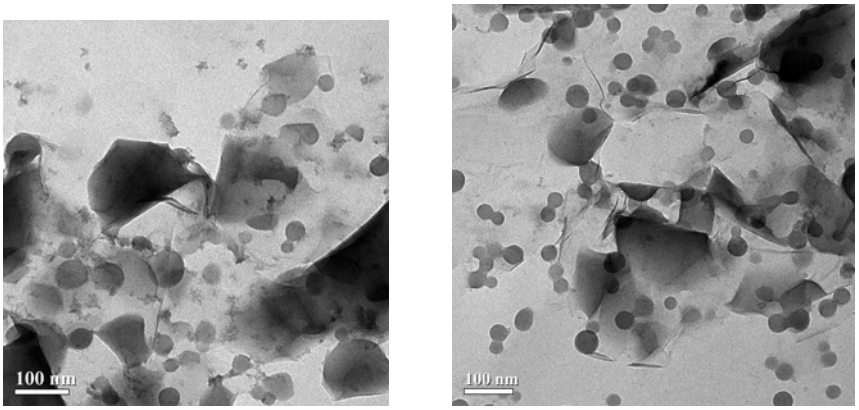

d) PIP24-CS15A_10 e) PIP27-CS15A_10

Figure 4.16 Transmission electron micrographs of PIP-CS15A nanocomposites: a) PIP (x80,000 and x300,000), b) PIP24-CS15A_5 (x40,000), c) PIP27-CS15A_5 (x40,000), d) PIP24-CS15A_10 (x40,000) and e) PIP27-CS15A_10 (x40,000)

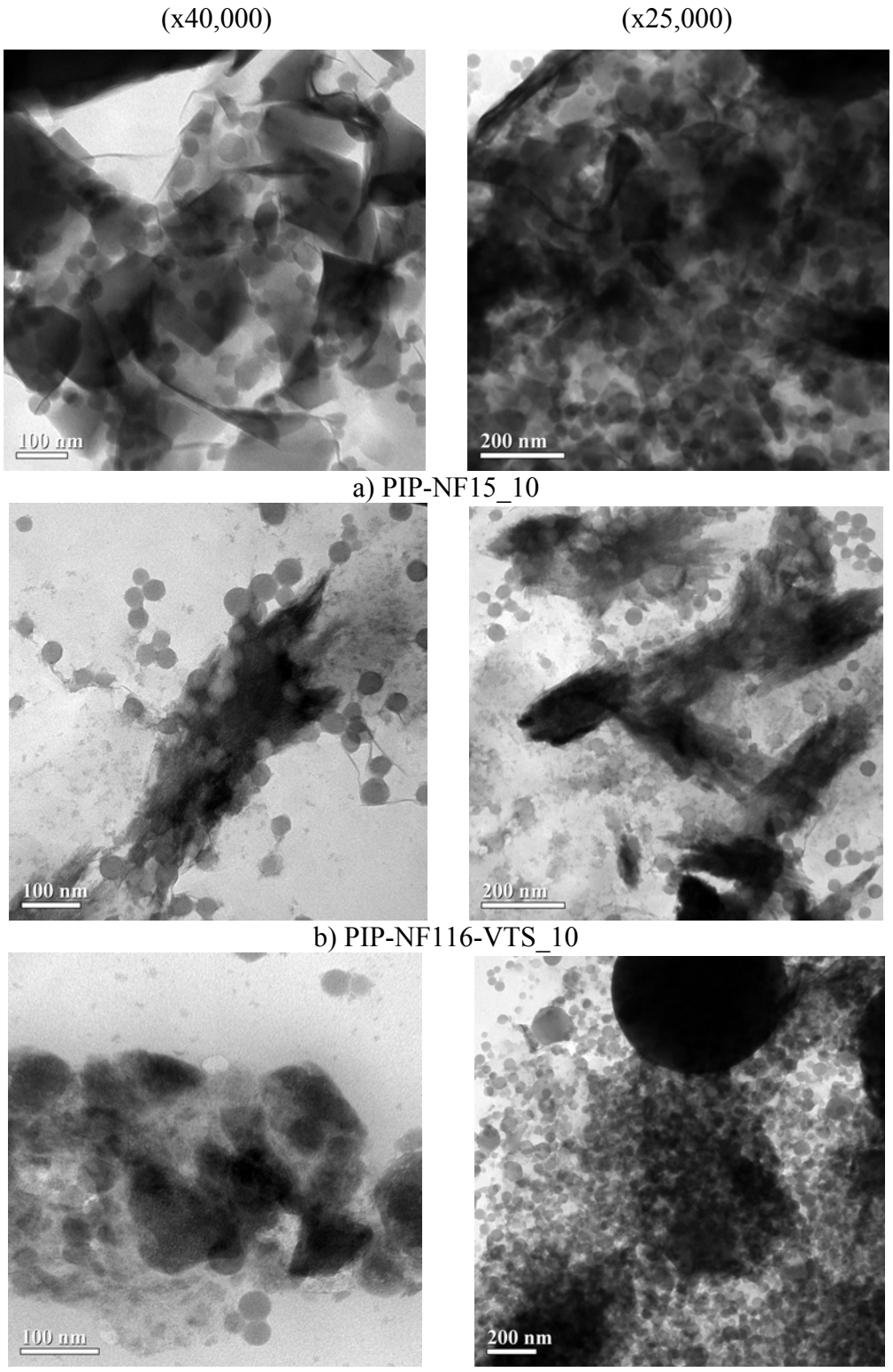

Figure 4.17 Transmission electron micrographs of PIP-MMT nanocomposites with various clay types: a) PIP-NF15_10, b) PIP-116-VTS_10 and c) PIP-CS30B_10

4.3 Properties of NR/PIP-MMT Blend

4.3.1 Mechanical Properties of NR/PIP-MMT Blends

Mechanical properties in terms of tensile strength, modulus and elongation at break of PIP-MMT filled NR with different clay types before and after ageing are shown in Table 4.10 and Figure 4.18. For the influence of clay types, NR/ PIP-CS15A_10 composites had highest tensile strength (TS)(13.4 MPa) and elongation at break (EB). Moreover, the TS and EB retention of all rubber composites was higher than 80%, except NR/PIP-NF116-VTS_10 that had the retention of 72% in tensile strength and 70% in modulus of elasticity at 300% strain (ME).

Table 4.10 Mechanical properties of NR/PIP-MMT compounds before and after ageing with various clay types

Rubber composite	Tensile Strength (MPa)			Modulus at 300% Strain (MPa)			Elongation at break (%)	
	Before ageing	After ageing	RT[a] (%)	Before ageing	After ageing	RT (%)	Before ageing	RT (%)
NR/PIP-CS15A_10	13.4 (0.1)	13.1 (1.0)	97.8	1.8 (0)	1.6 (0)	88.1	920 (45)	84.9
NR/PIP-NF15_10	11.9 (0.1)	10.2 (0.3)	85.7	1.8 (0.1)	1.5 (0)	81.9	819 (3.5)	94.9
NR/PIP-NF116-VTS_10	10.1 (0.4)	7.3 (1.5)	72.3	1.7 (0.1)	1.2 (0)	70.6	759 (37)	90.6
NR/PIP-CS30B_10	8.9 (1.8)	7.3 (0.7)	82.0	1.4 (0.1)	1.3 (0)	92.9	868 (33)	94.6

PIP-CS15A_10: PIP with 10 %wt CS15A loading

PIP-NF15_10: PIP with 10 %wt NF15 loading

PIP-NF116-VTS_10: PIP with 10 %wt NF116-VTS loading

PIP-CS30B_10: PIP with 10 %wt CS30B loading

NR ratio: NR/PIP-MMT =70/30. %MMT content based on total rubber = 3%.

[a]%Retention (RT) = (properties after ageing/properties before ageing) x 100.

(-): Standard diviation, SD

For direct mixing of NR filled with 3 and 5 %wt untreated CS15A (NR/untreated CS15A), the tensile strength (13.6 and 13.1 MPa) were closed to

From the results in Table 4.11 and Figure 4.19, PIP-CS15A and PIP-CS30B latex were selected to blend with NRL at various blend ratios (equivalent to 1-6 %wt MMT based on total rubber). The tensile strength of rubber nanocomposites was significantly affected by the addition of PIP-CS15A. From Table 4.11, tensile strength was increased from 11.1 MPa (unfilled NR) to 17.3 and 17.7 MPa for NR/PIP-CS15A_10 at blend ratio of 90/10 and 80/20 (equivalent to 1 and 2 %wt CS15A, respectively). The tensile strength of NR/PIP-CS15A_10 at blend ratio of 70/30 (equivalent to 3 %wt CS15A) was 11.1 MPa. This implied that for the low content of CS15A (equivalent to 1 and 2 %wt CS15A) in NR, the PIP-CS15A was effectively dispersed and compatible to rubber matrix.

For NR/PIP-CS30B composites, the tensile strength gradually increased with increasing PIP-CS30B loading from 10 to 15 %wt (equivalent to 3 and 4.5 %wt CS30B) and then decreased at high PIP-CS30B loading of 20 %wt (equivalent to 6 %wt CS30B). In addition, modulus at 300% strain of NR/PIP-CS30B increased with increasing CS30B loading. This implied that loading of PIP-CS30B was required at more than 1.5 times to achieve the similar properties with PIP-CS15A loading in NR.

However, the TS, EB and ME retention of all NR/PIP-CS30B was high above 80% as shown in Figure 4.20.

Generally, the tensile strength of NR prevulcanizated at 60°C was 21.8 MPa [55]. However, in this work, low tensile strength of NR/PIP-MMT composites was obtained due to low prevulcanization temperature at 40°C. Moreover, increasing prevulcanizing temperature of NR/PIP-MMT composites higher than that 40°C caused more bubbles presented in latex during vulcanization process and the latex was coagulated.

Hardness of all rubber nanocomposites was increased with increasing the MMT content and the hardness retention after the accelerated aging process were high (95%). This indicated that clay content significant affected the hardness of rubber nanocomposites due to the clay strength.

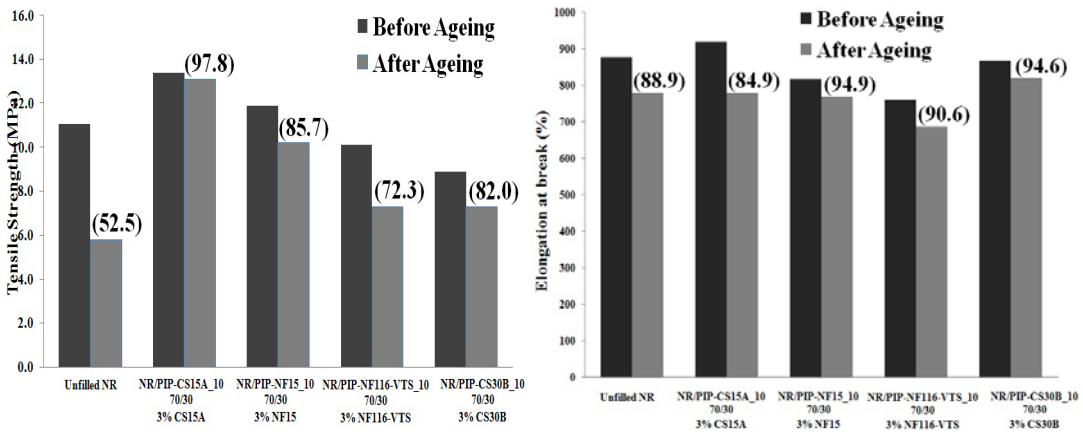

a) b)

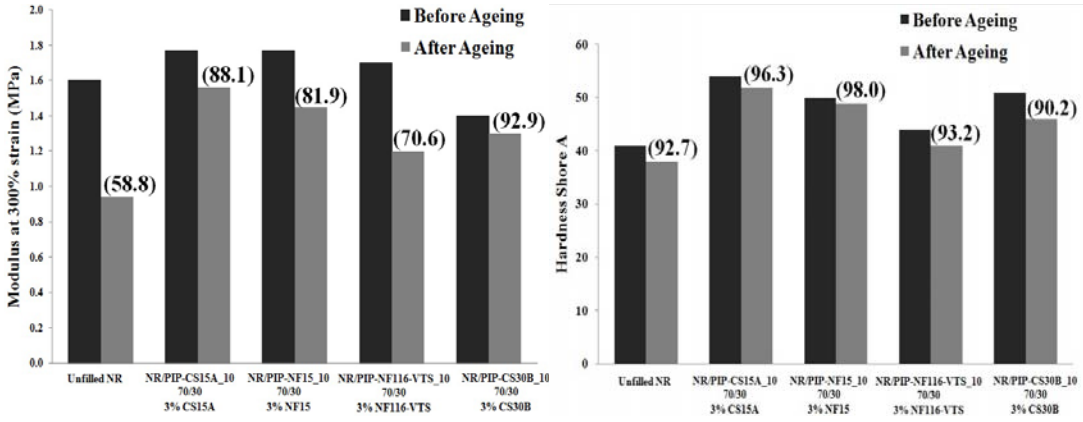

c) d)

Figure 4.18 Mechanical properties of PIP-MMT filled NR with various clay types before and after ageing: a) Tensile strength b) Elongation at break c) Modulus at 300% strain and d) Hardness Shore A
(-) = %Retention

Table 4.11 Mechanical properties of NR/PIP-MMT composites before and after ageing

Rubber composite	NR/ PIP-MMT[a]	% MMT[b]	Tensile Strength (MPa)			Modulus at 300% Strain (MPa)			Elongation at Break (%)	
			Before ageing	After ageing	RT[c] (%)	Before ageing	After ageing	RT (%)	Before ageing	RT (%)
Unfilled NR		0	11.1 (0.3)	5.8 (0.1)	52.5	1.6 (0)	0.9 (0)	58.8	877 (14)	88.9
Direct Mixing										
NR/untreated CS15A		3.0	13.6 (1.5)	8.6 (0.2)	63.2	1.6 (0.9)	0.9 (0.1)	58.1	875 (2.5)	95.1
		5.0	13.1	8.8	67.2	1.0	0.8	85.7	893	94.7

			(0.5)	(0.1)		(0)	(0.1)		(18)	
NR/PIP-CS15A_5	70/30	1.5	6.1 (0.2)	5.1 (0.7)	83.6	2.0 (0.1)	1.8 (0.1)	90.0	658 (49)	95.0
	60/40	2.0	11.5 (0.3)	9.4 (18)	81.7	2.3 (0)	2.2 (0)	95.7	820 (32)	85.6
NR/PIP-CS15A_10	90/10	1.0	17.3 (0.1)	11.9 (0.4)	68.8	1.8 (0)	1.6 (0)	84.8	788 (2)	97.8
	80/20	2.0	17.7 (0.1)	15.5 (0.1)	87.6	1.8 (0)	1.5 (0)	84.0	853 (14)	96.2
	70/30	3.0	13.4 (0.1)	13.1 (1)	97.8	1.8 (0)	1.6 (0)	88.1	920 (45)	84.9
NR/PIP-CS30B_10	70/30	3.0	8.9 (1.8)	7.3 (0.7)	82.0	1.4 (0.1)	1.3 (0)	92.9	868 (33)	94.6
NR/PIP-CS30B_15	70/30	4.5	11.3 (0.4)	9.6 (0.4)	85.0	1.7 (0)	1.6 (0)	94.1	823 (14)	89.6
NR/PIP-CS30B_20	70/30	6.0	6.4 (0.4)	5.9 (0.2)	92.2	2.2 (0.1)	2.2 (0.1)	100.0	593 (32)	100.5

PIP-CS15A_5: PIP with 5 %wt CS15A loading, PIP-CS15A_10: PIP with 10 %wt CS15A loading, PIP-CS30B_10: PIP with 10 %wt CS30B loading, PIP-CS30B_15: PIP with 15 %wt CS30B loading and PIP-CS30B_20: PIP with 20 %wt CS30B loading.

[a]NR/PIP-MMT: ratio of NR to PIP-MMT.

[b]%MMT: content based on total rubber.

[c]%Retention (RT) = (properties after ageing/properties before ageing) x 100.

(-): Standard diviation, SD

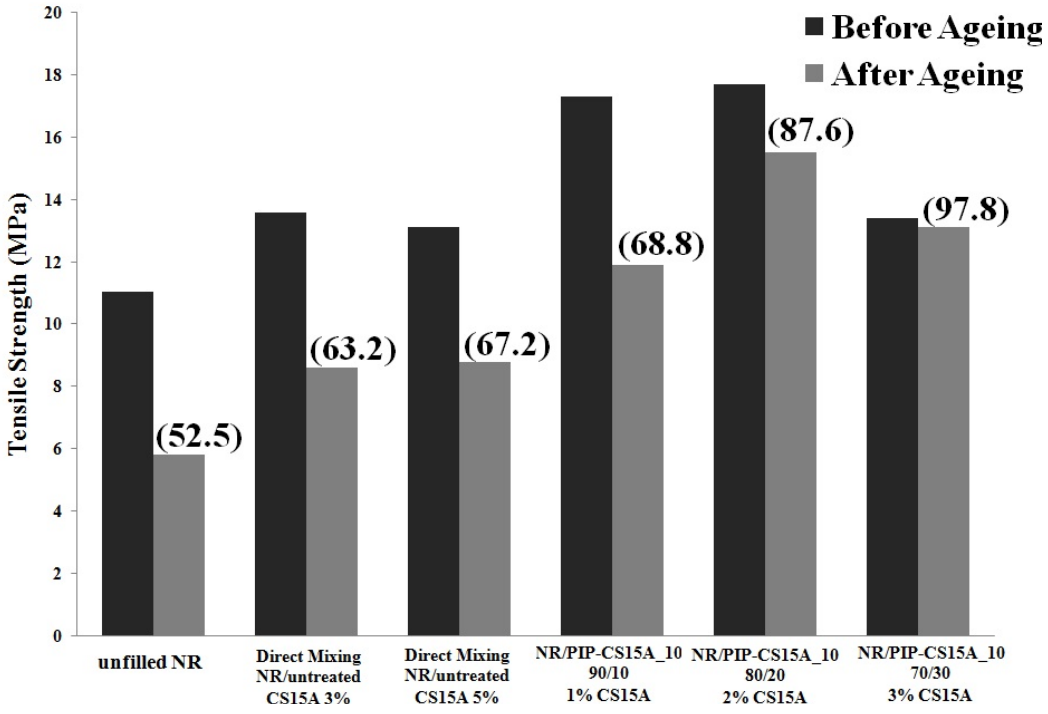

a)

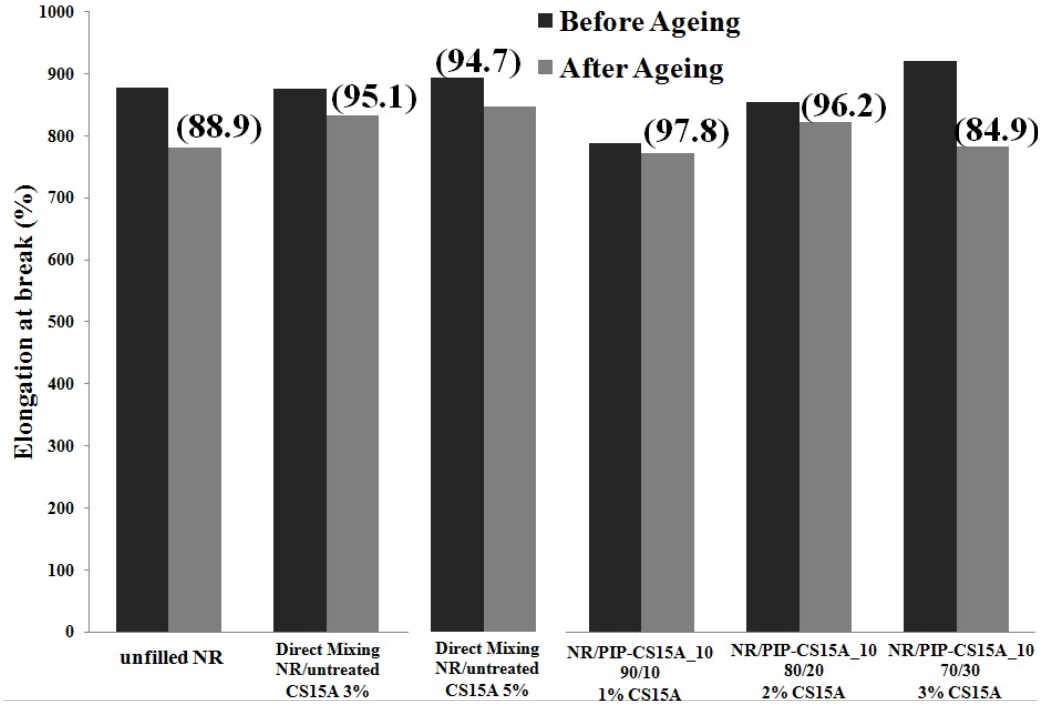

b)

Figure 4.19 Mechanical properties of PIP-CS15A filled NR with various CS15A loading before and after ageing: a) Tensile strength b) Elongation at break, c) Modulus at 300% strain and d) Hardness shore A
(-) = %Retention

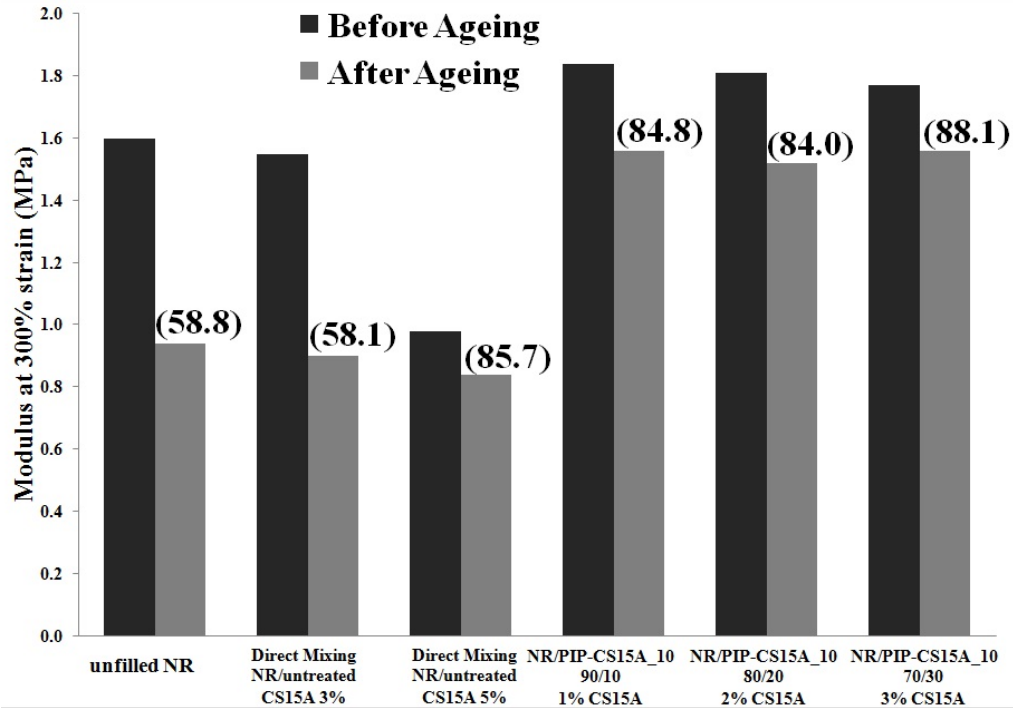

c)

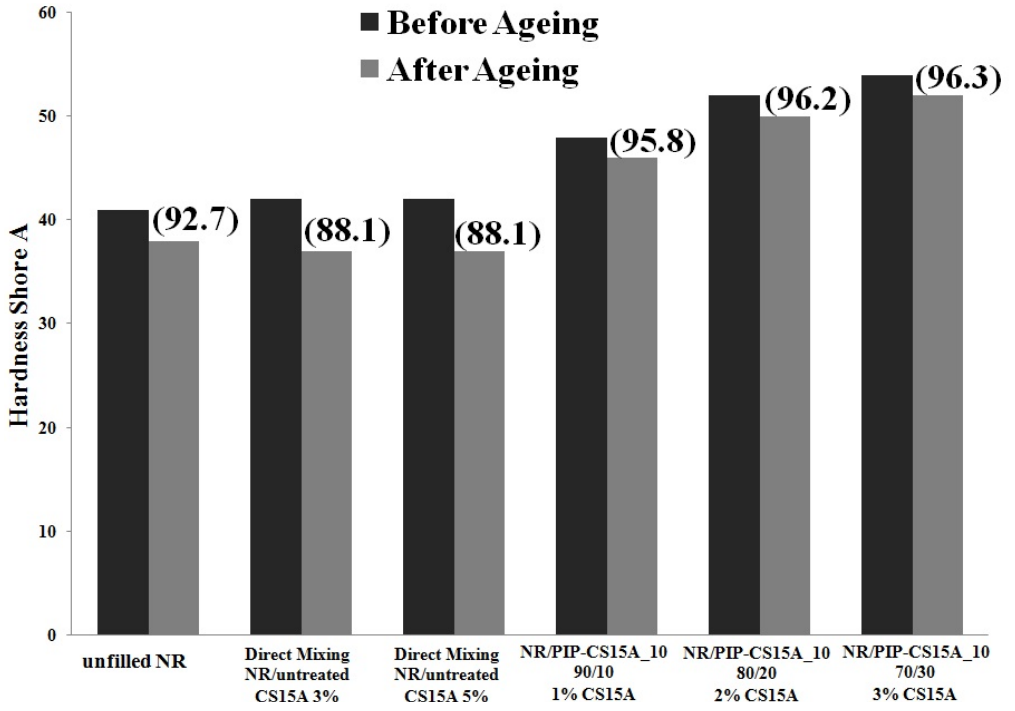

d)

Figure 4.19 (Continued)

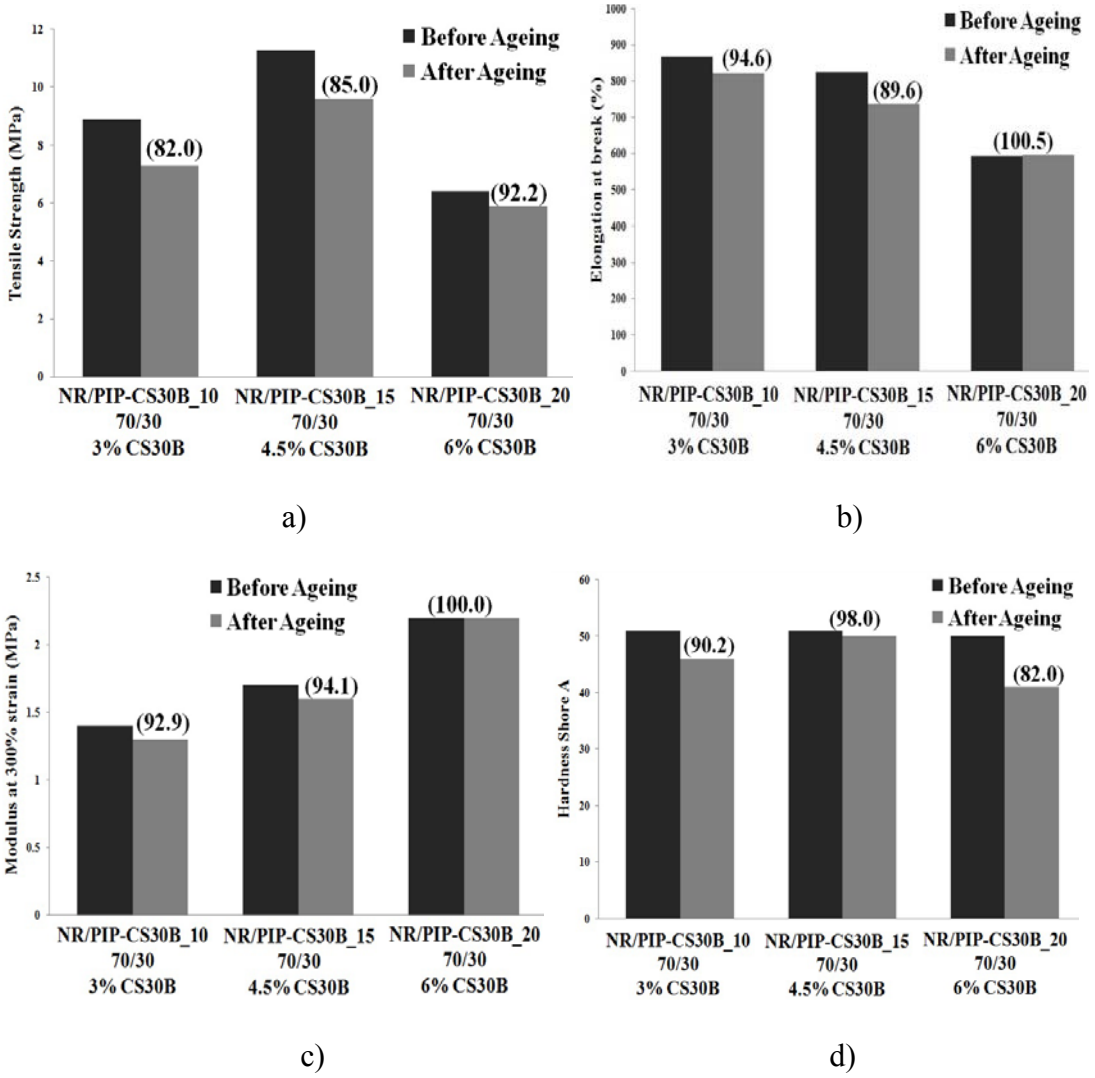

Figure 4.20 Mechanical properties of PIP-CS30B filled NR with various of CS30B loading before and after ageing: a) Tensile strength b) Elongation at break, c) Modulus at 300% strain and d) Hardness shore A
(-) = %Retention

4.4.2 Thermal Properties of NR/PIP-MMT Blend

In general, the thermal stability of NR/PIP-MMT nanocomposites was higher than that of unfilled NR due to the good gas barrier action of organo-montmorillonite layers which hinder the evaporation of small molecules generated during the thermal decomposition and restrict the continuous decomposition of the rubber matrix [54]. For CS15A, the decomposition initially occurred at about 268°C and ended at 650°C as shown in Figure 4.21. The total weight loss was about 35.1%. The decomposition of PIP-CS15A was early described in the section of 4.1.2 and the effect of montmorillonite loading on decomposition of PIP-CS15A was already discussed.

The NR showed one step degradation at T_{id} 357°C to T_{max} of 412°C and provided smooth weight loss curves of 98.4%. However, the thermal decomposition of NR/PIP-MMT was similar to NR when MMT content increased due to a low CS15A loading (1-3%). However, T_{max} of NR/PIP-MMT composites were slightly increased from 413 to 420°C). Furthermore, the weight loss of NR/PIP-MMT composites (89.7 - 94.8%) decreased with increasing MMT loading. Thus, NR/PIP-MMT composites at high MMT loading had the high trace of MMT as residue. It can be noted that the thermal stability of the NR/PIP-MMT could be improved. The similar results were earlier reported for NR/PIP-SiO_2 nanocomposites that T_{max} increased with increasing SiO_2 (455-475°C of 10-15 %wt SiO_2 loading) [55].

DSC curves of NR/PIP-CS15A composites are shown in Figure 4.22. T_g onset of NR/PIP-CS15A composites (-64.71°C) was the same as unfilled NR (-65.45°C). This implied that PIP-CS15A loading did not significantly affect T_g onset of NR.

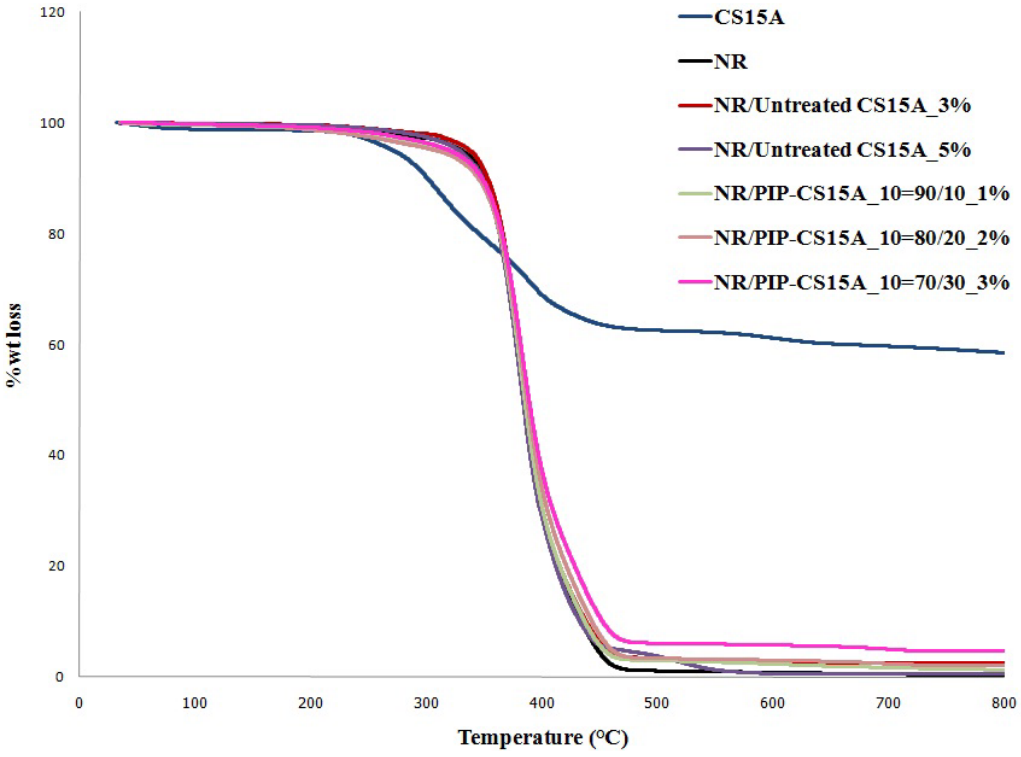

a)

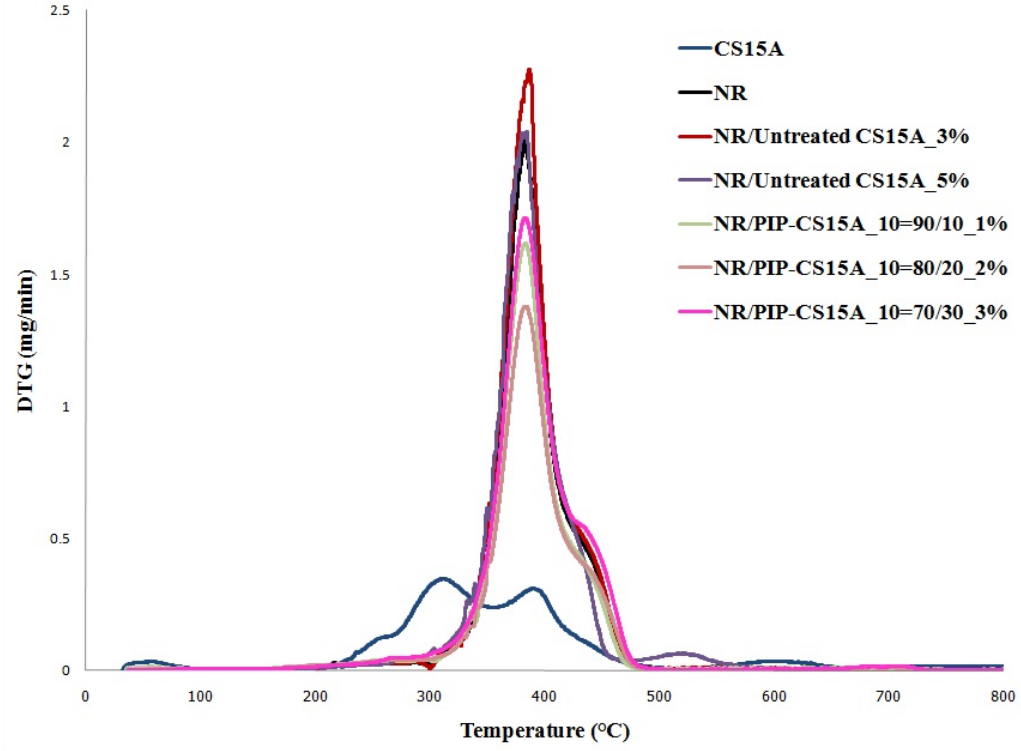

b)

Figure 4.21 a) TGA and b) DTG curves of NR/PIP-CS15A nanocomposites.

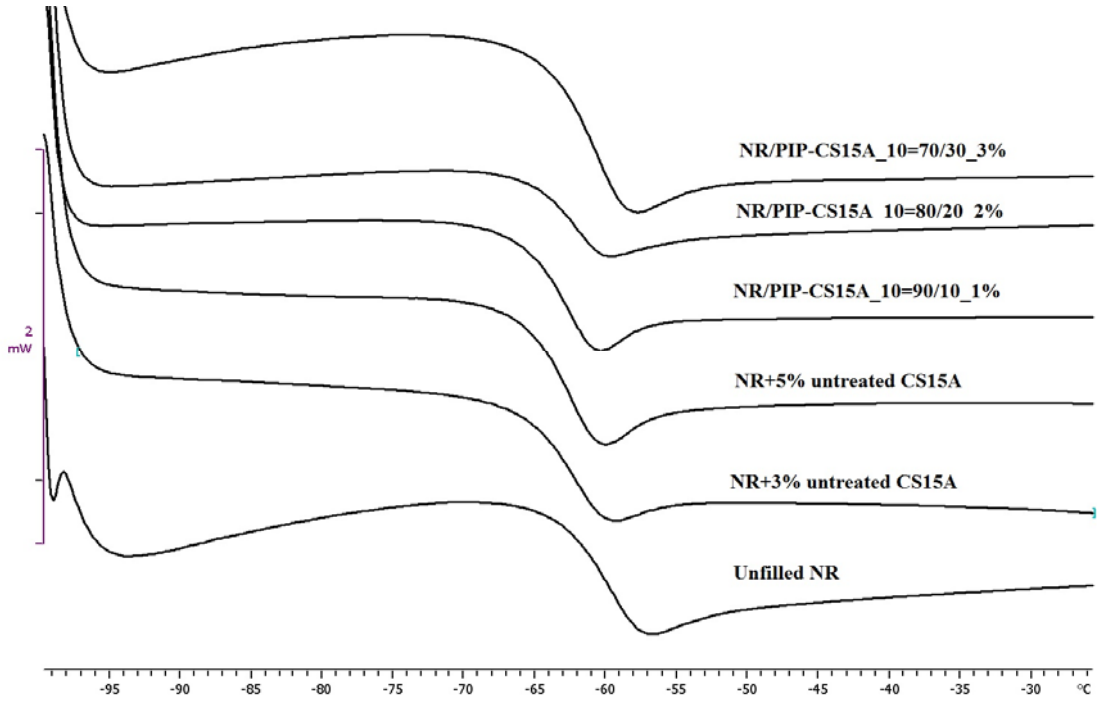

Figure 4.22 DSC curves of NR/PIP-CS15A nanocomposites.

Table 4.12 Glass transition temperature and decomposition temperature of NR/PIP-MMT composites before and after ageing

Sample	NR/PIP-MMT[a]	% MMT[b]	%wt Loss	T_{id} (°C)	T_{max} (°C)	T_g (°C)
NR			98.4	357.6	412.5	-64.7
CS15A			35.1	268.5	407.9	-NA-
NR/untreated CS15A		3.0	97.3	358.9	411.3	-65.4
		5.0	95.4	353.7	412.7	-65.5
NR/PIP-CS15A_5	70/30	1.5	93.8	357.1	418.5	-65.6
	60/40	2.0	93.9	354.2	419.0	-64.9
NR/PIP-CS15A_10	90/10	1.0	93.4	356.5	413.1	-66.2
	80/20	2.0	94.5	355.1	417.6	-65.6
	70/30	3.0	92.8	357.1	418.5	-64.5
NR/PIP-CS30B_10	70/30	3.0	93.3	355.0	420.0	-64.9
NR/PIP-CS30B_15	70/30	4.5	92.9	352.8	418.8	-65.6
NR/PIP-CS30B_20	70/30	6.0	90.9	354.1	420.1	-66.1
NR/PIP-NF15_10	70/30	3.0	89.7	355.7	417.0	-65.5
NR/PIP-NF116-VTS_10	70/30	3.0	94.8	354.9	417.1	-65.7

4.4.3 Morphology of NR/PIP-MMT Blends

The surface morphologies of CS15A, unfilled NR and NR/PIP-CS15A composites (2 and 3 %wt CS15A based on total rubber) before and after ageing were characterized by scanning electron microscopy at high magnification are shown in Figure 4.23 and 4.24.

Figure 4.23 shows the surface morphology of CS15A powder. The CS15A particles seem to be stack together due to moisture. Figure 4.24a – 4.24f show the morphology of NR/PIP-CS15A composites after tensile fracture. Surface morphology of unfilled NR before and after ageing is shown in Figure 4.24a and b, respectively. It can be seen that the fracture surface of unfilled NR is quite smooth. In addition, the unfilled NR was showed roughness surface (brittle) implying the deformation failure in NR after high thermal ageing.

Surface morphologies of NR/PIP-CS15A composites before and after ageing (2 and 3 %wt CS15A based on total rubber) are shown in Figure 4.24c, d and Figure 4.24e, f, respectively. For NR/PIP-CS15A composites before ageing, smooth surface with some aggregates flake layer of CS15A and the cavitations between CS15A layers in NR matrix were observed. The aggregates flake layer of CS15A on NR matrix increased with increasing CS15A amount was observed. After thermal ageing, the surface roughness of NR/PIP-CS15A was observed more than that of before ageing implying the deformation failure of tensile sample. This result was quite similar to the morphology of polyacrylamide/OMMT nanocomposites [60] and NR/PIP-SiO_2 composites [61].

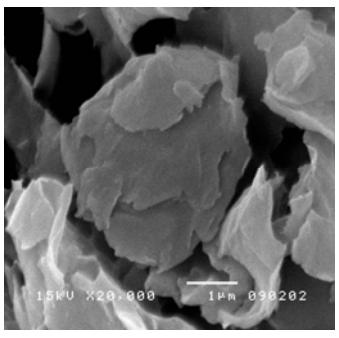

Figure 4.23 Scanning electron micrograph of CS15A (x20,000).

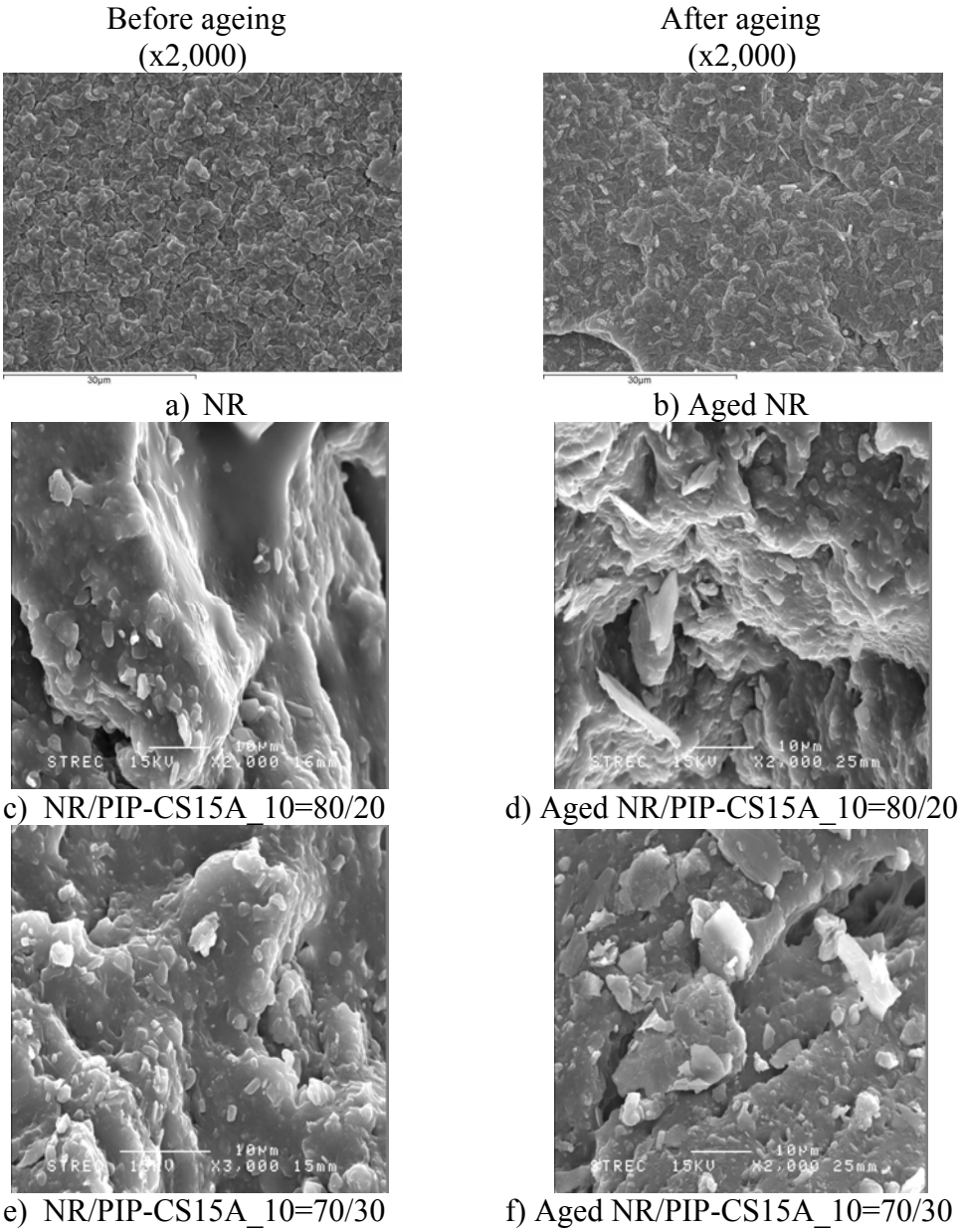

Figure 4.24 Scanning electron micrographs of NR and NR/PIP-CS15A nanocomposites: a) Unfilled NR, b) Aged NR, c) NR/PIP-CS15A_10=80/20, d) Aged NR/PIP-CS15A_10=80/20 e) NR/PIP-CS15A_10=70/30 and f) Aged NR/PIP-CS15A_10=70/30

CHAPTER V

CONCLUSION AND SUGGESTION

5.1 Conclusions

Polyisoprene-montmorillonite nanocomposite was successfully synthesized by differential microemulsion polymerization and the nanosized polyisoprene well-dispersed with montmorillonite was obtained. The influences of surfactant concentration, monomer to water ratio and CS15A loading were investigated. The high monomer conversion of 81% was achieved at 10 %wt CS15A loading, monomer to water ratio of 0.24:1, initiator concentration of 0.25 %wt and surfactant concentration of 12 %wt based on isoprene monomer. PIP-MMT latex with particle size of 30 nm and narrow size distribution was obtained. PIP was well-dispersed and intercalated between the layers of CS15A, as confirmed by X-ray diffractometer that d-spacing of CS15A layer expanded from 3.11 nm to 3.82 nm. Furthermore, TEM micrograph of PIP-CS15A nanocomposites showed spherical shape with particle size of PIP in the range of 30 to 50 nm and montmorillonites with 20-30 nm thick and 100-200 nm long.

PIP-MMT nanoparticles could be used as nanofiller in natural rubber. The addition of PIP-CS15A nanocomposites into NR latex (equivalent to 0-3 %wt CS15A) affected the mechanical properties of NR filled with PIP-CS15A. Tensile strength of NR/PIP-CS15A blends at the ratio of 90/10 (1 %wt), 80/20 (2 %wt) and 70/30 (3 %wt) was higher than that of unfilled NR and high elongation at break was maintained. Hardness of NR filled with PIP-MMT nanocomposites increased with increasing of MMT content, due to the clay strength. Interestingly, the stability of NR/PIP-CS15A composites after thermal ageing increased, maintaining 87.6% of its tensile strength and 84.0% of its modulus of elasticity at 2 %wt of CS15A content.

Thermal stability of NR/PIP-CS15A composites was improved (decrease in %wt loss) with increasing of PIP-CS15A amount. In addition, PIP-CS15A was well dispersed and had good adhesive interaction in NR matrix as confirmed by SEM micrograph.

5.2 Suggestions of the Future Work

The modification of nanosized PIP with montmorillonite should be further studied with the following aspects:

1. Synthesis of polyisoprene-montmorillonite nanocomposites

The synthesis of montmorillonite encapsulation with PIP should be further studied by using ammonium salts and coupling agent (silane group) for providing the strong interaction and good compatibility between montmorillonite within PIP matrix. In addition, the effect of surfactant concentration and monomer to water ratio on preparation of PIP-NF16, PIP-CS30B and PIP-NF116-VTS should be further studied.

2. Synthesis of styrene-butadiene rubber-montmorillonite nanocomposites

The synthesis of montmorillonite encapsulation with SBR should be further studied by using ammonium salts and coupling agent for providing the strong interaction and good compatibility between montmorillonite within SBR matrix.

3. Application of PIP-MMT nanocomposites

The preparation of NR/PIP-MMT nanocomposites at high pre-vulcanization temperature (60-70°C) and high vulcanization temperature (more than 70°C) should be further studied for improving the mechanical properties in tensile strength. In addition, gas barrier properties (permeability of film) should be explored.

REFERENCES

[1] Synthetic Polyisoprene. [Online]. 2011. Available: http://www.hmc polymers.com/ [2011, May 31]

[2] Alexander, B. Morgan, L. and Richard, H. Flammability of polystyrene layered silicate (clay) nanocomposites: carbonaceous char formation. Fire and Materials 26 (2002): 247–253.

[3] Gao, J. Gu, Z. and Song, G. Octadecylammonium montmorillonite/natural rubber/cis-1,4-polybutadiene nanocomposites. Applied Clay Science 50 (2008): 272–275.

[4] Nhumnunjai, P. Prasassarakich, P. and Supaphol, P. Preparation and properties of poly(methyl methacrylate)/clay nanocomposites, Master's Thesis. Program of Petrochemical and Polymer Science, Faculty of Science, Chulalongkorn University, (2003).

[5] Liu, Y.; Fan, Z.; Ma, H.; Tan, Y.; Qiao, J. Application of nano powdered rubber in friction materials, Wear 261 (2006): 225-229.

[6] He, G., Pan, Q., and Rempel, G. L. Synthesis of poly(methyl methacrylate) nanosize particles by differential microemulsion polymerization. Macromolecular Rapid Communications 24 (2003): 585-588.

[7] Suppaibulsuk, B. Prasassarakich, P. and Rempel, G.L. Synthesis styrene-g-polyisoprene nanoparticles by emulsion polymerization and its effect on properties of polyisoprene composites. Polymers for Advanced Technology. (2011) doi: 10.1002/pat.2069.

[8] Navrotsky, A. Nanomaterials in the environment, agriculture, and technology (neat). Journal of Nanoparticle Research 2 (2000): 321-323.

[9] Birnbaum, D. T., Kosmala, J. D., and Brannon-Peppas, L. Optimization ofpreparation techniques for poly(lactic acid-co-glycolic acid) nanoparticles. Journal of Nanoparticle Research 2 (2000): 173-181.

[10] Hillaireau, H. and Couvreur, P. Polymeric nanoparticles as drug carriers. In: Polymers in drug delivery., Uchegbu, I., Schaetzlein, AG., Editor. 2006, CRC Press Boca Raton, FL, USA. p. 101-110.

[11] Chern, C.S. Principles and applications of emulsion polymerization. 2008, John Wiley & Sons: New Jersey, Canada. p. 6-10.

[12] Xu, X.-J. and Gan, L. M. Recent advances in the synthesis of nanoparticles of polymer latexes with high polymer-to-surfactant ratios by microemulsion polymerization. Current Opinion in Colloid & Interface Science 10 (2005): 239-244.

[13] Odian, G. Other emulsion polymerization systems, in principles of polymerization. 2004, John Wiley & Sons: New Jersey, US. p. 367-368.

[14] Atik, S. S. and Thomas, J. K. Polymerized microemulsions. Journal of the American Chemical Society 103 (1981): 4279-4280.

[15] Stoffer, J. O. and Bone, T. Polymerization in water- in- oil microemulsionsystems. I. Journal of Polymer Science: Polymer Chemistry Edition 18 (1980): 2641-2648.

[16] Matsumoto, A. Kodama, K. Aota, H. and Capek, I. Kinetics of emulsion crosslinking polymerization and copolymerization of allyl methacrylate. European Polymer Journal 35 (1999): 1509-1517.

[17] Capek, I. Microemulsion polymerization of styrene in the presence of anionic emulsifier. Advances in Colloid and Interface Science 82 (1999): 253-273.

[18] He, G. Synthesis and characterization of nano-sized polymer particles using differential microemulsion polymerization. Doctoral dissertation, Chemical Engineering, University of Waterloo, 2006.

[19] Suppaibulsuk, B.; Prasassarakich, P.; Rempel, G. L. Synthesis of nanosize polyisoprene and isoprene copolymer by microemulsion polymerization and their diimide hydrogenation, Doctoral dissertation, Department of Chemical Technology, Faculty of Science, Chulalongkorn University, 2011.

[20] Pinnavaia, T.J. and Beall, G.W. Polymer-Clay Nanocomposites. 2000, John Wiley & Sons: West Sussex, England. p. 97-109.

[21] Grim R.E. Clay mineralogy. 2nd ed., New York: Mc Graw-Hill, 1968.

[22] Alexandre, M. and Dubois, P. Polymer-layered silicate nanocomposites: preparation, properties and used of a new class of materials. Material Science and Engineering 28 (2000): 1-63.

[23] Lee, S.Y. and Kim. S.J. Delamination behavior of silicate layers by adsorption of cationic surfactants. Journal of Colloid and Interface Science 248 (2002): 231-238.

[24] Hang, P.T. and Brindley, G.W. Methylene blue absorption by clay minerals: determination of surface areas and cation exchange capacities (clay-organic studies XVIII). Clays and Clay Minerals 18(1970): 203-212.

[25] Mitchell, J.K. Fundamentals of soil behavior. 2nd ed. New York: John Wiley & Sons, 1993.

[26] Paul F.L. and Sylvia R. The colloidal and rheological properties of bentonite suspensions. Advances in Colloid and Interface Science 82 (1999): 43-92.

[27] Santamarina J.C., Klien K.A., Wang Y.H. and Prencke E. Specific surface: determination and relevance. Canadian Geotechnical Journal 39 (2002): 233-241.

[28] Shinoda, K. Nakagawa, T. Tamamushi, B. and Isemura, T. Colloidal and Surfactants. New York: Academic Press, 1963.

[29] Vaia, R. Thermal degradation chemistry of alkyl quaternary ammonium montmorillonite, Chemistry of Materials 13 (2001): 2979-2990.

[30] Vaia R.A., Ishida H. and Giannelis E.P. Synthesis and properties of two-dimensional nanostructures by direct intercalation of polymer melts in layered silicates. Chemistry of Materials 5 (1993): 1694-1696.

[31] Whitting, L.D. "X-ray diffraction technique for menerals identification and mineralogical composition" Methods of soil Analysis Part I Agronomy No.9, C.A. Black, ed. Wisconsin: America. Agron, 1965.

[32] Xie, W. et al., Singh in thermal characterization of organically modified montmorillonite, Thermochimica Acta, (2001): 367-368

[33] Xu, S. and Boyd, S.A. Cationic surfactant adsorption by swelling and non-swelling layer silicates. Langmuir 11, (1995): 2508.

[34] Moore, D.M.; Robert, C. and Reynolds, Jr. X-ray diffraction and the identification and analysis of clay minerals. 2nd edition. New York: Oxford University Press, 1997.

[35] Deer, W.A., Howie, R.A. and Zussman, J. An introduction to the rock-forming minerals. China: Addition Wesley Longmann Ltd., 1996.

[36] LeBaron, P.C. Wang, Z. Pinnavaia, T.J. Polymer-layered silicate nanocomposites: an overview. Applied Clay Science 15 (1999):11–29.

[37] Zeng, Q.H. Yu, A.B. Lu, G.Q. and Paul, D.R. Clay-based polymer nanocomposites: research and commercial development. Journal of Nanoscience and Nanotechnology 5 (2005):1574–92.

[38] Zanetti, M. Lomakin, S. and Camino, G. Polymer layered silicate nanocomposites. Macromolecule Materials Engineering 279 (2000): 1–9.

[39] Ke, Y.C. and Stroeve, P. Polymer-layered silicate and silica nanocomposites. Amsterdam, The Netherlands: Elsevier BV; 2005. p. 1–68.

[40] Beyer G. Nanocomposites: a new class of flame retardants for polymers. Plastic Additive Compound. (2002): 22–8.

[41] Chen, G. Pan, J. Han, B. and Yan, H. Adsorption of methylene blue on montmorillonite. Journal of Dispersion Science and Technology 20 (1999): 1179-1187.

[42] Cho, G.C. and Santamarina, J.C. Unsaturated particulate materials-particle level studies. Journal of Geotechnical and Geoenvironmental Engineering 127 (2001):84-96.

[43] Morgan, B.A. Polymer-Clay Nanocomposites: design and application of multi-functional materials, Sigma-Aldrich Material Matters 2 (2007): 20-23.

[44] Fukushima, Y. and Ingaki, S. Synthesis of an intercalate compound of montmorillonite and 6-polyamide. Journal of Inclusion Phenomena 5 (1987):473-482.

[45] Paiva, L. B. Morales, A.R. and Valenzuela Diaz, F.R. Organoclays: properties, preparation and applications. Applied Clay Science 42 (2008): 8-24.

[46] Zhang, C. Wang, Q. Xia, H. and Qiu, G. Ultrasonically induced microemulsion polymerization of styrene, European Polymer 38 (2002): 1769-1776.

[47] Xu, X., Ge, X., Zhang, Z., Zhang, M.; Zuo, J., Niu, A. Microemulsion polymerization of methyl methacrylate initiated with BPO, European Polymer 73 (1999): 2621–2626.

[48] Norakankorn, C., Pan, Q., Rempel, G. L., and Kiatkamjornwong, S. Synthesis of poly(methyl methacrylate) nanoparticles initiated by 2,2-azoisobutyronitrile via differential microemulsion polymerization. Macromolecular Rapid Communications 28 (2007): 1029-1033.

[49] Norakankorn, C. Pan, Q. Rempel, G.L. and Kiatkamjornwong S., Synthesis of poly(methyl methacrylate) nanoparticles initiated by azobisisobutyronitrile using a differential microemulsion polymerization technique. Applied Polymer Science 113 (2009): 375-382.

[50] Suppaibulsuk, B. Prasassarakich, P. and Rempel, G.L. Factorial design of nanosized polyisoprene synthesis via differential microemulsion polymerization, Polymer Advanced Technology 21 (2010): 467-475.

[51] Jankovic, L. Madejova, J. Komadel, P. Moskova, D.J. and Chodak, I. Characterization of systematically selected organo-montmorillonites for polymer nanocomposites, Applied Clay Science 51 (2011): 438-444.

[52] Valadares, L.F. Leite, C.A.P. and Galembeck, F. Preperation of Natural rubber-montmorillonite nanocomposites in aqueous medium: evidence for polymer-platelet adhesion, Polymer 47 (2006): 672-678.

[53] Gu, Z. Song, G. Liu, W. Li, P. Gao, L. Li, H. and Hu, X. Preparation and properties of styrene butadiene rubber/natural rubber/organo-bentonite nanocomposites prepared from latex dispersion, Applied Clay Science 46 (2009): 241-244.

[54] Pojanavaraphan, T. Schiraldi, D. A. and Magaraphan, R. Mechanical, rheological, and swelling behavior of natural rubber/montmorillonite aerogels prepared by freeze-drying. Applied Clay Science 50 (2010): 271-279.

[55] Kongsinlark, A. Rempel, G.L. and Prasassarakich, P. Synthesis of monodispersed polyisoprene-silica nanoparticles via differential microemulsion polymerization and mechanical properties of polyisoprene nanocomposite. Chemical Engineering Journal 21 (2010): 467-475.

[56] Jinghua Tan, Xiaoping Wang, Yuanfang Luo, Demin Jia, Rubber/clay nanocomposites by combined latex compounding and melt mixing: A masterbatch process. Materials and Design 34 (2012): 825-831.

[57] Limpanart, S.; Udomkichdecha, W.; Srikhirin, T. Surface modification of montmorillonite for polymer-clay nanocomposite preparation, Doctoral dissertation, Department of Material Science, Faculty of Science, Chulalongkorn University, 2003.

[58] Product bulletin. [Online]. 2012 Available: http://www.nanoclay.com/ [2011, June 15]

[59] Larissa, C. Cassio, R. Aline, Z. Raquel, M. Marcelo, G. Roosmary, B and Janaina, C. Characterization of natural rubber nanocomposites filled with organoclay as a substitute for silica obtained by the conventional two-roll mill method. Applied Clay Science 52 (2011): 56-61.

[60] Mansoori, Y. Atghia, S.V. Zamanloo, M.R. Imanzadeh, Gh. and Sirouszar, M. Polymer-clay nanocomposites: Free radical grafting of polyacrylamide onto organophillic montmorillonite. European Polymer Journal 46 (2010): 1844-1853.

[61] Chuayjuljit, S. and Boonmahitthisud, A. Natural rubber nanocomposites using polystyrene-encapsulated nanosilica prepared by differential microemulsion polymerization. Applied Surface Science 256 (2010): 7211-7216.

APPENDICES

Appendix A

The Overall Compositions of Rubbers and Montmorillonite

Table A-1 Properties of natural rubber latex

Properties	Test Results
Total Solid Content, %	61.79
Dry Rubber Content, %	60.12
Non Rubber Solid, %	1.67
Ammonia Content (on Total Weight), %	0.69
Ammonia Content (on Water Phase), %	1.81
pH Value	10.32
KOH Number	0.6020
Volatile Fatty Acid Number (VFA)	0.0288
Mechanical Stability Time at 55% TS., Sec	900
Specific Gravity at 25C	0.9461
Magnesium Content (ppm)	33.75
Viscosity (60%. TS.spindle no 1.60 rpm) cps.	76
Coagulum Centent (80 mesh),ppm	28

All tests are perform according to relevant ISO 2004-1997(E) specification

Table A-2 Properties of montmorillonite

Treatment /Properties	Organic Modifier	Modifier Concentration (meg/100g Clay)	%Weight loss on ignition	Color	d_{001} (nm)
Cloisite15A (CS15A)	2M2HT	125	43	Off white	3.15
Cloisite30B (CS30B)	MT2EtOH	90	30	Off white	1.85
Nanofil15 (NF15)	2M2HT	93	38	Off white	2.80
Nanofil116 (NF16)	none	none	8	Off white	1.25

All results from product bulletin of Southern Clay Product

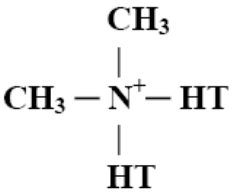

Where HT is Hydrogenated Tallow (~65% C18; ~30% C16; ~5% C14)
Anion: Chloride
2M2HT: dimethyl, dihydrogenatedtallow, quaternary ammonium

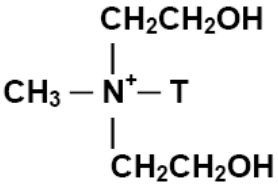

Where T is Tallow (~65% C18; ~30% C16; ~5% C14)
Anion: Chloride
(1) MT2EtOH: methyl, tallow, bis-2-hydroxyethyl, quaternary ammonium

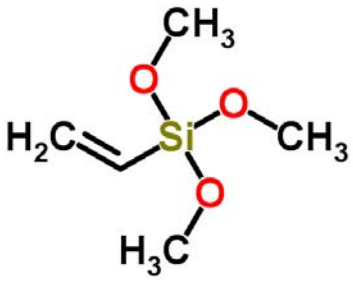

Vinyl trimethoxysilane

Appendix B

Calculation of Monomer Conversion and Solid Content

$$\text{Monomer conversion (\%)} = (M_0\text{-}M_1 / M_2) \times 100 \quad \text{(B.1)}$$

$$\text{Solid content (\%)} = (M_3 / M_4) \times 100 \quad \text{(B.2)}$$

where; M_0 = Mass of the resulting composite particles

M_1 = Mass of the charged MMT particles

M_2 = Mass of the charged isoprene monomer

M_3 = Mass of dried PIP-MMT

M_4 = Mass of PIP-MMT latex

Table B.2 Solid content and monomer conversion calculation

Experiment	MMT loading (%)	M_0 (g)	M_1 (g)	M_2 (g)	M_3 (g)	M_4 (g)	%Solid Content	%Monomer Conversion
SDS 6%wt based on monomer weight								
PIP27-CS15A-01	5	15.2	1.235	24.7	1.14	7.81	14.6	56.5
PIP27-CS15A-02	5	14.8	1.235	24.7	1.20	7.78	15.4	54.9
PIP27-CS15A-03	5	15.3	1.235	24.7	1.11	7.85	14.1	56.8
Mean							14.7	56.0
SD							0.65	0.99
SDS 8%wt based on monomer weight								
PIP27-CS15A-01	5	16.9	1.235	24.7	0.75	4.43	16.9	63.4
PIP27-CS15A-02	5	16.5	1.235	24.7	0.72	4.42	16.3	61.8
PIP27-CS15A-03	5	16.7	1.235	24.7	0.76	4.48	17.0	62.6
Mean							16.7	62.6
SD							0.38	0.81
SDS 10%wt based on monomer weight								
PIP27-CS15A-01	5	20.8	1.235	24.7	0.52	2.54	20.47	79.2
PIP27-CS15A-02	5	21.1	1.235	24.7	0.30	1.51	19.87	80.4
PIP27-CS15A-03	5	21.4	1.235	24.7	0.69	3.37	20.47	81.6
Mean							20.3	80.4
SD							0.35	1.21
SDS 12%wt based on monomer weight								
PIP27-CS15A-01	5	21.3	1.235	24.7	0.68	3.18	21.4	81.2
PIP27-CS15A-02	5	21.5	1.235	24.7	0.87	4.06	21.4	82.0
PIP27-CS15A-03	5	21.2	1.235	24.7	1.24	5.71	21.7	80.8
Mean							21.5	81.4
SD							0.17	0.62
SDS 14%wt based on monomer weight								
PIP27-CS15A-01	5	20.8	1.235	24.7	0.50	2.18	22.9	79.2
PIP27-CS15A-02	5	21.2	1.235	24.7	1.62	6.94	23.3	80.8
PIP27-CS15A-03	5	21.4	1.235	24.7	1.24	5.71	21.7	81.4
Mean							22.6	80.5
SD							0.83	1.15

Table B.2 Solid content and monomer conversion calculation (continued)

Experiment	MMT loading (%)	M_0 (g)	M_1 (g)	M_2 (g)	M_3 (g)	M_4 (g)	%Solid Content	%Monomer Conversion
PIP27-CS15A-01	10	22.2	2.47	24.7	1.07	4.74	22.6	79.7
PIP27-CS15A-02	10	22.3	2.47	24.7	0.96	4.45	21.6	80.2
PIP27-CS15A-03	10	22.4	2.47	24.7	1.19	5.53	21.5	80.8
Mean							21.9	80.2
SD							0.61	0.53
PIP27-CS15A-01	15	16.3	3.29	24.7	0.75	4.43	16.9	52.8
PIP27-CS15A-02	15	16.6	3.29	24.7	0.72	4.42	16.3	53.7
PIP27-CS15A-03	15	16.7	3.29	24.7	0.78	4.48	17.4	54.1
Mean							16.9	53.5
SD							0.56	0.65
PIP27-CS15A-01	20	12.1	4.39	24.7	0.98	7.81	12.5	31.3
PIP27-CS15A-02	20	11.9	4.39	24.7	0.96	7.78	12.3	30.4
PIP27-CS15A-03	20	12.0	4.39	24.7	1.02	7.85	13.0	30.7
Mean							12.6	30.8
SD							0.33	0.45
PIP24-CS15A-01	5	19.8	1.097	21.95	1.11	4.54	24.4	85.0
PIP24-CS15A-02	5	19.7	1.097	21.95	1.09	4.52	24.1	84.9
PIP24-CS15A-03	5	19.8	1.097	21.95	1.10	4.58	24.0	85.0
Mean							24.2	85.0
SD							0.23	0.05
PIP24-CS15A-01	10	20.2	2.194	21.95	0.42	2.17	19.4	81.9
PIP24-CS15A-02	10	20.1	2.194	21.95	0.21	1.08	19.4	81.7
PIP24-CS15A-03	10	19.8	2.194	21.95	0.23	1.10	20.9	80.2
Mean							19.9	81.3
SD							0.87	0.91
PIP30-CS15A-01	5	22.0	1.372	27.4	0.78	3.52	22.2	75.3
PIP30-CS15A-02	5	22.7	1.372	27.4	0.76	3.55	21.4	77.8
PIP30-CS15A-03	5	22.4	1.372	27.4	0.75	3.54	21.2	76.7
Mean							21.6	76.6
SD							0.51	1.28
PIP30-CS15A-01	10	14.9	2.744	27.4	0.12	0.55	21.8	44.4
PIP30-CS15A-02	10	14.5	2.744	27.4	0.51	2.36	21.6	42.9
PIP30-CS15A-03	10	14.8	2.744	27.4	0.44	2.13	20.7	44.0
Mean							21.4	43.8
SD							0.62	0.76
PIP40-CS15A-01	5	27.8	1.783	35.67	1.40	4.92	28.5	72.9
PIP40-CS15A-02	5	27.2	1.783	35.67	1.35	4.88	27.7	71.3
PIP40-CS15A-03	5	28.2	1.783	35.67	1.36	4.90	27.8	74.1
Mean							28.0	72.8
SD							0.43	1.41
PIP40-CS15A-01	10	14.8	3.566	35.67	1.08	4.46	24.2	31.4
PIP40-CS15A-02	10	14.8	3.566	35.67	1.02	4.42	23.1	31.4
PIP40-CS15A-03	10	14.9	3.566	35.67	1.06	4.45	23.8	31.6
Mean							23.7	31.5
SD							0.58	0.13

Table B.2 Solid content and monomer conversion calculation (continued)

Experiment	MMT loading (%)	M_0 (g)	M_1 (g)	M_2 (g)	M_3 (g)	M_4 (g)	%Solid Content	%Monomer Conversion
PIP24-NF15-01	10	17.2	2.194	21.95	0.16	0.78	20.5	68.3
PIP24-NF15-02	10	17.1	2.194	21.95	0.27	1.35	20.0	68.0
PIP24-NF15-03	10	17.0	2.194	21.95	0.27	1.32	20.5	67.3
Mean							20.3	67.8
SD							0.28	0.52
PIP24-CS30B-01	10	17.1	2.194	21.95	0.21	0.91	23.1	67.9
PIP24-CS30B-02	10	17.0	2.194	21.95	0.19	0.86	22.1	67.4
PIP24-CS30B-03	10	16.9	2.194	21.95	0.18	0.81	22.2	66.9
Mean							22.5	67.4
SD							0.53	0.52
PIP24-NF116-VTS-01	10	8.8	2.194	21.95	0.12	0.55	21.8	30.1
PIP24-NF116-VTS-02	10	8.8	2.194	21.95	0.50	2.36	21.2	29.9
PIP24-NF116-VTS-03	10	8.8	2.194	21.95	0.45	2.13	21.1	30.0
Mean							21.4	30.0
SD							0.38	0.09
PIP24-CS30B-01	15	16.9	3.291	21.95	0.18	0.79	22.8	61.9
PIP24-CS30B-02	15	17.3	3.291	21.95	0.71	3.30	21.5	63.8
PIP24-CS30B-03	15	17.2	3.291	21.95	0.46	2.14	21.5	63.4
Mean							21.9	63.0
SD							0.74	1.03
PIP24-CS30B-01	20	17.4	4.388	21.95	0.24	1.14	21.1	59.2
PIP24-CS30B-02	20	17.4	4.388	21.95	0.26	1.15	22.6	59.5
PIP24-CS30B-03	20	17.5	4.388	21.95	0.24	1.12	21.4	59.6
Mean							21.7	59.4
SD							0.81	0.19

Appendix C

Appearance of NR/PIP-MMT nanocomposites

a) b) c) d) e) f) g)

Figure C.1 Appearance of a) NR, b) nanosized PIP24, c) PIP24-CS15A_5, d) PIP24-CS15A_10, e) nanosized PIP27, f) PIP27_CS15A_5 and g) PIP27-CS15A_10 latex.

a) b) c) d) e)

Figure C.2 Appearance of dipping pre-vulcanized rubber film samples: a) unfilled NR, b) NR/PIP, c) NR/PIP-CS15A_10 (1 %wt CS15A), c) NR/PIP-CS15A_10 (2 %wt CS15A) and d) NR/PIP-CS15A_10 (3 %wt CS15A)

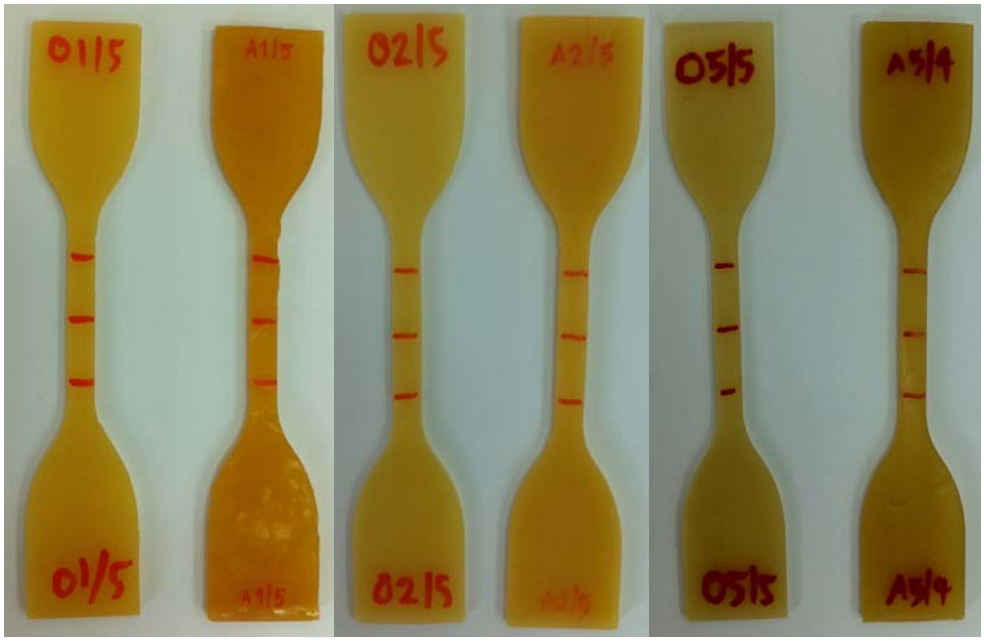

a) b) c)

Figure C.3 Dumbbells specimen before and after ageing of a) unfilled NR, b) NR filled with PIP-CS15A_10=80/20 (2%), and c) NR filled with PIP-CS15A_10=70/30 (3%).

Appendix D

I. NR/PIP-CS15A/PIP-SiO_2 composites

Table D.1 Mechanical properties of NR/PIP-MMT/PIP-SiO_2 composites before and after ageing

Rubber composite	NR/ PIP-MMT/ PIP-SiO_2[a]	% MMT[b]	Tensile Strength (MPa)			Modulus at 300% Strain (MPa)			Elongation at Break (%)	
			Before ageing	After ageing	RT[c] (%)	Before ageing	After ageing	RT (%)	Before ageing	RT (%)
NR/PIP-CS15A/PIP-VTS-SiO_2	80/10/10	1.0	10.6 (1.3)	7.6 (0.2)	71.7	1.3 (0.1)	1.0 (0.1)	76.9	809 (67)	98.4
	70/15/15	1.5	11.0 (1.4)	6.7 (0.4)	60.9	1.4 (0.1)	1.2 (0)	85.7	856 (35)	88.1

Prevulcanization conditions: 40°C under vigorous stirred for 1h.

Ageing conditions: 100°C under air atmosphere for 24h.

[a]NR/PIP-MMT/PIP-SiO_2: ratio of NR to PIP-MMT and PIP-SiO_2.

[b]%MMT: content based on total rubber.

[c]%Retention (RT) = (properties after ageing/properties before ageing) x 100.

Table D.2 Glass transition temperature and decomposition temperature of NR/PIP-MMT compounds before and after ageing

Sample	NR/ PIP-MMT/PIP-SiO_2	% MMT[b]	%wt Loss	T_{id} (°C)	T_{max} (°C)	T_g (°C)
NR/PIP-CS15A/ PIP-VTS-SiO_2	80/10/10	1.0	94.0	356.4	416.2	-65.6
	70/15/15	1.5	94.0	356.4	416.8	-64.7

II. Solid blending of NR/PIP-CS15A composites

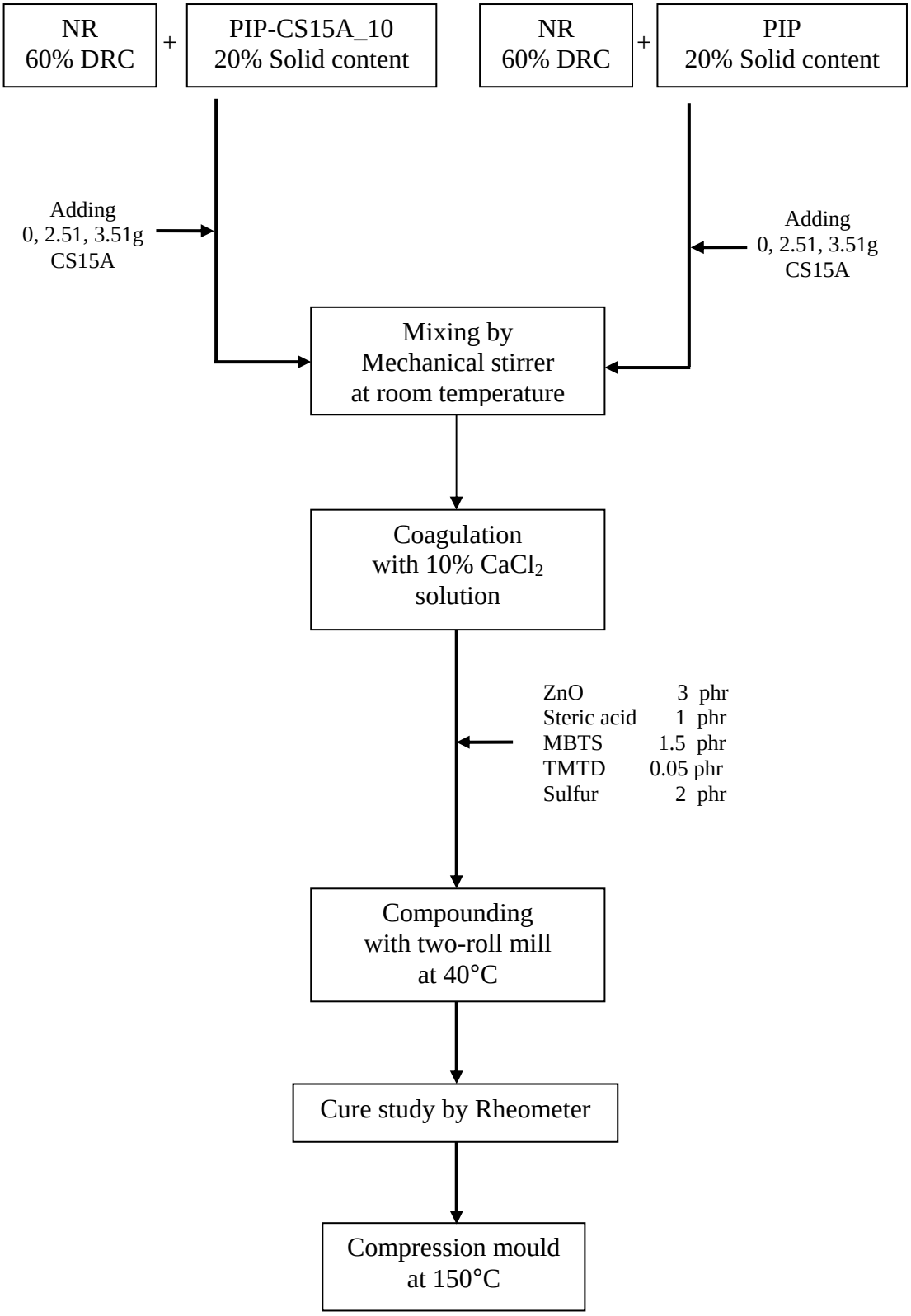

Figure D.1 The experimental procedure for solid compounding of NR/PIP-CS15A

Table D.3 Cure characteristics of the rubber compounds

Rubber composite	%CS15A Total	Minimum torque	Maximum torque	Scorch time	Optimum cure time
		M_L (lbf.in)	M_H (lbf.in)	t_{s2} (min)	t_{90} (min)
Unfilled NR	0	0.16	4.64	1:49	2:56
NR/PIP-CS15A_10 = 50/50	5	0.52	5.74	1:18	3:09
NR/PIP-CS15A_10 = 50/50	8	0.46	6.32	1:25	3:29
NR/PIP-CS15A_10 = 50/50	10	0.61	6.53	1:30	3:55
NR/PIP = 50/50	5	0.57	5.73	1.21	2:45
NR/PIP = 50/50	8	0.58	5.74	1:23	3:02
NR/PIP = 50/50	10	0.51	5.15	1:28	2:58

Die temperature: 155 °C

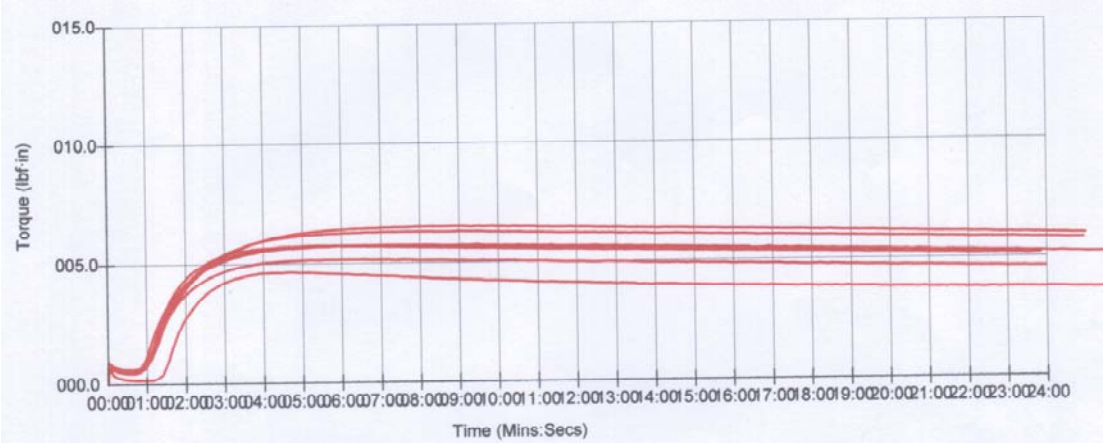

Figure D.2 Rheometric curve of rubber compounds

Table D.4 Mechanical properties of NR/PIP-MMT composites (solid blending) before and after ageing

Rubber composite	NR/ PIP-MMT[a]	% MMT[b]	Tensile Strength (MPa)			Modulus at 100% Strain (MPa)			Elongation at Break (%)		
			Before ageing	After ageing	RT[c] (%)	Before ageing	After ageing	RT (%)	Before ageing	After ageing	RT (%)
Unfilled NR	100/0	0	19.5 (2.2)	6.5 (0.8)	33.6	0.9 (0.1)	0.8 (0.1)	96.3	763 (51)	561 (52)	73.7
NR/PIP-CS15A_10	50/50	5	2.6 (0.7)	2.3 (0.4)	89.6	1.9 (0.4)	2.1 (0.1)	113	228 (41)	132 (98)	58.0
		8	3.0 (0.3)	1.7 (0.5)	56.6	2.5 (0.2)	2.1 (0.9)	85	164 (18)	136 (66)	83.3
		10	3.6 (0.8)	3.0 (0.3)	84.4	1.6 (0.1)	2.7 (0.2)	164	309 (47)	126 (75)	40.9
NR/PIP +CS15A direct mixing	50/50	5	8.0 (1.1)	4.6 (0.7)	57.2	1.8 (0.3)	3.6 (0.7)	196	494 (49)	182 (41)	36.9
		8	3.6 (0.6)	3.1 (1.4)	87.5	1.5 (0.2)	2.3 (0.2)	154	338 (72)	178 (24)	52.6
		10	9.1 (5.6)	3.9 (1.3)	42.5	1.2 (0.1)	2.8 (0.9)	236	608 (112)	174 (97)	28.6

Ageing conditions: 100°C under air atmosphere for 24h.

[a]NR/PIP-MMT/: ratio of NR to PIP-MMT mixing.

[b]%MMT: content based on total rubber.

[c]%Retention (RT) = (properties after ageing/properties before ageing) x 100.

Appendix E

Data of Mechanical Properties

Table E.1 Tensile strength of NR/PIP-MMT compounds before ageing.

Rubber Composites	NR	NR/Untreated CS15A Directed load		NR/PIP-MMT_10=70/30				NR/PIP-CS15A_5		NR/PIP-CS15A_10		NR/PIP-CS30B_15	NR/PIP-CS30B_20	NR/PIP-CS15A /PIP-VTS-SiO_2	
				CS15A	NF15	NF116 -VTS	CS30B	=70/30	=60/40	=90/10	=80/20	=70/30	=70/30	=80/10/10	=70/15/15
%Clay	**0**	**3.0**	**5.0**	**3.0**	**3.0**	**3.0**	**3.0**	**1.5**	**2.0**	**1.0**	**2.0**	**4.5**	**6.0**	**1.0**	**2.0**
TS (MPa)	10.86	15.34	12.91	13.34	11.93	9.92	7.78	5.91	11.76	17.34	17.70	11.08	6.45	11.55	12.00
	11.35	12.96	12.66	13.26	11.75	10.60	7.92	6.30	11.18	17.29	17.82	11.72	5.99	11.11	11.50
	10.94	12.56	13.58	13.45	11.95	9.79	10.93	6.05	11.65	17.40	17.58	11.11	6.83	9.14	9.40
Mean	11.05	13.62	13.05	13.35	11.88	10.10	8.88	6.09	11.53	17.34	17.70	11.30	6.42	10.60	10.97
SD	0.3	1.5	0.5	0.1	0.1	0.4	1.8	0.2	0.3	0.1	0.1	0.4	0.4	1.3	1.4

Table E.2 Elongation at break of NR/PIP-MMT compounds before ageing.

Rubber Composites	NR	NR/Untreated CS15A Directed load		NR/PIP-MMT_10=70/30				NR/PIP-CS15A_5		NR/PIP-CS15A_10		NR/PIP-CS30B_15	NR/PIP-CS30B_20	NR/PIP-CS15A /PIP-VTS-SiO_2	
				CS15A	NF15	NF116 -VTS	CS30B	=70/30	=60/40	=90/10	=80/20	=70/30	=70/30	=80/10/10	=70/15/15
%Clay	**0**	**3.0**	**5.0**	**3.0**	**3.0**	**3.0**	**3.0**	**1.5**	**2.0**	**1.0**	**2.0**	**4.5**	**6.0**	**1.0**	**2.0**
EB (%)	876	791	656	922	816	796	854	656	805	788	853	818	604	778	889
	892	786	674	874	819	761	845	674	857	790	868	840	556	870	820
	864	789	645	963	823	719	906	645	799	786	840	813	618	740	859
Mean	877	789	658	920	819	759	868	658	820	788	853	824	593	796	856
SD	14	2.5	18	45	3.5	39	33	15	32	2.0	14	14	33	67	35

Table E.3 Modulus at 300%Elongation of NR/PIP-MMT compounds before ageing.

Rubber Composites	NR	NR/Untreated CS15A Directed load		NR/PIP-MMT_10=70/30				NR/PIP-CS15A_5		NR/PIP-CS15A_10		NR/PIP-CS30B_15	NR/PIP-CS30B_20	NR/PIP-CS15A /PIP-VTS-SiO_2	
				CS15A	NF15	NF116 -VTS	CS30B	=70/30	=60/40	=90/10	=80/20	=70/30	=70/30	=80/10/10	=70/15/15
%Clay	**0**	**3.0**	**5.0**	**3.0**	**3.0**	**3.0**	**3.0**	**1.5**	**2.0**	**1.0**	**2.0**	**4.5**	**6.0**	**1.0**	**2.0**
300% Modulus (MPa)	0.97	2.59	2.09	1.54	1.77	1.59	1.56	2.09	2.34	1.84	1.81	1.73	2.17	1.39	1.38
	0.91	1.03	1.91	1.52	1.88	1.86	1.34	1.91	2.31	1.88	1.80	1.70	2.28	1.18	1.50
	0.94	1.05	2.03	1.52	1.65	1.63	1.43	2.03	2.34	1.81	1.82	1.71	2.17	1.35	1.40
Mean	0.94	1.56	2.01	1.53	1.77	1.69	1.44	2.01	2.33	1.84	1.81	1.71	2.21	1.31	1.43
SD	0	0.9	0.1	0	0.1	0.1	0.1	0.1	0	0	0	0	0.1	0.1	0.1

Table E.4 Hardness shore A of NR/PIP-MMT compounds before ageing.

Rubber Composites	NR	NR/Untreated CS15A Directed load		NR/PIP-MMT_10=70/30				NR/PIP-CS15A_5		NR/PIP-CS15A_10		NR/PIP-CS30B_15	NR/PIP-CS30B_20	NR/PIP-CS15A /PIP-VTS-SiO_2	
				CS15A	NF15	NF116 -VTS	CS30B	=70/30	=60/40	=90/10	=80/20	=70/30	=70/30	=80/10/10	=70/15/15
%Clay	**0**	**3.0**	**5.0**	**3.0**	**3.0**	**3.0**	**3.0**	**1.5**	**2.0**	**1.0**	**2.0**	**4.5**	**6.0**	**1.0**	**2.0**
Hardness shore A	41	42	42	54	50	44	51	47	51	48	52	52	51	48	50
	41	42	42	54	50	44	51	50	49	48	52	51	50	48	51
	42	42	42	54	50	44	51	48	49	48	52	51	50	48	51
Mean	41.3	42	42	54	50	44	51	48	50	48	52	51	50	48	51
SD	0.6	0	0	0	0	0	0	1.5	1.2	0	0	0.6	0.6	0	0.6

Table E.5 Tensile strength of NR/PIP-MMT compounds after ageing.

Rubber Composites	NR	NR/Untreated CS15A Directed load		NR/PIP-MMT_10=70/30				NR/PIP-CS15A_5		NR/PIP-CS15A_10		NR/PIP-CS30B_15	NR/PIP-CS30B_20	NR/PIP-CS15A /PIP-VTS-SiO_2	
				CS15A	NF15	NF116 -VTS	CS30B	=70/30	=60/40	=90/10	=80/20	=70/30	=70/30	=80/10/10	=70/15/15
%Clay	**0**	**3.0**	**5.0**	**3.0**	**3.0**	**3.0**	**3.0**	**1.5**	**2.0**	**1.0**	**2.0**	**4.5**	**6.0**	**1.0**	**2.0**
TS (MPa)	5.72	7.86	8.84	12.92	10.30	8.41	7.12	4.37	8.59	14.80	15.50	9.71	5.81	7.75	7.06
	5.91	8.23	8.65	12.95	10.40	8.01	6.62	5.23	8.15	14.41	15.45	9.93	5.81	7.39	6.88
	5.91	7.88	8.78	13.38	9.80	5.60	8.05	5.82	11.40	15.20	15.56	9.14	6.08	7.66	6.30
Mean	5.85	7.99	8.76	13.08	10.17	7.34	7.26	5.14	9.38	14.80	15.50	9.59	5.90	7.60	6.75
SD	0.1	0.2	0.1	0.3	0.3	1.5	0.7	0.7	1.8	0.4	0.1	0.4	0.2	0.2	0.4

Table E.6 Elongation at break of NR/PIP-MMT compounds after ageing.

Rubber Composites	NR	NR/Untreated CS15A Directed load		NR/PIP-MMT_10=70/30				NR/PIP-CS15A_5		NR/PIP-CS15A_10		NR/PIP-CS30B_15	NR/PIP-CS30B_20	NR/PIP-CS15A /PIP-VTS-SiO_2	
				CS15A	NF15	NF116 -VTS	CS30B	=70/30	=60/40	=90/10	=80/20	=70/30	=70/30	=80/10/10	=70/15/15
%Clay	**0**	**3.0**	**5.0**	**3.0**	**3.0**	**3.0**	**3.0**	**1.5**	**2.0**	**1.0**	**2.0**	**4.5**	**6.0**	**1.0**	**2.0**
EB (%)	775	791	959	856	772	650	821	569	687	771	821	751	613	848	741
	770	869	854	837	747	700	819	655	669	767	814	732	749	745	778
	796	818	893	891	791	714	823	651	750	774	828	729	625	834	743
Mean	780	826	902	861	770	688	821	625	702	771	821	737	596	809	754
SD	14	40	53	27	22	34	2	49	43	3.5	7	12	41	56	21

Table E.7 Modulus at 300%Elongation of NR/PIP-MMT compounds after ageing.

Rubber Composites	NR	NR/Untreated CS15A Directed load		NR/PIP-MMT_10=70/30				NR/PIP-CS15A_5		NR/PIP-CS15A_10		NR/PIP-CS30B_15	NR/PIP-CS30B_20	NR/PIP-CS15A /PIP-VTS-SiO_2	
				CS15A	NF15	NF116 -VTS	CS30B	=70/30	=60/40	=90/10	=80/20	=70/30	=70/30	=80/10/10	=70/15/15
%Clay	**0**	**3.0**	**5.0**	**3.0**	**3.0**	**3.0**	**3.0**	**1.5**	**2.0**	**1.0**	**2.0**	**4.5**	**6.0**	**1.0**	**2.0**
300% Modulus (MPa)	0.95	0.97	0.78	1.54	1.42	1.25	1.24	1.76	2.27	1.56	1.52	1.62	2.19	1.01	1.19
	0.92	0.81	0.90	1.52	1.47	1.19	1.28	1.69	2.22	1.54	1.53	1.55	2.39	1.11	1.18
	0.95	0.90	0.86	1.53	1.47	1.27	1.25	1.91	2.22	1.57	1.51	1.59	2.16	1.01	1.13
Mean	0.94	0.89	0.85	1.53	1.45	1.24	1.26	1.79	2.24	1.56	1.52	1.59	2.25	1.04	1.17
SD	0	0.1	0.1	0	0	0	0	0.1	0	0	0	0	0.1	0.1	0

Table E.8 Hardness shore A of NR/PIP-MMT compounds after ageing.

Rubber Composites	NR	NR/Untreated CS15A Directed load		NR/PIP-MMT_10=70/30				NR/PIP-CS15A_5		NR/PIP-CS15A_10		NR/PIP-CS30B_15	NR/PIP-CS30B_20	NR/PIP-CS15A /PIP-VTS-SiO_2	
				CS15A	NF15	NF116 -VTS	CS30B	=70/30	=60/40	=90/10	=80/20	=70/30	=70/30	=80/10/10	=70/15/15
%Clay	**0**	**3.0**	**5.0**	**3.0**	**3.0**	**3.0**	**3.0**	**1.5**	**2.0**	**1.0**	**2.0**	**4.5**	**6.0**	**1.0**	**2.0**
Hardness shore A	38	37	37	52	49	40	47	44	49	46	50	51	42	42	48
	38	37	36	52	50	41	46	46	50	46	50	50	42	41	47
	38	38	37	52	49	41	46	44	50	46	50	50	42	41	46
Mean	38	37	37	52	49	41	46	45	50	46	50	50	42	41	47
SD	0	0.6	0.6	0	0.6	0.6	0.6	1.2	0.6	0	0	0.6	0	0.6	1.0

VITA

Miss Parat Boonchoo was born on March 7, 1985 in Phang-Nga, Thailand. She received her Bachelor's degree of Science in Chemistry, King Mongkut's University of Technology, Thonburi in 2007. Parat joined the Program of Petrochemistry and Polymer Science, Chulalongkorn University as Master Degree student in 2009 and finished her study in 2012.

Presentations at the National Conference

"Synthesis of Polyisoprene/Montmorillonite Nanocomposites via Differential Microemulsion Polymerization", January 11-13, 2012. Pure and Applied Chemistry International Conference 2012 (PACCON 2012), Chiang Mai, Thailand.